2016

Novel therapeutic approach for regulating the susceptibility of epitheliato adenovirus infection

Mahmoud Soliman Salem Alghamri
Wright State University

NOVEL THERAPEUTIC APPROACH FOR REGULATING THE SUSCEPTIBILITY OF EPITHELIA TO ADENOVIRUS INFECTION

A Dissertation submitted in partial fulfillment of the requirements for the degree of

Doctor of Philosophy

By

Mahmoud S Alghamri

B.Pharm, Alazhar University, Gaza, Palestine

M.S., Wright State University, Dayton, USA

2016

Wright State University

WRIGHT STATE UNIVERSITY

GRADUATE SCHOOL

August 1, 2016

I HEREBY RECOMMEND THAT THE DISSERTATION PREPARED UNDER MY SUPERVISION BY Mahmoud S Alghamri ENTITLED Novel Therapeutic Approach for Regulating the Susceptibility of Epithelia to Adenovirus Infection BE ACCEPTED IN PARTIAL FULFILMENT OF THE REQUIREMENTS FOR THE DEGREE OF Doctor of Philosophy

Katherine J.D.A. Excoffon, Ph.D.
Dissertation Director

Mill W. Miller, Ph.D.
Director, Biomedical Sciences Ph.D program

Robert E. W. Fyffe, Ph.D.
Vice President for Research and Dean of the Graduate School

Committee on Final Examination

David R. Cool, Ph.D.

David R. Ladle, Ph.D.

Quan Zhong, Ph.D.

Weiwen Long, Ph.D.

Abstract

Mahmoud S Alghamri Ph.D. Biomedical Sciences Ph.D. Program. Wright State University, 2016. Novel therapeutic approach for regulating the susceptibility of epithelia to adenovirus infection.

Human Adenoviruses (AdVs) are etiologic agents for respiratory tract, digestive tract, heart, and eye infections. Although most AdV infections are self-resolving, some infections progress to acute respiratory disease with up to 50% mortality, particularly in immunosuppressed people. Except for vaccines for serotypes, 4 and 7, serotypes that are prevalent in the military, no vaccines or therapeutics that specifically prevent or treat AdV infection exist. On the other hand, AdV remains the most common vector system used in gene therapy clinical trials worldwide and several AdV vectors show promise in phase III clinical trials.

The majority of AdVs use the coxsackievirus and adenovirus receptor (CAR) as a primary receptor. We have characterized an alternatively spliced eight-exon containing isoform (CAR^{Ex8}) that localizes at the apical surface of epithelial cells and is responsible for the initiation of apical AdV infection. A cellular scaffold protein named Membrane Associated Guanylate Kinase, WW and PDZ Domain Containing 1 (MAGI-1) directly interacts with and alternatively regulates CAR^{Ex8} through the C-terminal PDZ-binding domain. The alternative regulation is due to the interaction with two different domains, namely PDZ1 and PDZ3, within the same molecule (MAGI-1). I hypothesized that cell permeable peptides that target the interaction between MAGI-1 PDZ1 domain and CAR^{Ex8} (TAT-PDZ1) would be able to decrease CAR^{Ex8} protein levels and prevent AdV

infection. On the other hand, peptides that target the interaction between MAGI-1 PDZ3 domain and CAR^{Ex8} (TAT-PDZ3) would be able to increase CAR^{Ex8} and enhance AdV mediated gene therapy. Decoy peptides that target the assigned domain were synthesized and conjugated to TAT cell permeable peptide to facilitate peptide entry (TAT-PDZ1; TAT-NET1, TAT-E6) or (TAT-PDZ3; TAT-CAR^{Ex8}-9c, TAT-ESAM). Peptide entry into the polarized epithelia was confirmed by mass spectroscopy and fluorescence microscopy. Treatment with TAT-PDZ1 peptides decreased the cellular levels of CAR^{Ex8} and suppressed AdV transduction in MDCK, human airway epithelia (HAE), as well as epithelia from cotton rats, an animal model of AdV pathogenicity. To determine the mechanism of peptide action, CAR^{Ex8} localization was tracked by immunofluorescence. Interestingly, TAT-PDZ1 caused nuclear translocation of CAR^{Ex8} C-term domain, an effect that was reversed by ADAM17 inhibitor (TIMP3) and γ-secretase inhibitor (Comp E), implicating the regulated intramembrane proteolysis (RIP) pathway. Immunoprecipitation and direct ligand binding assays showed that ADAM17 interacts specifically with MAGI-1 PDZ2 domain, suggesting that TAT-PDZ1 peptides caused CAR^{Ex8} degradation by enhancing the proximity of the substrate (CAR^{Ex8}) and enzyme (ADAM17). Finally, ADAM17 caused CAR^{Ex8} extracellular domain (ECD) shedding that was able to significantly decrease AdV-GFP transduction, indicating a second protective role against AdV entry by the shed ECD of CAR^{Ex8}. By contrast, TAT-PDZ3 peptides increased the levels of CAR^{Ex8} and significantly increased AdV entry and transduction in MDCK, HAE, and cotton rat epithelia. Upon TAT-PDZ3 peptide administration, CAR^{Ex8} was localized in vesicular pattern compartments distinct from MAGI-1 and spread throughout the apical trafficking pathway and at the apical surface of the epithelium.

Investigation of the trafficking pathway of CAR^{Ex8} using Rabs reveal the possibility of CAR^{Ex8} is residing within the recycling Endosomal-Golgi pathway. Neither TAT-PDZ1 nor TAT-PDZ3 binding peptides altered epithelium formation, as measured by transepithelial resistance (TER) as well as dextran permeability across the epithelia, indicating the safety of the peptides on epithelial integrity. Moreover, intranasal administration of TAT-PDZ3 peptides increased AdV transduction by 300-500% while TAT-PDZ1 peptides decreased AdV transduction by 80-95% after intranasal administration in mice demonstrating *in vivo* activity. Taken together, these results validate a potential therapeutic approach of TAT-PDZ1 that can be used as a prophylactic agent to protect susceptible populations from AdV infections or the TAT-PDZ3 which can enhance adenovirus transduction and offer the potential to increase the efficacy of adenovirus-mediated gene therapy.

CONTENTS

List of Figures

List of Tables

CHAPTER1: INTRODUCTION

Adenoviruses

Adenovirus (AdV) gained its name due to first being isolated from contaminated "adenoid" cells where it caused cell deformation (1). At the same time, another group discovered that it was the agent that was responsible for causing the common cold in military recruits (2). Soon after, the two microorganisms were recognized as the same virus (3) and both groups agreed on the common name as "adenovirus" based on the cell type from which it was first isolated.

The non-enveloped capsid of adenoviruses is approximately 90-100 nanometers in size and icosahedral in structure. The predominant proteins in the structure of AdV are: 1) The hexon base trimeric structure with more than 240 trimeric structures distributed equally over the twenty faces of AdV; 2) The penton base proteins distributed evenly to the 12 vertices of the capsid structure and join it with 3) the fiber knobs that project out of the icosahedral architecture (Figure 1). The fiber knobs have a crucial role because they are the first component of the AdV that interact with host cells. The AdV core structure contains a 35-40 kb double stranded DNA structure, which enables AdV to deliver a large amount of DNA into the host cell.

Human AdV are classified into more than 57 serotypes, grouped into 7 species (A-G, Table 1). Most species (all except species B) use the Coxsackie and Adenovirus receptor (CAR) as their primary receptor. AdV is a serious etiologic human pathogen for

respiratory tract, digestive tract, heart, and eye infection, and can progress to acute respiratory distress syndrome (ARDS) and disseminated disease, with up to 50% mortality rate in ARDS patients (4-7).

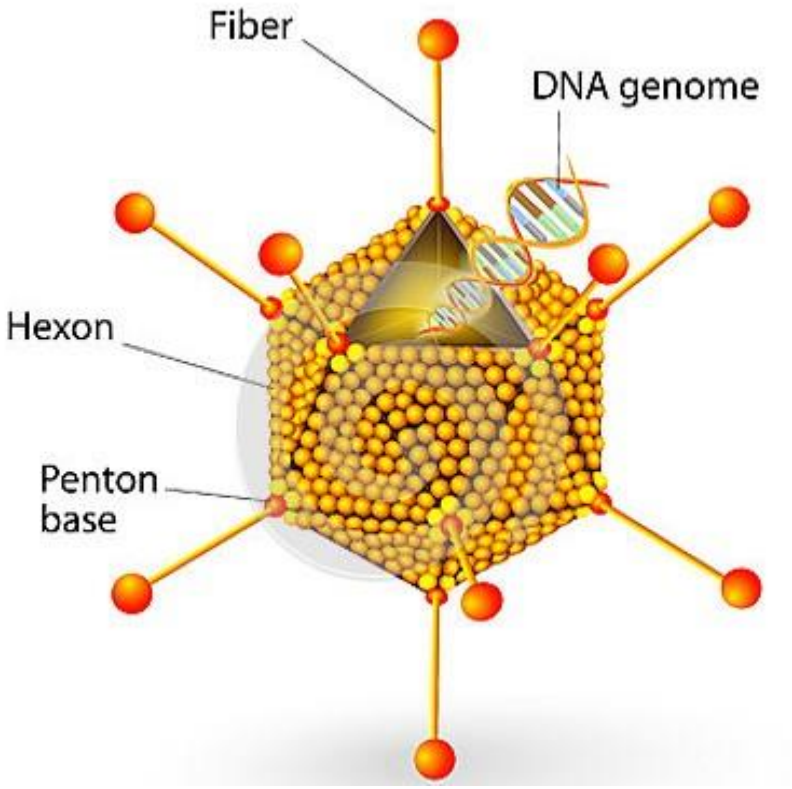

Figure 1. Model structure of the human adenovirus (AdV).

The penton base protein and hexon are within the core structure that package the double stranded DNA. The fiber knobs are trimeric protein structure that radiate out from the core structure and facilitate the AdV binding and entry into the host cell. Adapted from www.shutterstock.com

Depending on serotype, AdV can also cause gastroenteritis with prolonged fecal shedding, or keratoconjunctivitis that can lead to blindness. In highly susceptible, immunosuppressed populations, such as in the transplant setting, AdV infections can be lethal. AdV are easily transmitted by airborne droplets from the infected individual to another, and it can survive in extreme conditions of low humidity and high temperature (8, 9). Due to its stability and ease of spread, many cases of AdV outbreaks have been reported (10-13). Epidemic AdV outbreaks occur in closed or crowded communities, particularly among children and military recruits (4, 14). Such characteristics render AdV as a highly virulent and opportunistic microorganism and mandate immediate invention for novel therapeutics. Unfortunately, no therapeutics that specifically treat or prevent AdV infection are available, and supportive care remains the primary treatment option.

Table 1. Classification of Human AdV serotype

Species	Serotype	Site of infection	Receptor (s)
A	12, 18, 31	Gastrointestinal tract	CAR
B	3, 7, 11, 14, 16, 21, 34, 35, 50,55	Respiratory tract, Urinary tract	CD46, CD80, CD86
C	1, 2, 5, 6, 57	Upper respiratory tract	CAR, Sialic acid, CD46
D	8, 9, 10, 13, 15, 17, 19, 20, 22-30, 32, 33, 36-39, 42-49, 51, 53, 54,56	Ocular, Gastrointestinal tract	CAR
E	4	Respiratory tract	CAR
F	40, 41	Gastrointestinal tract	CAR
G	52		

Current vaccination and therapeutic strategies to control AdV infection

The first AdV vaccination was developed and administered to military recruits in 1971. It successfully reduced the AdV-associated respiratory diseases by 95% (15). However, the vaccine production was discontinued in 1996 which caused a re-emergence of AdV infections and associated symptoms among military population (15, 16). The same vaccine was reinstated in 2011 (17) and resulted in a steep decline in adenovirus cases from approximately 13,000 per year to a few hundred per year. Interestingly, only certain adenovirus types (4, 7, and 14) are problems in the military and are distinct from the types circulating in the civilian population (2, 5, 8, 11, and 21). Therefore, the current vaccines are relatively military specific.

Over the decades since it was discovered, many attempts have been made to make additional therapeutics that inhibit AdV infection. Most of these trials have targeted the viral progeny which develop from the fully mature virus later during the replication stage of the AdV. One of the most commonly used strategies to block AdV infection is the inhibition of viral replication. More than 25 agents have been investigated to determine if they inhibit AdV viral replication. Notably, these agents were initially developed to treat DNA viruses in general, therefore they are non-specific for AdV infection. They prevent viral DNA replication by integration into the viral DNA and interfere with viral DNA elongation. An example (cidofovir) is commercially available anti-DNA viral agent, however, its selectivity against AdV infection is questionable due to the fact that it works in the late stage of viral entry and replication. In addition, the side effects developed from such agent limits its applicability specifically against AdV infection (18-20). Other antiviral agents that target the DNA replication include the cyclin-dependent kinase

(CDK) inhibitors which have been shown to inhibit the spread of AdV *in vitro* (21). A major consideration of this group is the wide range of off-target effects, due to the significant number of substrates available for CDK. Protease inhibitors are another group of antiviral agents that work by targeting proteases produced by the progeny virions in infected cells. Recently released simeprevir, the first FDA approved protease inhibitor against hepatitis C, could give hope for the potential development of anti-AdV protease inhibitors (22, 23). However, AdV produces many proteases and screening for potent and selective anti-AdV protease inhibitor may be time consuming process.

As of today, there is no approved or effective treatment for AdV infection. Some antiviral drugs that non-selectively target DNA viruses are available and anecdotally used as a last resort against AdV infection due to limited efficacy and wide variety of side effects (24-26). Inhibition of AdV binding and entry is expected to be the most effective and prominent strategy to abolish AdV infection. The strategy for inhibition of AdV binding can be accomplished mainly by targeting the host cell receptor. AdV hijacks cellular proteins on the surface of host cells to bind and enter, hence, targeting one of the host cellular proteins may be an efficient way to prevent AdV entry or reduce spread in the body. There is an increased acceptance of targeting the host cells as an antiviral strategy. An example is the development of a sialic acid mimetic that would neutralize and inhibit AdV entry (27). The drug targets some of AdV species C, which use sialic acid as a co-receptor for binding and entry. The drug is now in phase II clinical trials in eye drop formulation under the name “APD-209” for prevention and treatment of conjunctivitis caused by AdV.

Targeting the host cell as potential new anti-AdV or pro-gene therapy strategies

In contrast to anti-viral agents that target the specific viral pathogen, molecules that target the host may have promising outcomes for preventing AdV infection. A hallmark of such strategy is to target host proteins that are being hijacked by the AdV. This strategy would broaden the biological applications of the agent due to the fact that many AdVs use CAR as a receptor for binding and entry. Moreover, it can be used against other types of viruses that potentially use the similar cellular proteins. One advantage of targeting the host cell is the AdV life cycle depends on many cellular proteins within host cells. If these cellular proteins are targeted it will make it less likely for the virion to develop antiviral resistance, in comparison to the other antiviral agents that target the virions. For example, many microorganisms developed resistance against their antiviral agents either by releasing proteolytic enzymes to degrade the agent or by causing mutations in the drug active site. It would not be expected for the virions, however, to change its main cellular receptor, for example CAR, used for binding and entry. Therefore, agents that block AdV receptor would be more efficient against AdV infection with no resistance. Another advantage in targeting the host cell is to broaden the antiviral activity since many viruses share the same mode of infection toward their host cells. Finally, it is plausible that the effectiveness of traditional antiviral agents (i.e. acyclovir) would be enhanced if used in combination with an agent that targets one of the proteins necessary for viral cycle in the host cells. Such combination would also lower the required dose of the therapeutic agent which lowers the potential of developing side effects.

Adenovirus as a vector for gene therapy

AdV is the most widely used vector for gene therapy (28, 29). It gives high expression of the gene it carries and it can infect both dividing and quiescent cells. Besides that, it has the capacity to deliver a large gene load efficiently and the dsDNA genome can be manipulated through standard molecular methods.

The most common AdV used as vector in gene therapy is AdV5 of which CAR is the primary receptor, and its transduction efficacy is dependent on CAR expression (30-32). Experimentally substituting the transmembrane and C-terminus of CAR with a glycophosphatidylinositol (GPI) tail (GPI-CAR) causes exclusive localization at the apical membrane of polarized epithelia and increases viral infection (33-35). Therefore, cells with high CAR expression at the apical membrane are transduced more efficiently than cells with low CAR levels and targeting the upregulation of apical CAR would be a good strategy for enhancing AdV mediated gene therapy.

Upon intravenous administration in mice, AdV accumulates mainly in the liver, followed by spleen, heart, lung, kidney (36). Attempts have been made to change the distribution of AdV and tissue targeting of the AdV by targeting alternative surface receptors. One approach was the incorporation of an adaptor within the AdV fiber-knob structure that would recognize and target a ligand on the cell surface. In such way, the AdV will travel to the tissue were the receptor for the added ligand is expressed. An example of that is conjugation of Ad-FAB against a cellular receptor, such as fibroblast growth factor 2 (EGF2) (37, 38) to target cells with EGF2 receptor expression, or angiotensin converting enzyme (ACE) to target AdV to the pulmonary endothelium (39). Other adaptors used include an AdV that was fused with soluble CAR extracellular domain (sCAR ECD) along with EGF. This adaptation leads to increase AdV

transduction in EGF positive cells. The disadvantage of the adaptor-AdV fusion is that the two components were produced separately then fused together by chemical or physical ways. Such ways could affect the AdV structure or the genetic material that is being carried. Another disadvantage is that the progeny and nascent virions would lack these modifications, and therefore will bind to their original cellular receptor CAR, which may reduce viral transduction.

Another strategy is genetic engineering of ligand within the AdV capsid structure so that it targets alternative cellular receptors. One of the most common engineered AdV was by incorporating the RGD motif within AdV structure (40-42). RGD are the 3 amino acid signals (Arginine, Glycine, Aspartic acid) that interact with surface integrins. AdV-RGD, Ad5.SSTR/TK.RGD is the most promising example which has passed phase I clinical trials (43) and has proven to have high efficacy of gene transduction *in vitro*.

In spite of the successful clinical trials using AdV as a vector, a major setback occurred in 1999 when 18-years old Jesse Gelsinger died after administration of a large inoculum (3.8×10^{13} particles) of AdV to restore ornithine transcarbamylase, an enzyme responsible for amino acid de-amination and ammonia metabolism in the body. Gelsinger died due to multi-organ failure and disseminated intravenous coagulation (44). Interestingly, a female patient who received a similar dose did not experience any such adverse effects (44). Although the administered AdV was replication deficient, high inoculums of AdV can still cause adverse effects. Therefore, molecules that increase the efficacy of AdV transduction would be able to overcome this drawback by allowing the administration of a low AdV inoculum.

Coxsackie and Adenovirus Receptor (CAR)

CXADR, the gene for CAR, was cloned and characterized in 1997 by three different groups (30-32). It is located on chromosome 21q11.1 and is composed of eight exons (45) spread over 54,000 nucleotides. The most abundant form of CAR protein is composed of one polypeptide chain (365 amino acids) which belongs to class I transmembrane protein (Figure 2). Its protein structure is composed of four domains, two of them form the extracellular D1 and D2 (214 aa), transmembrane domain (23 aa), and 107 aa intracellular domains (30). The D1 extracellular domain forms homodimers and, thus, it is responsible for the cell adhesion function of CAR (46-49). The same aa within the D1 loop that mediate CAR-CAR adhesion also compose the binding site for AdV fiber knob. Neither the transmembrane domain nor the intracellular domain are important for viral binding and entry since replacement of these domains with a GPI-linked tail is sufficient to maintain equivalent infection (33). The cytoplasmic domain does play an important role in regulation and stability of the cellular levels of CAR. CAR is prone to many post translational modifications including, 1) phosphorylation at many tyrosine (Y269, Y294, Y313, and Y318), threonine (T29), or serine (S293, S323, and S332) residues (50) , 2) palmitoylation on cysteine C259, C260 (51), and 3) ubiquitination (52). Of particular importance, the extreme cytoplasmic domain of CAR encodes a PDZ binding domain motif -GSIV (or –ITTV in the 8 exon isoform of CAR), a motif that enables CAR to interact with PDZ domain containing proteins. The significance of CAR PDZ domain interactions is discussed in detail below (CAR interactions with PDZ domains containing protein).

CAR expression

CAR is expressed in most organs, but is predominantly expressed in the developing heart, airway epithelium, and brain (31, 53). In the heart, CAR levels change dramatically during embryonic development. During the early embryonic stage, CAR levels are high in the myocardium; this high concentration drops progressively as the heart matures (31, 54). Deletion of CAR leads to the formation of lesions and cardiac hemorrhaging (54, 55), ventricular hypertrophy, and defects in the sinoatrial valve (56). Asher et al. and others showed that in CAR KO mice, all embryos died 11-14.5 days post conception due to myocardial dysfunction (54-56). This indicates that CAR is essential for normal cardiac function during the early stages of embryonic development and suggests that CAR is a "pathfinder" receptor that mediates cardiomyocyte junction formation and integrity (57).

CAR expression levels remain relatively high in the epithelial cells of several organs such as lung, liver, and intestine in adult organisms (58). It was predominantly expressed in cell layers lining body cavities including polarized epithelia (59). In well-differentiated airway epithelia the eight exon isoform (CAR^{Ex8}) is localized at the apical surface (45), where it can function as an anchor site for neutrophil binding on the epithelial apical surface (60). CAR was also found to localize at the apical membrane of retinal epithelial cells (61).

Splicing of CAR

Most adenoviruses and group B coxsackieviruses invade the human epithelium using CAR as a primary receptor (30, 31, 62). *CXADR* can express four isoforms of CAR, only two of them are transmembrane isoforms, namely CAR1 (CAR^{Ex7}) and hCAR2 (CAR^{Ex8}), which differ in their intracellular domain (ICD). The two isoforms are

structurally similar except for the cytoplasmic extreme C-terminal domain; 13 aa in CAR^{Ex7} and 26 aa in CAR^{Ex8} (Figure 2). Another crucial difference between the two isoforms is their localization in polarized cells. Whereas CAR^{Ex7} is buried within the basolateral junction adhesion complex of the human epithelium, and therefore, it is not directly accessible to the incoming airborne viruses, CAR^{Ex8} is localized at the apical and sub-apical air-exposed surface of human epithelial cells and provides a direct binding site for the incoming virus (45, 63, 64). Viral receptor isoform-specific localization and function has also been described for the poliovirus receptor. The poliovirus receptor (hPVR/CD155) has two transmembrane isoforms with differential localization in polarized epithelia (65). While hPVRα resides on the basolateral surface, hPVRδ appears on the apical surface where it can mediate apical poliovirus entry. The regulation of apical versus basolateral localization for hPVR is also currently unknown but may rely on overlapping mechanisms with the CAR isoforms.

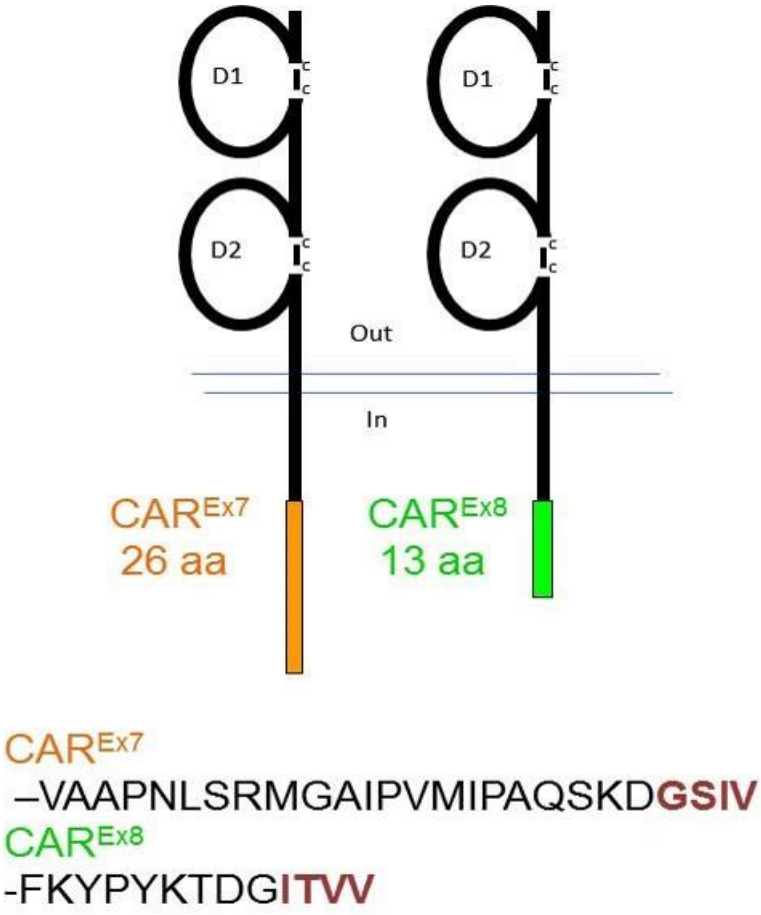

Figure 2. Alternative Coxsackievirus and adenovirus receptor (CAR) spliceforms.

The two isoforms are only different in the extreme C-terminal domain with 26 aa in CAR^{Ex7} replaced with 13 aa in CAR^{Ex8}. Adapted from (45).

CAR^{Ex8} mediates adenovirus infection of primary airway epithelia

The first step for initiation of AdV infection is binding to a cell surface receptor. Except for group B AdV which use CD46 for binding and entry (66-69), most AdV serotypes use CAR as a common receptor for binding and entry into cells (70, 71). Following binding, AdV requires a secondary interaction with integrins (72). Integrins are heterodimeric cell surface transmembrane proteins known to be involved in cell adhesion, migration, growth, and differentiation. Integrins $\alpha_v\beta_1$, $\alpha_v\beta_3$, and $\alpha_v\beta_5$ are the best described AdV co-receptors and are known to enhance the AdV entry step into host cells (72, 73). They promote AdV entry by binding to the RGD motif found within the AdV penton base which facilitate virus entry. AdV then internalized via clathrin-mediated endocytosis (74). The signaling pathway that causes dynamin and clathrin triskelions to be recruited to the AdV binding site and the surrounding milieu is currently unknown. However, endocytosis of the clathrin-coated vesicle is followed by stepwise dismantling of the virion fiber knobs and endosomal escape of virion to the cytoplasm by pH dependent process (75, 76). Adenovirus has also been shown to enter by non-clathrin mediated endocytosis pathways including macro- and micropinocytosis (77, 78). Once in the cytoplasm, the virion capsid interacts with microtubule motor proteins that lead to the nucleus. Additional uncoating of the capsid occurs at the nuclear pore which then allows transfer of viral DNA into the nucleus (Figure 3) (79, 80).

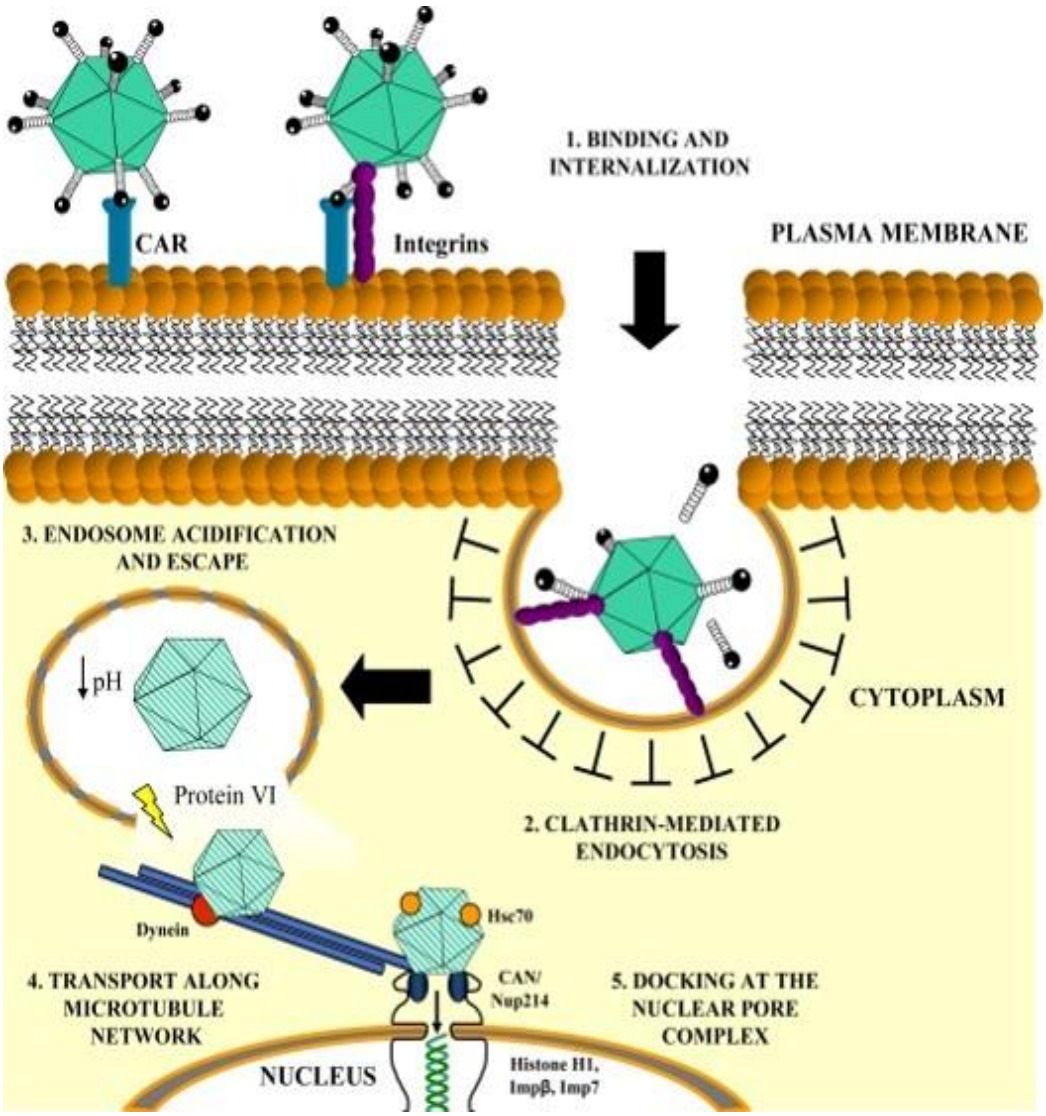

Figure 3. The process of AdV entry and infection.

AdV binds the cell surface receptor CAR. Integrins function as co-receptor for AdV to facilitate its entry. AdV is endocytosed by clathrin-mediated endocytosis followed by viral escape by endosomal acidification which causes stepwise dismantling of the virion structure. The virion travels along microtubules and binds to nuclear pore complex. The virion then ejects its DNA into the nucleus which triggers viral replication. Adapted from Coughlan et al., 2010 (81).

The pulmonary epithelium is a highly characterized system lining the respiratory tract. It exposes a vast surface area to the ambient air, thereby allowing efficient gas exchange of oxygen and the metabolic waste product carbon dioxide. It is also the first line of defense for an airborne microorganism to infect the respiratory system. The pulmonary epithelium is characterized by its ability to polarize and form tight junctions that seal the basolateral surface of the respiratory tract from pathogenic microorganisms on the apical surface. For a long time, the dominant isoform, CAR^{Ex7}, was believed to be the only primary epithelial AdV receptor and viral access to basolateral CAR^{Ex7} required a transient or sustained break in the tight junction (77). The discovery of CAR^{Ex8} causes paradigm shift from the traditional knowledge about AdV infection and gives incentives to researchers to look for a strategy to target the apically localized CAR^{Ex8} isoform.

We have discovered that the eight-exon CAR isoform (CAR^{Ex8}) localizes to the apical membrane of polarized primary human airway epithelia and mediates apical AdV entry (Figure 4) (45, 63, 64). CAR^{Ex8} is the AdV receptor at the apical surface of polarized epithelia and the susceptibility of an epithelium to adenoviral infection can be directly impacted by either increasing or decreasing CAR^{Ex8} expression (Figure 5). This discovery has opened the doors toward investigations and discovery of new therapeutic strategies aimed to downregulate CAR^{Ex8} for the purpose of inhibition of AdV infection, or to upregulate CAR^{Ex8} in order to enhance AdV gene therapy in target tissues.

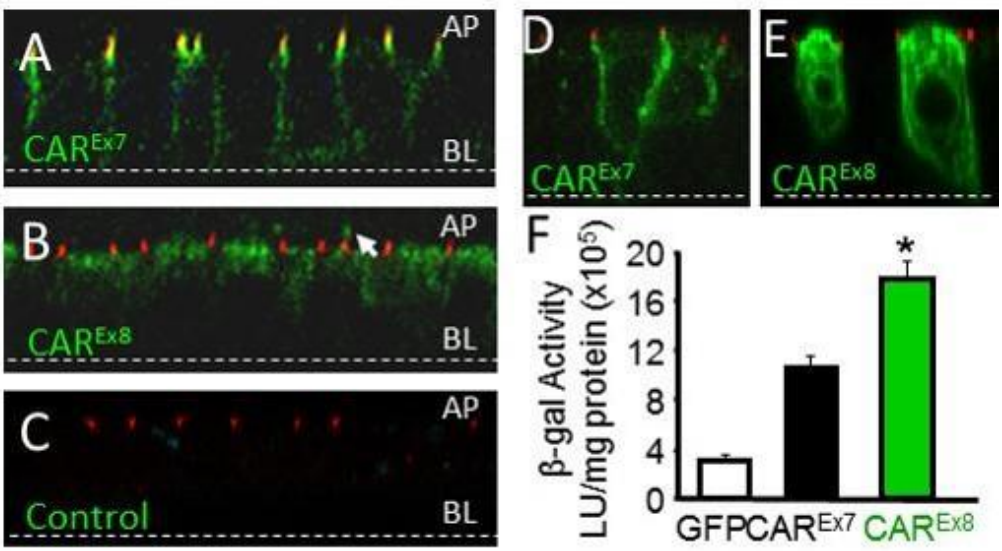

Figure 4. CAR^{Ex7} and CAR^{Ex8} localize and behave distinctly in well-differentiated primary human airway epithelia (HAE).

(A) CAR^{Ex7} (green) overlaps (yellow) and is basolateral to the tight junction protein ZO-1 (red). (B) CAR^{Ex8} (green) localizes to an apical compartment and is distinct from ZO-1 (red). The arrow indicates CAR^{Ex8}-specific staining above the ZO-1 delineated tight junction. (C) Background staining with pre-immune rabbit serum (green) and ZO-1 (red). Over-expression results in (D) CAR^{Ex7} localization primarily at the basolateral junctions and E) CAR^{Ex8} localization diffusely and at the apical surface of HAE. (F) Augmenting CAR^{Ex8} expression significantly increases apical adenovirus, encoding the gene for β-Galactosidase (Adβ-Gal), transduction over GFP or CAR^{Ex7} expressing epithelia *$p<0.01$. Dotted line represents support membrane; AP, Apical surface; BL, Basolateral surface. Confocal microscopy (60x oil immersion). Adapted from (45).

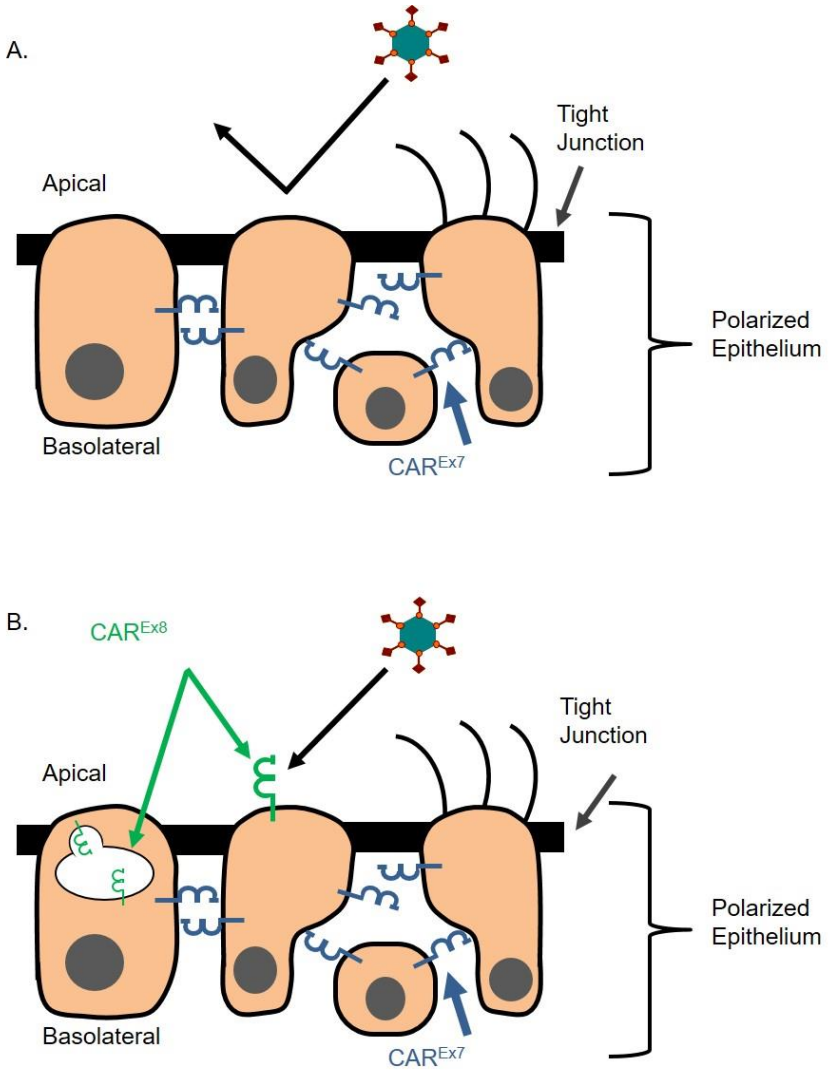

Figure 5. Accessibility of CAR to adenovirus entering from the lumen of the airway.

(A) CAR^{Ex7} localizes beneath the tight junctions at the basolateral surface of polarized epithelia and is not accessible to incoming AdV. (B) CAR^{Ex8} localizes at the apical surface and in a recycling endosome. Apical CAR^{Ex8} allows AdV to bind, internalize, and infect cells from the airway lumen.

PDZ interactions

PDZ domains were first identified in three proteins: postsynaptic density protein (PSD95) (82), its *Drosophila* homologue discs large tumor suppressor (DlgA) gene product (83) and zonula occludens-1 (ZO-1) (84), a tight-junction protein. PDZ domain containing proteins are a huge class of "scaffolding proteins" that can simultaneously interact with several proteins and are involved in screening and sorting of many intracellular and transmembrane proteins. They play an important role in the trafficking and stability of many proteins, including apically localized proteins such as CFTR (85). The membrane-associated guanylate kinases (MAGUKs) are a family of scaffolding proteins responsible for organizing many groups of proteins at the cell-cell junctions (86, 87). MAGUKs are characterized by having a SH3 domain, a guanylate kinase domain (GK), WW domains, and multiple PDZ domains (Figure 6). Most MAGUKs family members localize at the cell junction and this localization occurs in the absence of the GK domains as well as the extended carboxyl terminus (88).

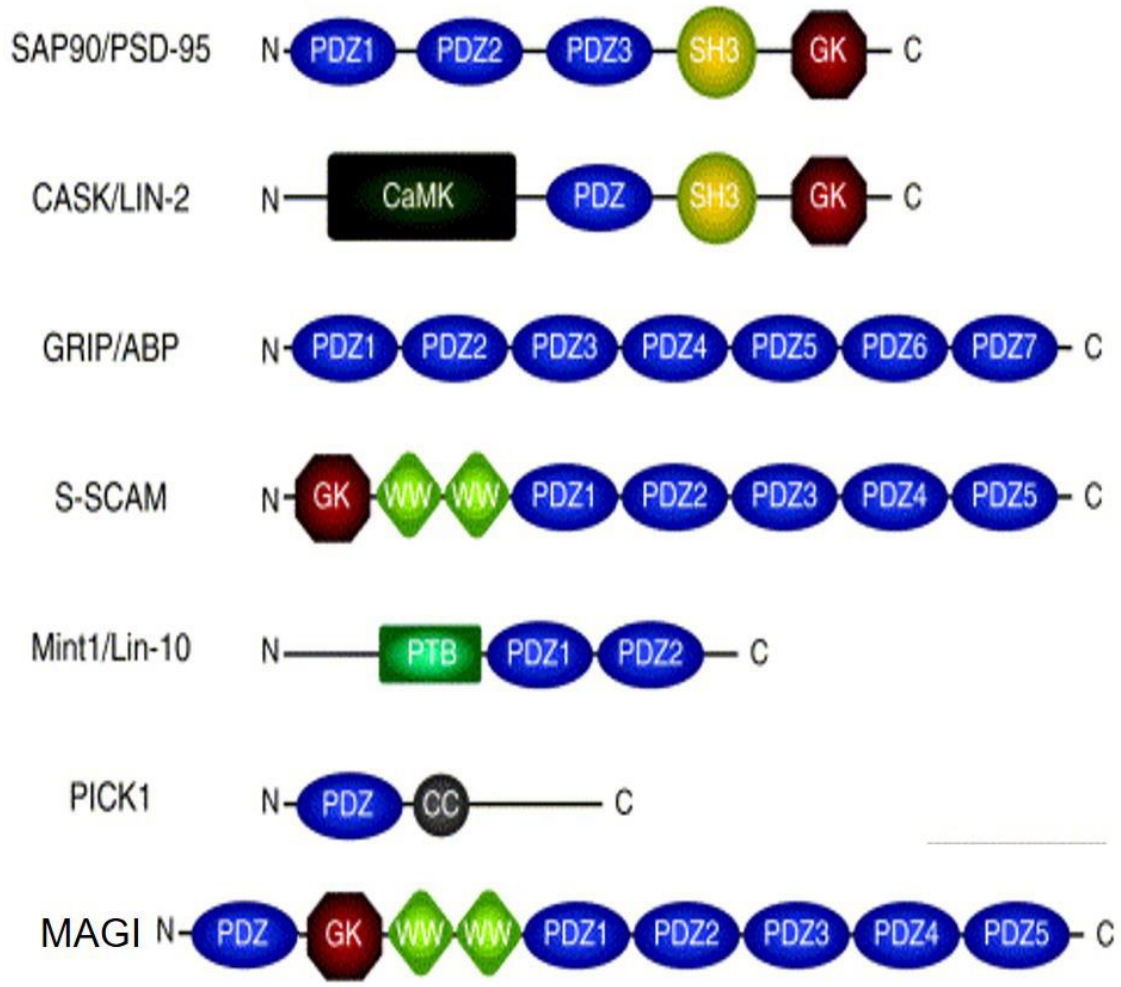

Figure 6. Examples of members of the membrane associated guanylyl kinases (MAGUK) family.

Most MAGUKs share a SH3 domain (yellow), a guanylate kinase domain (red) and PDZ domains (blue). Modified from (89)

Individual PDZ domains are composed of 80-100 amino acids that have a structurally well-defined interaction 'pocket' that interacts with PDZ binding domains (90). The domains can recognize short C-terminal sequences in target proteins, called PDZ binding domains that contain one of four classes of consensus sequences, type I (S/T-x-Φ–COOH), type II (Φ-x-Φ–COOH), type III (Ψ-x-Φ–COOH) and type IV (D-x-V–COOH) where (X) is any amino acid, (Φ) is hydrophobic aa (V, I, L, A, G, W, C, M, F), and (Ψ) is basic aa (H, R, K) (90-93). We have shown that the PDZ domain containing cellular protein, MAGI-1 (member of MAGUKs family), is a master switch for CAR^{Ex8} protein levels and apical AdV infection of polarized cells (63).

The function of each PDZ domain containing protein is diverse. Many of them such as LNX1 (94), MARCH2 (95), and PDLIM2 (96) were shown to contain a ubiquitin ligase in their structure. Others, such as Crumbs, Scribble, and Par are suggested to be responsible for establishing apical and basolateral polarity in epithelia cells (97). The majority of them, MUPP1, PATJ, MAGI-1, and ZO-2, lack a catalytic domain and instead form a multiple protein-protein interaction module with tight junction molecules. Alternatively, they may be responsible for proper trafficking and subcellular localization of many receptors and ion channels such as such as the β-adrenergic receptor (98), potassium channels (99), sodium channels (100), and NMDA receptors (101).

CAR interactions with PDZ domains containing protein

The cellular stability of CAR^{Ex8} protein level is regulated by a PDZ domain containing protein called MAGI-1 (Membrane Associated Guanylate Kinase, WW and PDZ Domain Containing 1). MAGI-1, is a master switch for CAR^{Ex8} protein levels and apical AdV infection of polarized cells (Figure 7) (63). We found that the effect of

MAGI-1 on CAR^{Ex8} is mediated by the PDZ binding domain of CAR^{Ex8} located at its extreme C-terminus domain. Interestingly, two PDZ domains within MAGI-1 recognizes the C-terminal domain of CAR^{Ex8}, namely PDZ1 and PDZ3. It is speculated that the concentration of CAR at the membrane is regulated mainly by PDZ domain containing proteins. Indeed, CAR has been shown to interact with many PDZ domain containing proteins located at the interior side of the membrane including MUPP-1 (102), MAGI-1b, PICK1 and PSD-95 (103), LNX and LNX-2 (104, 105), and ZO-1 (47). These interactions are not only relevant for regulating the concentration of CAR via interactions with scaffolding proteins such as MAGI-1b (63), but also for the proper trafficking of ion channel proteins such as, acid sensing ion channel 3 (ASIC3) (106).

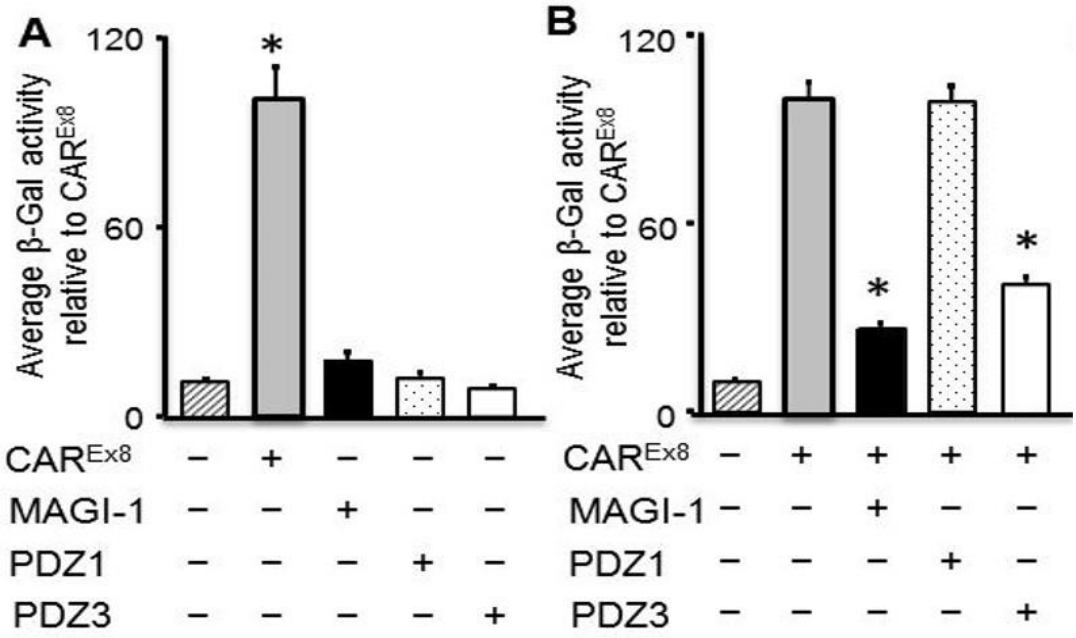

Figure 7. MAGI-1 PDZ3 decreases viral infection, while PDZ1 inhibits MAGI-1-mediated CAR^{Ex8} suppression to allow adenovirus infection.

CAR-deficient CHO-K1 cells were (A) single, or (B) double transfected with CAR^{Ex8}, full length MAGI-1 (black bars), PDZ1 domain (dotted bars), or PDZ3 domain (white bars), and balanced with empty pcDNA3.1 plasmid (gray bars), followed by AdV-β-Gal (MOI 100) transduction. Adapted from (63).

MAGI-1, an easy viral target

Many viral proteins contain PDZ binding domains and subvert the activity of cellular PDZ domain containing proteins to enhance the viral lifecycle and/or increase the virulence of the virus (107-109). Of particular importance here, MAGI-1 interacts with over 40 cellular and viral proteins (110). One of these proteins is the human papilloma virus (HPV) E6 protein which binds to and stimulates MAGI-1 degradation to disrupt tight junctions and promote oncogenesis (108). MAGI family proteins exhibit the strongest binding to and most efficient degradation by E6 via proteasome-mediated degradation (108, 111-113). Recent findings suggest that HPV E6-mediated degradation of MAGI-1 promotes tight junction disruption in epithelial cells (114). Therefore, many viral proteins may have been developed to hijack the host cell function in order to promote their virulence and enhance their replication.

Targeting protein interactions by cell permeable peptides

Rapid transduction of proteins into cells can be facilitated by cell permeable peptides (CPP; also called cell penetrating peptides) (115-117). The 11-amino acid minimal transduction domain of HIV-1 TAT (residues 47-57) can facilitate protein entry into a wide variety of cells both *in vitro* and *in vivo* (118, 119). Many other CPPs have been described from octa-arginine to AdV dodecahedrons (115, 120, 121). TAT-CPPs are in clinical trials and clinically approved protein-based therapies are available (e.g. surfactant proteins, DNase) (122-124). Interactions with the fifth MAGI-1 PDZ domain (PDZ5) has been targeted in MDCK cells using CPP and caused the disruption of the MAGI-1 interaction with β-catenin, an important cellular cell junction and signaling protein (125). Moreover, CPP that target PDZ domain interactions with the neuronal scaffolding protein PSD-95

protect against neuropathic pain and ischemic brain damage in murine models (126, 127). Interestingly, the PDZ binding domain motif of CFTR is required for its degradation (95) and modified cell permeable peptide has been used recently to rescue CFTR activity from its PDZ domain containing protein that mediates CFTR degradation (128). Moreover, disturbing the PDZ interactions has been used to protect against long term potentiation and depression (129), Huntington's disease (130, 131), cystic fibrosis (132), and cancer (133). Therefore, targeting PDZ dependent interactions are potential future therapeutics for many diseases and disorders (90).

Model for altering CAR trafficking and degradation in polarized cells

CAR^{Ex8} can interact with two MAGI-1 PDZ domains, PDZ1 and PDZ3, which regulate CAR^{Ex8} levels in opposing ways. Results showed that the MAGI-1 PDZ3 domain is responsible for CAR^{Ex8} degradation. However, when CAR^{Ex8} interacts with the MAGI-1 PDZ1 domain, CAR^{Ex8} was rescued from MAGI-1 induced CAR^{Ex8} degradation (Figure 8). The mechanisms behind how these domains have opposing activities are currently unknown. Understanding these mechanisms will have significant clinical implications for prevention of wild-type viral infection or improving AdV-mediated gene therapy and is the focus of this thesis.

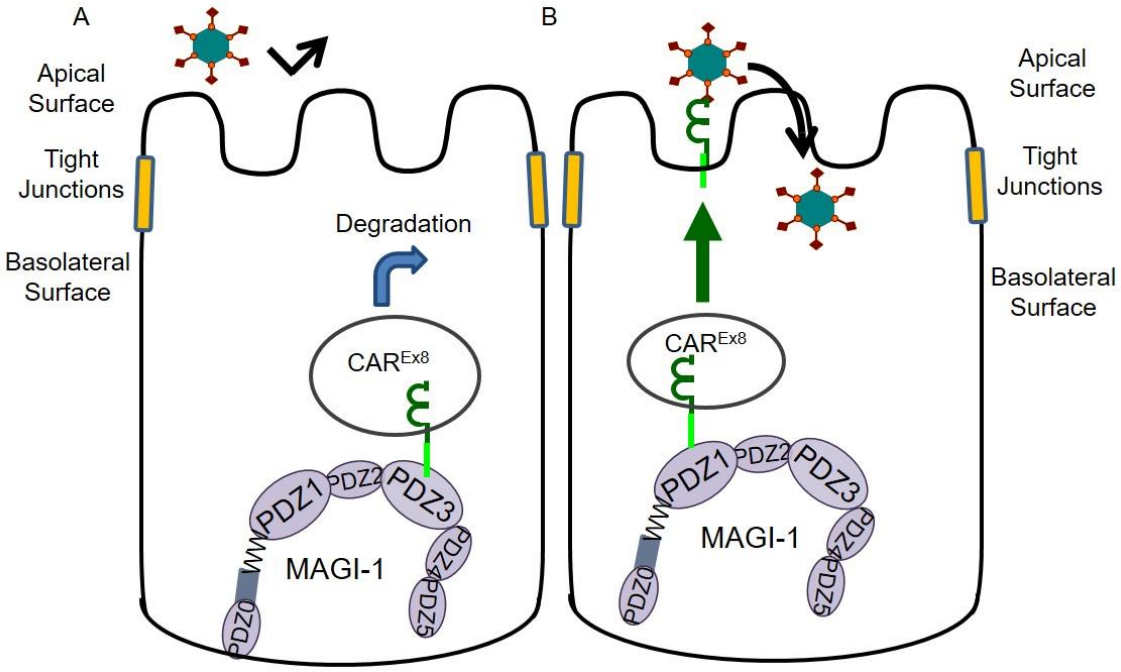

Figure 8. Model of MAGI-1 mediated CAR^{Ex8} regulation.

(A) MAGI-1 PDZ3 domain mediates CAR^{Ex8} degradation which suppresses AdV entry. (B) MAGI-1 PDZ1 domain rescues CAR^{Ex8} and promotes AdV entry into the epithelial cells.

The interaction of CAR^{Ex8} with MAGI-1 requires the CAR^{Ex8} PDZ binding domain (45). Previous data showed that deletion of the CAR^{Ex8} C-terminal ITVV PDZ binding domain sequence allows CAR^{Ex8} protein expression at cell junctions**,** where no co-localization with MAGI-1 is observed (45). However, the PDZ binding domain is not sufficient and the degradation phenotype requires the upstream CAR^{Ex8}-specific sequence. Interestingly, switching the CAR^{Ex7} GSIV sequence with the CAR^{Ex8} ITVV sequence does not switch the degradation phenotype between the two isoforms (45). These data show that the ITVV sequence interacts with MAGI-1 but that the last 9 amino acids of the CAR^{Ex8} C-terminal domain sequence play an important role in degradation. We hypothesize that this reflects a CAR^{Ex8} specific interaction with MAGI-1 directly and that such interactions can be controlled by using specific cell permeable peptides to interrupt the MAGI-1 PDZ domain interactions with CAR^{Ex8} (Figure 9). Notably, other proteins may also modulate this direct interaction between CAR^{Ex8} and MAGI-1.

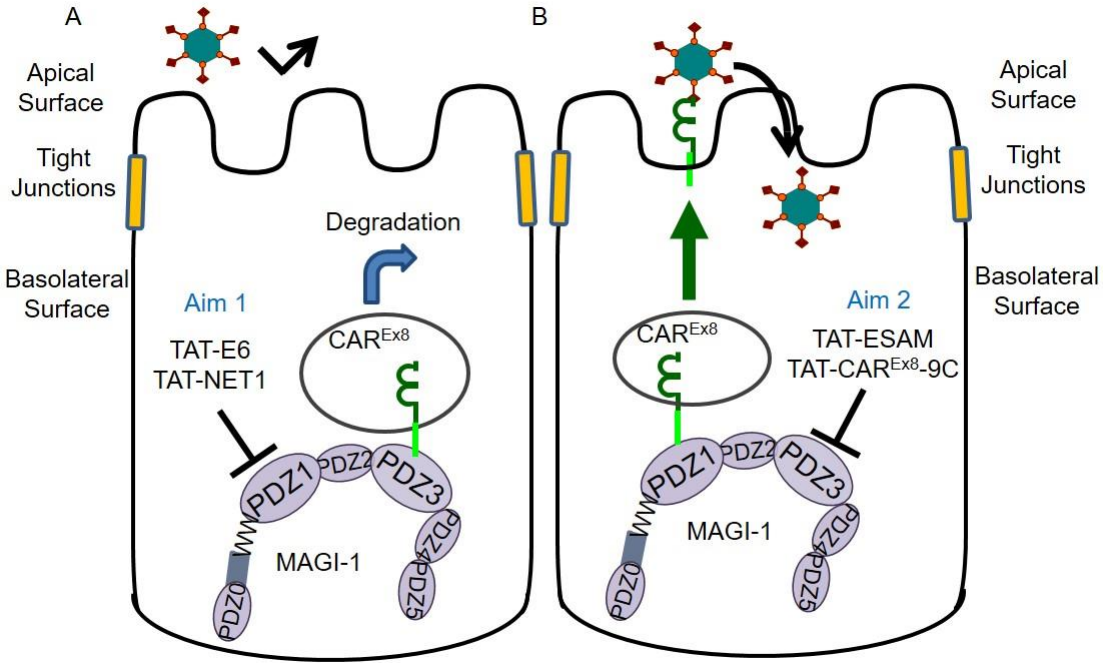

Figure 9. Model of TAT-peptide-mediated MAGI-1 PDZ domain blockers.

(A) It is hypothesized that TAT-PDZ1 binding peptides (TAT-E6 and TAT-NET1) bind to and block the PDZ1 domain increasing CAR^{Ex8} - PDZ3 domain interactions that promote CAR^{Ex8} degradation and suppress AdV entry. (B) It is hypothesized that TAT-PDZ3 binding peptides (TAT-ESAM and TAT-CAR^{Ex8}-9C) bind to and block the PDZ3 domain increasing CAR^{Ex8} – PDZ1 domain interactions that rescue CAR^{Ex8} from degradation and increase AdV entry into the epithelial cells. Note that it is expected that TAT-CAR^{Ex8}-9C will bind to both PDZ1 and PDZ3 but will function like a PDZ3 blocker due to its high affinity binding to PDZ3 domain.

Hypothesis

My **central hypothesis** is that *decoy peptides that interrupt one or both of the interactions between MAGI-1 and CAR^{Ex8} can destabilize apical CAR^{Ex8} protein to abrogate adenoviral entry or upregulate apical CAR^{Ex8} protein to enhance AdV gene therapy*.

Specific aims

Specific aim 1: To determine the cellular mechanism of "attenuator" cell permeable peptides that bind to the endogenous MAGI-1-PDZ1 domain and their effect on AdV infection.

Specific aim 2: To determine the cellular mechanism of "potentiator" cell permeable peptides that bind to the endogenous MAGI-1-PDZ3 domain and their effect on AdV infection.

Specific aim 3: To determine whether cell permeable peptides that bind to the endogenous MAGI-1-PDZ1 or MAGI-1-PDZ3 domain would change AdV infection *in vivo*.

Model illustrative diagram of the hypothesis and specific aims is shown in Figure 10.

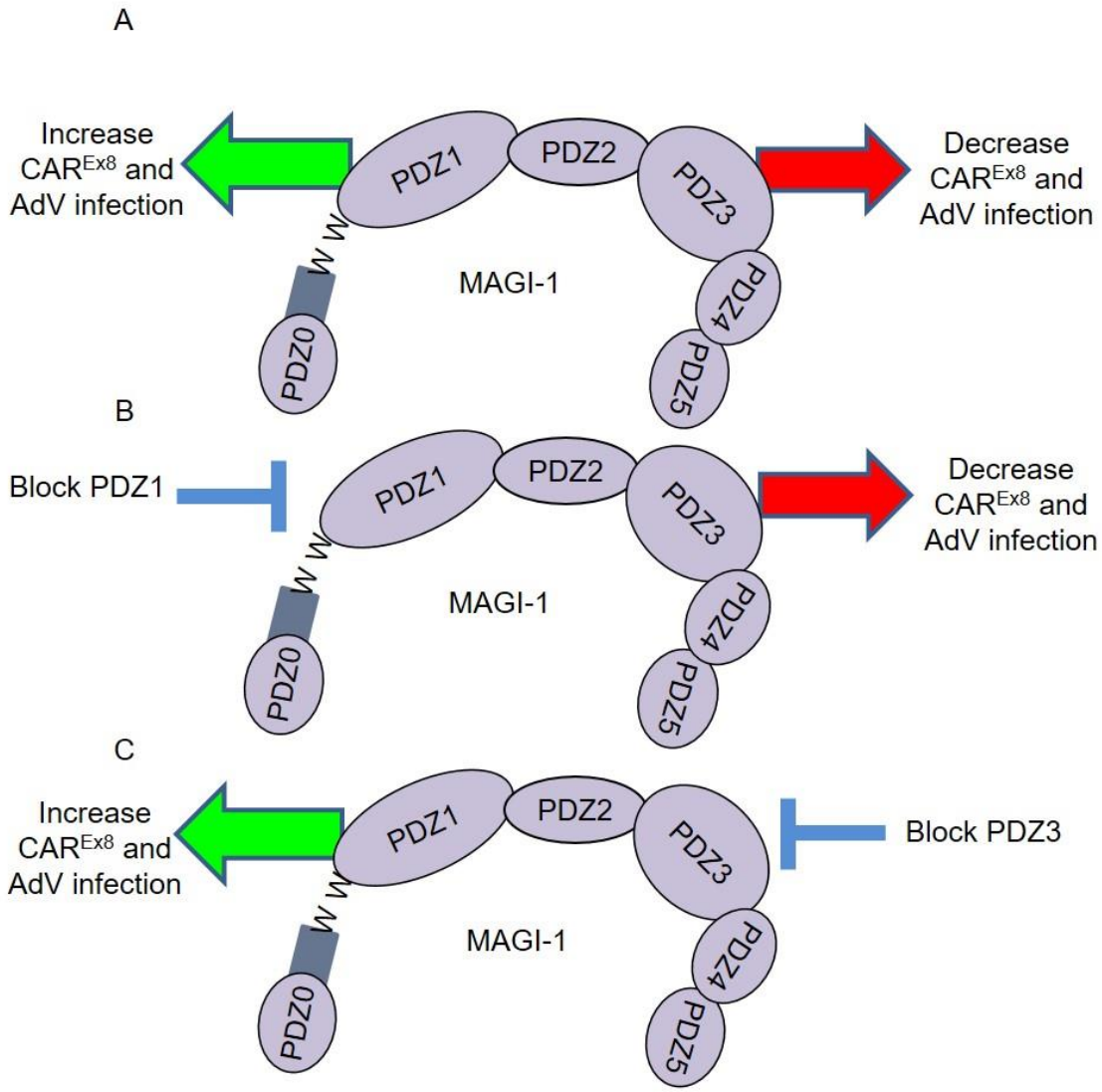

Figure 10. Model illustration of the hypotheses and specific aims.

(A) MAGI-1 regulates the protein level of CAR^{Ex8} by two of its PDZ domains. (B) TAT-PDZ1 peptides bind to and block the PDZ1 domain forcing CAR^{Ex8} - PDZ3 domain interactions that promote CAR^{Ex8} degradation and suppress AdV entry (Aim 1). (C) TAT-PDZ3 peptides bind to and block the PDZ3 domain forcing CAR^{Ex8} – PDZ1 domain interactions that rescue CAR^{Ex8} from degradation and increase AdV entry into the epithelial cells (Aim 2).

Table 2. MAGI-1 PDZ domain interacting partners

Protein (Gene)	Amino acid sequence	MAGI-1 PDZ domain	Ref.
α-actinin 4 (ACTN4)	STALYGESDL	5	**(134)**
BAI-1	QDIIDLQTEV	3, 4	**(135)**
β-Catenin (CTNNB1)	NQLAWFDTDL	5	**(136)**
Cadherin 23 (Cdh23)	METPLEITEL	4	**(137)**
CAR^{Ex8}	PYKTDGITVV	1, 3	**(63)**
Carom (FCHSD2)	KIEDVEITLV	4, 5	**(138)**
ESAM	PAQSQAGSLV	3	**(139)**
JAM4	PQKVRNVTLV	1, 4	**(140)**
Kir4.1	SALSVRISNV	5	**(141)**
Megalin (LRP2)	ANLVKEDSDV	5	**(142)**
Nephrin	LPFELRGHLV	2, 3	**(143)**
NET1	QSGGKKKETLV	1	**(144)**
PTEN	DQHTQITKV	2	**(125)**
TRIP6	ELSATVTTDC	5	**(145)**
Beta1AR (ADRB1)	PGFASESKV	1	**(146)**
RapGEP	EDEDEQVSAV	0, 1	**(147)**
Slo1 (KCNMA1)	KQKYVQEERL PPIREVEDEC	3	**(148)**
HPV E6	SRTRRETQL	1	**(112)**
Ad9 E4Orf1	FPSVKIATLV	1, 3	**(108)**
Influenza A virus NS1	KMARTARSKV	1, 5	**(149)**
CAR^{Ex7}	PAQSKDGSIV	3	**(150)**

CHAPTER 2: Materials and Methods

Materials

Cell Lines

Epithelial and non-epithelial cell lines were used for various experiments (Table 3). 3T3 J2 cell line was obtained from Howard Green, MD (Harvard University). Primary HAE (Donor 2) and the HEK 293 cell line were obtained from the University of Iowa Cell Culture

Core. The remaining cell lines were purchased from ATCC, Virginia. All cell lines were stored in liquid nitrogen in the Department of Biological Sciences at Wright State University, Dayton OH.

Culture Media

Cells were cultured in appropriate sterile culture medium (GibcoTM Invitrogen Corporation, Grand Island, NY) supplemented with 10% fetal bovine serum (except MDCK, supplemented with 5% FBS) immediately after removing the cells from liquid nitrogen. After stimulation of growth, the culture medium was further substituted with a final medium-serum mix containing penicillin and streptomycin antibiotics. The powdered culture medium, containing L-glutamine and 25 mM HEPES buffer, was dissolved in distilled deionized water (ddH2O) from a Nanopure Millipore Water System.

All culture media were supplemented with 2.024 g/L sodium bicarbonate. The solution was adjusted to pH 7.0 to 7.1 with 1 N HCl dropwise. The culture media

solutions were sterilized through a 0.2 μm-pore cellulose nitrate Nalgene vacuum filtration apparatus.

Sterile media were supplemented with 0.5% penicillin/streptomycin and the appropriate heat inactivated fetal bovine serum by appropriate volume percentage. The final culture media was stored in 500 ml Pyrex bottles and kept at 4ºC.

Competent Cells

BL21 derivative competent cells (Rosetta) were used for transformation and protein purification experiments according to their unique properties (see protein purification section). Competent *E. coli* DH5 alpha were used to store the transformed plasmid expression protein in glycerol stock (-80ºC).

TAT-PDZ Peptides

TAT-PDZ peptides used in this study and their binding affinities are listed in Table 4.

Antibodies

The antibodies used in this study are listed in Table 5.

Primers

The list of primers used in this study is shown in Table 6.

SiRNA

The list of siRNA used in this study and their target sequences is shown in Table 7.

Inhibitors

The list of inhibitors used in this study is shown in Table 8.

Table 3. List of cell lines used in the study

Cell Name	Cell Type	ATCC No	Media	Seeding (0.5 ml)
Cotton rats	Rat Lung Epithelia	PTA-3930	F-media	2×10^5
CHO-K1	Chinese Hamster Ovary	CCL-61	DMEM (low glucose)	1×10^5
COS-7	Transformed Monkey Kidney	CRL-1651	DMEM (low glucose)	1×10^5
HEK 293	Human Embryonic Kidney		DMEM	1×10^5
3T3-J2	Embryonic Mouse Fibroblast		DMEM	1×10^5
MDCK	Madin Darby Canine Kidney	CCL-34	EMEM	4×10^5
HeLa	Cervix Epithelia	30-2003	EMEM	2×10^5
HAE	Donor 2		F-media/ differentiation media	2×10^5

Table 4. TAT-PDZ peptides used in this study and their binding affinities

Peptide name	**sequence**	**Kd (nM), PDZ1**	**Kd (nM), PDZ2**	**Kd (nM), PDZ3**
TAT-CAR^{Ex8}-9c	YKTDGITVV	23± 10	N.I	4 ± 2
TAT- CAR^{Ex8}- AA-9c	YKTDGIAVA	113± 28	N.I	71± 19
TAT-NET1	SRTRRETQL	28 ± 11	N.I	N.I
TAT-E6	GGKKKETLV	15 ± 4	N.I	N.I
TAT-Scramble	QGDITVKVT	N.I	N.I	N.I
TAT-ESAM	AQSQAGSLV	N.I	N.I	17 ± 5
TAT-ADAM17-9c	RVDSKETEC	N.I	35 ± 8	N.I

N.I, No detectable interactions

Table 5. Antibodies used in the study

Table 2. Antibodies used in the study			
Antibody	**Vendor**	**Cat #**	**Dilution for WB/IF**
Mouse primary antibody			
Actin	Ambion	AM4302	1:2000-1:3000
DAPI	Vectashield	H-1200	1:20000
Flag	Fisher Scientific	MA1-91878	1:1000
GST	GenScript	A00865	1:1000
MAGI-1	Novus Biologicals	9223-M03	1:500
Myc	Cell Signaling	2276S	1:1000
ZO-1 (dog)	Invitrogen	33-9100	1:200
ZO-1 (human)	BD Bioscience	610967	1:200
Rat Primary Antibody			
Rab 4,5,7,9,11	Cell Signaling	9385S	1:500-1:1000
Flag	Cell Signaling	14793S	1:1000
CAR (1605)	University of Iowa		1:1000-1:2000
CAR^{Ex8} (5678)	University of Iowa		1:200
GFP	Invitrogen	A11122	1:1000-1:2000
MAGI-1	Novus		1:200
Myc	Cell Signaling	2278S	1:1000
PPRP-YY1	University of Iowa	AB3792	1:200
ZO-1	Invitrogen	61-7300	1:200
ADAM17	Thermo Scientific	PA5-19872	0.5µg/ml
ADAM17	Thermo Scientific	RB1660P0	5µg/ml
Donkey IgG HRP Labeled Secondary Antibody			
Mouse	Jackson Immuno Research	715035150	1:10000
Rabbit	Jackson Immuno Research	715035150	1:10000
Goat IgG Alexa Fluor Labeled Secondary Antibody			
Mouse A488	Invitrogen	a10667	1:1000
Mouse A568	Invitrogen	a11004	1:1000
Rabbit A488	Invitrogen	a11008	1:1000
Rabbit A568	Invitrogen	a11036	1:1000

Table 6. List of primers and their sequence

Primer Set	**Forward Primer 5' → 3'**	**Reverse Primer 3' → 5'**
AdV Hexon specific primer	ACGCCTCGGAGTACCTGAG	GTGGGGTTTCTGAACTTGT
CAR^{Ex8}	TCGGCAGTAATCATTCATCCCTGG	ACTGTAATTCCATCAGTCTTGTAAGGG
GAPDH	CACCCTGTTGCTGTAGCCAAA	CAACAGCGACACCCACTCCT
Actin	AAGATCTGGCACCACACCTTCTAC	ATCTGGGTCATCTTCTCACGGTTG
CAR^{Ex8} (stable MDCK-CAR^{Ex8})	GTCCCTCCTTCAAATAAAGCTG	ACTGTAATTCCATCAGTCTTGTAAGGG
ADAM17	GGGGCCCCTGGGATCCATGAGGCAGTCTCTCC	GTCGACCCGGGAATTCGGCTAGCACTCTGTCTC

Table 7. List of siRNA used in the study

siRNA	Vendor	Cat #	Target Sequence
ADAM17	Dharmacon	A-003453-13	GGAUGUAAUUGAACGAUUU
ADAM17	Dharmacon	A-003453-14	CCAAGAUUUUGAUAUGGGA
ADAM17	Dharmacon	A-003453-15	GCAUCAAUACUUUUGGAAA
ADAM17	Dharmacon	A-003453-16	GGUCUAUUUCUAGUUAUUA
ON-TARGET plus	Dharmacon	D-001810-01-05	UGGUUUACAUGUCGACUAA
MAGI-1 (A)	Invitrogen	1299001	Exon 21,22,23 SMARTpool

Table 8. Inhibitors used in this study

Inhibitor	Vendor	Cat #
MG-132	Fisher Scientific	AP81-5-15A
TAPI-1	Calbiochem	579051
TIMP3	R & D systems	973-TM
Compound E	Calbiochem	565790
Cyclohexamide	Sigma-Aldrich	01810

Methods

Cell culture maintenance

Cell culture techniques were performed under a laminar flow hood using aseptic techniques. Cell cultures were stored and grown in 25 or 75 cm^2 tissue culture flasks within a humidified incubator at 37ºC and 5% CO_2 concentration. The media-serum mix was changed in the flasks based upon a pH change from 7.1 to about 6.0, as indicated by a color change of the media from pink to yellow. As cells began to divide and reach approximately 80% confluency, the cell cultures were divided into new flasks using a cells to media ratio of between 1:5 and 1:20 after removing attached cells with 0.25% Trypsin-EDTA (Mediatech, Inc., Manassas, VA). All flasks were supplied with new media-serum mix to a final volume of 5 ml in a 25 cm^2 tissue culture flask and 10 ml in a 75 cm^2 tissue culture flask. Cell viability was verified before each experimental set using the trypan blue exclusion test (151). Dead cells appeared blue, as their cell membranes are permeable to the dye upon death. Cell viability above 80% was considered suitable for experiments.

Determination of cell concentration (hemocytometer)

The technique reported was used during cell seeding before transfection and adenovirus infection. Adherent monolayers of cells were trypsinized from 1-2 flasks and combined in a 50 ml centrifuge tube. The tube was centrifuged at 150 rcf for 5 min at 4ºC. The supernatant was aspirated and the cells resuspended in 1 ml culture medium and mixed gently by pipetting up and down. A clean coverslip was centered on a

hemocytometer between the outside railings over the two counting grids. A drop (10 µl) of well-mixed cell suspension was placed at each notch. The drop was added once to ensure even distribution of cells. Cells were counted with a push button counter using 400 X total magnification. Cells were counted in the four corner squares (1 mm X 1 mm) of the cytometer. These squares were 1/400 mm^2. The average value of the total cells counted in the 4 squares was multiplied by 10^4 to determine the number of cells per milliliter. The volume of the mixture was adjusted by dilution with culture media to an appropriate concentration, depending on the particular assay.

Peptide preparation and treatment

TAT-Peptides were synthesized by the Genescript peptide synthesis core (Genescript, MO) as a white powder. A list of all synthesized peptides and their binding affinities is shown in Table 4. A stock solution of approximately 1 mM of each peptide was prepared and dissolved in PBS. For peptide treatment, cells were washed with PBS 3 times and treated with small volume (50µl of 1 - 100 µM dose) of peptide directly into cells. Serum free Opti-MEM was added and incubated for 1 hr or as described in the text. Media was changed to Opti-MEM containing fetal bovine serum for 4-5 hrs. After that cells were washed again and either fresh media added or lysed with lysis buffer containing protease inhibitor depending on the experiment. Unless otherwise indicated, in conditions where CAR^{Ex8} was induced using inducible MDCK epithelial cells, 100 µM of TAT-peptides were used in treatment for a period of 4-5 hrs.

Matrix Assisted Laser Desorption Ionization-Mass Spectrometry (MALDI-MS)

Polarized MDCK cells (≈ $1*10^{6)}$ were incubated for 60 min at 37°C with 1 or 50 µmol/l TAT-CAR^{Ex8}-9c peptide in starvation media containing (Opti-MEM with earle's salt). After 1hr incubation, cells were washed with PBS, and lysed with lysis buffer containing 2 mmol/l PMSF and 0.1% Trifluoroacetic acid (TFA). Lysate was washed with 50 mM sodium acetate buffer containing 150 mM Nacl. Cells were centrifuged at 135,000 rpm. Equal amounts of protein lysate were transferred into new tubes. Peptides were purified using C_{18} Ziptips (Millipore, Billerica, MA) according to a previously published procedure (152). Briefly, the Ziptip was activated with 100% acetonitrile, followed by washing 3x with 0.1% TFA. After that, the sample was loaded into column by repeated pipetting 20-30 times. Column was washed again 3 times with 0.1% TFA. Finally, peptide was eluted with 95% acetonitrile containing 0.3% TFA. Elution was spotted on a Brucker protein plate chip containing (alpha cyano-4- hydroxycinnamic acid in 70% acetonitrile, 10% acetone, 0.3% TFA).

Mass spectra were obtained using a Bruker Autoflex III smart beam MALDI TOF/TOF instrument. A total of 7,000 laser shots were acquired randomly for each spot at a laser frequency of 100 Hz. The mass spectrum was accumulated and normalized to the peak m/z in each spectrum.

Fluorescently-labelled peptide internalization

TAT-CAR^{Ex8}-9c peptide was synthesized (genescript, NJ) and tagged with TAMRA (red fluorescence). Cells were treated with the fluorescent peptide at different time points after which they were washed with PBS, fixed with 1% PFA in methanol and cover slipped with DAPI solution. Images were taken by confocal microscope at 60X oil immersion magnification.

Testing for expression of proteins in *E. coli*

Confirmed clones of MAGI-1 PDZ domains (pHH2 plasmids) were transformed into *E.coli* using the Rosetta strain of competent cells (EMD chemicals, Gibbstown, NJ). Rosetta competent cells are BL21 derivatives that supply tRNAs for AGG, AGA, AUA, CUA, CCC, GGA codons on a chloramphenicol-resistant plasmid and are therefore capable of expressing eukaryotic proteins that contain codons rarely used by *E. coli*. Transformation was done by adding 100 ng pHH2 plasmids into 10 µL competent cells in a 2.0 ml centrifuge tube and kept on ice for 30 min. The tube was heat shocked for 45 sec at 42°C and kept back on ice for 2 min. 250 µL SOC medium was added to the cells and the tube incubated for 1 hr at 37°C with shaking at 200 rpm. Each vial of transformed cells was then spread on ampicillin (100 µg/ml) and chloramphenicol (10 µg/ml) containing LB agar plates (20% and 80%) and incubated overnight at 37°C. The next day, 3 - 9 colonies of each plasmid were grown overnight as 1 colony per 5 ml of LB broth containing ampicillin (100 µg/ml) and chloramphenicol (10 µg/ml). Next day, 500 µL of each overnight culture was subcultured into three 5 ml of LB (Amp+, Chl+) broth (a total of 15 ml culture/colony) and grown until an OD_{600} od 0.6-0.8 was contained, after which 1 ml of culture was transferred from each sample into another tube and stored at -20°C as the zero hour non-induced sample. 10 µL of 100 mM IPTG was added to each remaining 2 ml culture to induce protein expression and continued incubation at 37°C. 1 ml samples were taken at 1, 2, 4, 6, 8, 12, 24 hrs. All samples were centrifuged at 9,500 rpm, 4°C for 10 min. Each pellet was resuspended in 100 µL PBS and sonicated with pulses to completely lyse the cells. The lysate was again centrifuged after which the supernatant was transferred into fresh tubes on ice. Protein samples were mixed with 2X

SDS denaturing buffer and incubated at 75°C for 5-10 min with shaking at 300 rpm. Then, 35 µl of protein from each sample was subjected to SDS-PAGE and the gels were stained with Coomassie blue to look for a protein band of appropriate size. The sample with the highest amount of protein after induction was chosen and this clone was used to make and purify the protein of interest. Desired clones were grown in LB broth and stored at -80°C in cryogenic tubes containing 50% glycerol (1:1 50% glycerol: cell culture ratio) to make the glycerol stock.

Coomassie blue staining

Gel containing 10% acrylamide was fixed with solution contain 50% ethanol and 7% acetic acid. Then, the gel was immersed in 0.075% stain solution in 10% acetic acid and 50% ethanol for 10 min and then washed 3X with ddH_2O. To destain, the gel was placed in 100 ml of 5% ethanol and 7.5% acetic acid with gentle agitation and changed to fresh destain solution every half hour until the gel was clean enough to see protein bands clearly. The gel was transferred into 0.5% acetic acid and subsequently soaked in 4% glycerol for 2 hr. The gel was dried at 70°C for 50 min in a gel dryer vacuum system (BioRad, model 583) and scanned for image.

Purification of proteins from Rosetta bacteria

On the evening of the first day of purification, Rosetta *E. coli* containing the appropriate pHH2 plasmid were taken from a glycerol stock and streaked on a LB (amp+/chlo+) agar plate and grown at 37°C overnight. The plate was removed the next morning and kept at room temperature until evening. A 40 ml LB (amp+/chlo+) broth was inoculated with a single colony from the plate and incubated at 37°C and 200 rpm

overnight in a shaker. The overnight culture was subcultured into 1 L of pre-warmed LB broth and incubated at 37°C for about 4 hours (until OD600 1.5-1.9). 1 ml of uninduced sample was taken for gel analysis before adding 1 ml of 100 mM isopropyl β-D-1-thiogalactopyranoside (IPTG) and continued shaking for about 4 hours. 1 ml of induced sample was also taken for gel analysis. The 1 L culture was then centrifuged in 500 ml bottles at 8,500 rpm, 4°C for 10 min in a Sorvall centrifuge. The pellet was stored at -80°C with 400 µL of 100 mM PMSF.

Pellets from the 1 L culture were resuspended in 10 ml 2X L&C buffer (Tris-based elution buffer; 400 µL 1 M Tris, pH 8.0, 0.35 g NaCl, 2 ml glycerol in 10 ml solution), 10 ml 2X protease inhibitors cocktail (Sigma-Aldrich, St Louis, MO Cat # S8830), 40 µL 0.5 M EDTA and 20 µL 1 M DTT. The resuspended cells were sonicated on ice for 6 min with 30 sec pulses and centrifuged at 9,500 rpm at 4°C for 20 min. The supernatant was filtered through 1.2 micron filters then through 0.2 micron (Whatman, GE Healthcare REF 10 462 261) to remove any debris. The clarified lysate was pumped through a Fractogel GST-bind cartridge (EMD) using a BioRad pump at 4°C according to the manufacturer's instructions. The Fractogel cartridge bound the GST-tagged proteins while other synthesized proteins pass through the column. Briefly, after pumping the lysate through the cartridge, the column was washed with 2 ml 1X L&C buffer, followed by 5 ml ATP wash buffer (2X L&C buffer, 10 mM ATP, 50 mM MgCl2, 1.3 ml ddH2O) and finally, 12 ml 1X L&C buffer containing 1 mM DTT and 1 mM EDTA. To excise protein without any tag, a GST-tagged PreScission protease mix (1 ml L&C buffer containing DTT and EDTA and 50-100 µL of protease) was pumped in the column and allowed to circulate through the system for 4-6 hours. Typically, the protease was

originally at 1.5-6 mg/ml and desalted. The material in the recirculated tube was collected as elution 1 (E1). L&C buffer containing DTT and EDTA was pumped through the column to collect at least 3 more fractions of about 1 ml each and labeled E2, E3 and E4 respectively. The fractions contained tag-free proteins which were quantified and the quality verified using SDS-PAGE. 4 ml of reduced glutathione buffer (0.01 g/ml of 1X L&C buffer) without DTT or EDTA was pumped into the column to remove the GST tags and protease and the column was subsequently washed with 10 ml L&C buffer without DTT or EDTA to regenerate the column for future use. The column was stored at 4°C for other purifications while the purified protein was stored at -80°C. In any situation where GST-tagged protein was purified, the bound protein was eluted directly with reduced glutathione after washing thereby skipping the use of protease. In other situations, where a GST tagged protein band is noticed with the pure protein, the GST protein was removed by incubating with GST slurry beads (Goldbio, MO) for 4 hrs at 4°C. The protein-slurry mixture was separated by centrifugation at 4°C, then the pure protein is taken to be dialyzed. Results showed a high yield of pure protein of both PDZ1 and PDZ3 domain (Figure 11). ADAM17 cytoplasmic domain was cloned and purified using the same approach. First, ADAM17 coding sequence was confirmed by double digestion and sequencing (Figure 12). Then, ADAM17 cytoplasmic domain was cloned in pHH2 plasmid, transfected into Rosetta cells, and the protein was purified as explained above. A high concentrated purified ADAM17 cytoplasmic domain (MW = 17 KD) was eluted (Figure 13). Note that the protein band intensity decreases as more protein was eluted from the column (Figure 13).

Protein dialysis

Proteins were purified with a Tris-based buffer that did not allow proper labeling of the proteins with fluorophores for subsequent experiments. Tris-based buffer was replaced by dialysis against 3 changes of 2 L dialysis buffer (PBS) at 4°C for minimum of 16 hours (2 hrs; 2 hrs; overnight) using a Slide-a-lyzer dialysis cassette (Thermo scientific). Each cassette was removed aseptically from its pouch and immersed in dialysis buffer for 2 min to hydrate the membrane. 2 ml protein sample was added and the cassette was floated vertically in the dialysis buffer and stirred gently. A syringe was used to transfer protein samples into and to remove samples from the cassette after dialysis as directed by the manufacturer.

Protein labeling

Purified MAGI-1 PDZ domain proteins without GST tag were labeled with FluoroLink^{TM} Ab Cy3 labeling kit (GE Healthcare Cat # PA33000) according to the manufacturer's recommendations. Protein solution (1 mg/ml) was added to the vial of coupling buffer, mixed gently, then transferred to the vial of reactive dye and incubated at room temperature with mixing every 10 minutes. While the labeling reaction was incubating, 13 ml of fresh elution buffer was added to the column for priming. The antibody-labeling mixture was carefully added to the top of the column and allowed to enter the resin. 2 ml of elution buffer was added to the column to separate the mixture into a faster moving pink (Cy3) band of labeled protein from the unconjugated dye. An additional 2.5 ml of elution buffer was then added to the column that will help to elute the pink band. The labeled protein was collected in a clean tube.

Quantification and calculation of D/P ratio

Cy3 bisfunctional dye characteristics Cy3

Formula Weight 949.11

Absorbance max 550nm

Extinction max 150000M-1cm-1

Emission max 570nm

Quantum Yield >0.15*

* = for labeled proteins, D/P = 2

An aliquot of the labeled protein was diluted such that the maximum absorbance was 0.5 to 1.5 AU. The absorbance of each labeled protein was measured at 280 nm, 552 nm (Cy3) after which protein concentration was determined with Bio-Rad reagent.

Estimation of Cy3 final Dye/Protein (D/P) Ratios

[Cy3 dye] = (A @ 552nm) / 150000 ([ ])= concentration)

[Protein] = [A @ 280nm – (0.08 * A @ 552nm)]/ molecular weight of protein

D/P final = [dye]/[protein]

Graphing and data analysis

All graphs and data analysis were made using Prism software version 6 (GraphPad, CA). Each experiment was done in triplicate and data were plotted as Mean± SEM. The binding affinity (Kd) was determined using the function of non-linear regression- one site specific binding.

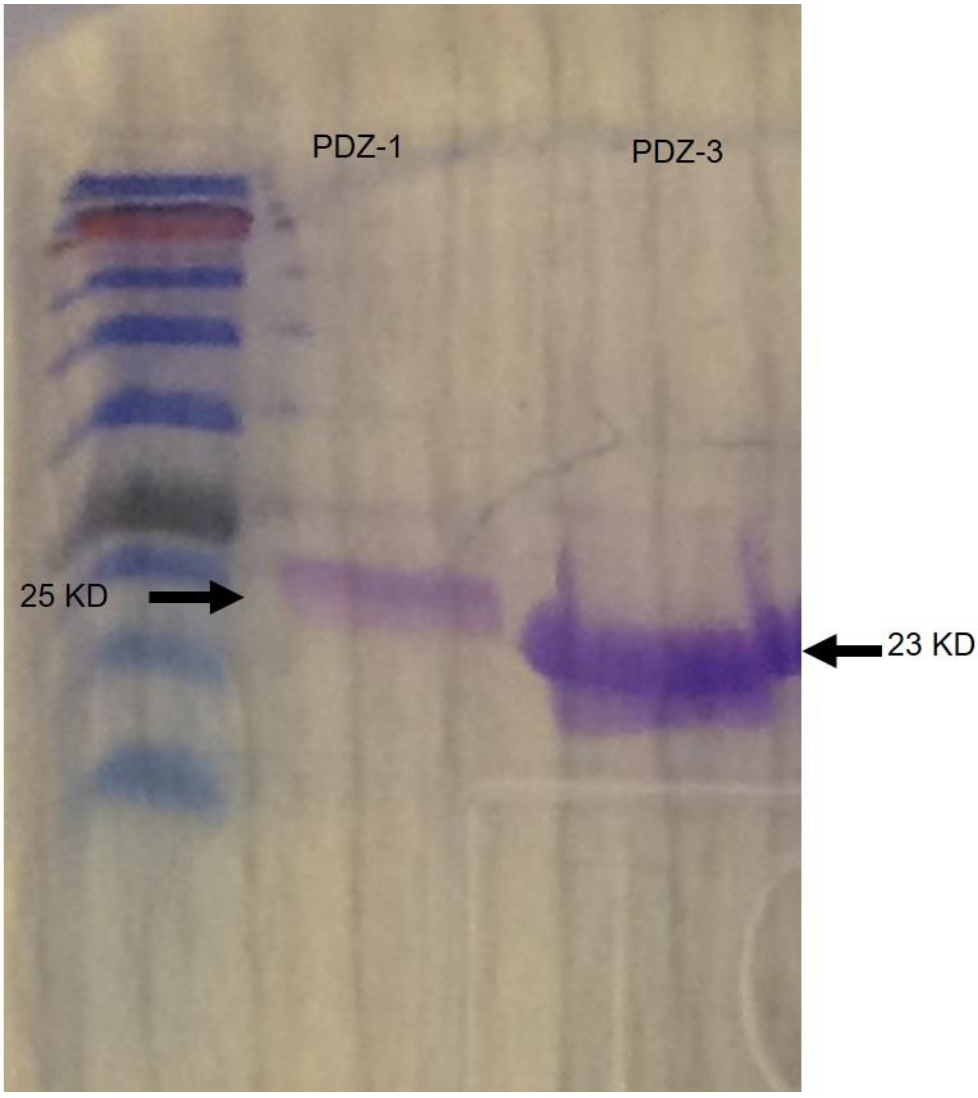

Figure 11. MAGI-1 PDZ domains protein purification.

PDZ1 and PDZ3 were purified using GST-tagged column purification. A band at 25 KD and 23 KD were obtained which correspond to PDZ1 and PDZ3 domain, respectively. Note that further purification was done to remove any GST tagged PDZ domain.

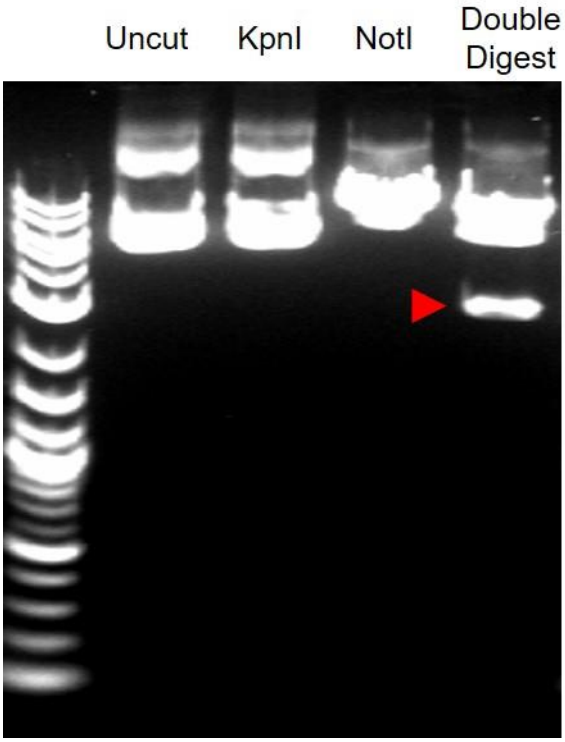

Figure 12. Confirmation of ADAM17 coding sequence using restriction enzyme double digestion of the vector.

A band of 3 kbp, corresponding to the expected length of the gene for ADAM17 (arrow), was detected upon double digestion with NotI and KpnI.

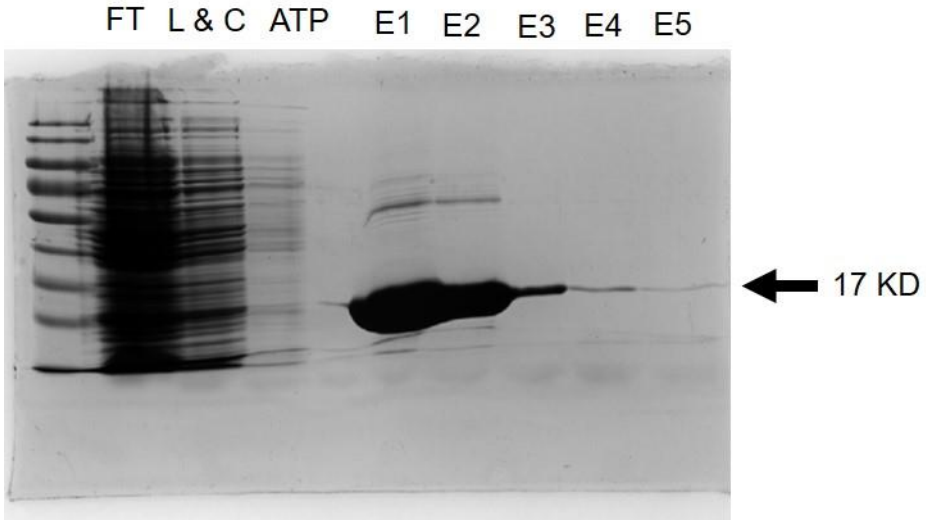

Figure 13. Purification of ADAM17 cytoplasmic domain by GST column purification.

The cytoplasmic domain of ADAM17 has MW of 17 KD. Elution 1 and 2 (E1, E2) had highly concentrated purified protein. Note that the band intensity decreased as more protein is eluted from the GST column. The upper band was mostly likely uncleaved GST-ADAM17 or precision protease. E1 and E2 were subsequently incubated with GST-beads to remove remnant GST proteins (data not shown). FT, flow through; L&C, wash step; ATP, wash step; E1-5, elusions.

Immunoprecipitation and Western blot

Cell cultures were placed on ice for 5 min, washed with ice-cold PBS, and lysed in buffer (50 mM Tris pH 7.4, 150 mM NaCl, 1% Triton X-100, protease inhibitors (20 µg/ml, leupeptin, aprotinin, 10 µg/ml pepstatin, and 17.4 µg/ml phenylmethylsulfonyl fluoride)) by rocking at 4°C for 10 min. Cells were scraped into a tube, sonicated five times with 5 pulses using Sonic Dismembrator (Fisher Scientific, model 100) and centrifuged at 14,000g for 10 min at 4°C. The supernatant was transferred to fresh tubes and subjected to protein estimation by Bio-Rad protein assay according to manufacturer's instructions. Aliquots of each lysate were saved for Western blot analysis of total protein in immunoprecipitation (IP) or co-immunoprecipitation (co-IP) experiments. For IP or co-IP, an appropriate amount of primary antibody was added to pre-cleared equal protein concentration of sample lysate in Eppendorf tubes and rotated at 4°C for 4 hours. Protein G Sepharose beads slurry (GE Healthcare) was prepared by washing 3 times with 2X volume of lysis buffer and once with lysis buffer minus Triton X-100, followed by resuspension in fresh lysis buffer (50% beads + 50% buffer). 50 µL washed beads was added to each sample tube with additional rotation at 4°C for overnight. Samples were washed 3 times with lysis buffer and once with lysis buffer minus Triton X-100 by centrifugation at 17000 rcf, 4°C for 1 min to pellet beads. Each IP sample was resuspended in 70-100 µL 2X denaturing buffer with dye (for WB) and incubated in a heat block at 65°C with shaking at 300 rpm for 10 min. Samples were then immediately vortexed vigorously before spinning at 17000 rcf, 30-60 sec. Only supernatant was subjected to SDS polyacrylamide gel electrophoresis (10% unless otherwise indicated). Proteins were transferred to a polyvinylidene difluoride membrane (Millipore, Bedford,

MA), blocked with 5% BSA in TBS-T, washed, probed with appropriate antibody diluted in 2% BSA in tris-buffered saline tween-20 (TBS-T) with sodium azide, followed by HRP-conjugated secondary antibodies (Jackson Immuno Research, West Grove, PA) diluted in TBS-T (1: 10,000). Protein bands were detected by adding ECL reagents (Pierce, Rockford, IL) and imaged on a ChemiDoc^{TM} MP imaging system (Biorad, CA).

Cell surface biotinylation

Cell surface proteins were biotinylated with 3 ml per 100 mm plate of 1 mg/ml sulfo-NHS-biotin (Cat # 21331 Thermo Scientific, Rockford, IL) for 1 hour at 4°C after first cooling cells on ice for 10 min and washing with ice cold PBS +/+. After washing the cells again with PBS +/+, any unreacted biotin was quenched with 100 mM glycine for 20 min at 4°C. Washed cells were then incubated with lysis buffer for another 20 min at 4°C. Cell lysate was immunoprecipitated with NeutrAvidin ultra link resin (Cat # 53150 Thermo Scientific) and Western blotting with antibody of interest.

Adenovirus infection

Adenovirus serotype 5 containing the β-galactosidase gene (AdV-β-Gal), or AdV-CAR^{Ex7}, or AdV-CAR^{Ex8} (University of Iowa Vector Core, Iowa City, IA) was diluted with Opti-MEM culture media (Gibco, Invitrogen) without serum to the multiplicity of infection (MOI) of 100. Growth media was aspirated from cells that had been seeded for 48 hours and the cells were rinsed with phosphate buffered saline containing Ca^{+2} and Mg^{+2} ions (PBS+/+). 250 uL of diluted adenovirus was added to each well in a 24 well plate (3 ml in 10 cm^2 dish) at a MOI of approximately 100 plaque forming units/cell (PFU/cell), unless otherwise indicated, and incubated for 1 hr at 37°C and 5% CO_2 with

gentle swirling every 15 min. The inoculum was then removed, cells were rinsed with Opti-MEM, and fresh complete media was added. The cells were then incubated at 37°C, 5% CO_2 until further analysis.

Quantitative Polymerase Chain Reaction (QPCR)

The PCR amplification was programmed for 40 cycles at 95ºC for 10 min (denaturation), 58ºC for 1 min (annealing), and 60ºC for 1 min. (extension). qPCR was performed using SYBR Green with low ROX (Quanta, Gaithersburg, MD; 10µl master mix qPCR reaction contained 2µl DNA, 2X reaction buffer with dNTPs, Accusat Taq DNA polymerase, $MgCl_2$ ROX reference dye and SYBR green dye that binds specifically to dsDNA) in Stratagene's Real Time PCR System (Agilent Technologies) using Mx4000p software v5 for data analysis.

Beta-galactosidase assay

The Galacto-Light Plus System (Applied Biosystems, USA) was used to analyze adenovirus-mediated beta-galactosidase activity according to manufacturer directions. Briefly, cells were lysed 24 hours after adenovirus infection. 100 µL of lysis buffer were added to each well in a 24-well plate for 10 min at room temperature. Cells were scraped and 2 µL of lysate was added into a 96-well plate followed by 120 µL of a 1X Tropix-Galacton substrate (Applied Biosystems) and 60 min incubation at room temperature. 150 µL of Tropix accelerator II was then added just before measuring β-galactosidase luminescence in Luminometer. Protein concentration was determined by Bradford protein estimation according to the manufacturer protocol. The optical density was measured at spectrophometer wavelength 595 nm as compared to a set of standard. Each experiment

was performed in 3-6 replicates and lysis buffer was used as control. Data was analyzed using Prism software (GraphPad, CA).

Nuclear Fractionation

Nuclear fractionation was done as previously described (153), with some modification. Inducible MDCK- CAR^{Ex8} ($1*10^7$ cells) were induced with 50 ng/ml of Dox for overnight. The next day, cells were treated with either TAT-NET1, TAT-E6 or TAT-scramble peptides for 4-5 hrs. By the end of the treatment period, cells were transferred into 4 ºC and kept for 10 min, washed with PBS without calcium and magnesium 3 times. Cells were lifted using Nelson lifting solution ($NaHCO_3$ 4.2 mM, glucose 5.6 mM, NaCl 137 mM, KCl 5.4 mM, EDTA 0.5 mM. PH 7.2-7.4). After that, cells were pelleted by centrifugation at 880 rpm for 6 min. The pellet was re-suspended in 50 µl of freshly prepared buffer A (10 mM Hepes, PH 7.9, 10 mM Kcl, 1.5 mM $MgCl_2$, 0.1 mM EDTA, 0.5mM DTT, 0.5% (v/v) NP-40, 1X protease inhibitor cocktail (Pierce Thermo scientific, MA)). Samples were centrifuged at 800 x g for 10 min at 4ºC and the supernatant was collected as the cytoplasmic extracts. Then, the pellets were re-suspended in 50 µl of buffer B (20 mM Hepes, PH 7.9, 400 mM NaCl, 1.5 mM $MgCl_2$, 0.1 mM EDTA, 5% glycerol, 0.5 mM DTT, 1X protease inhibitor cocktail (Pierce Thermo scientific, MA)) in order to extract the nuclear proteins. After incubation for 30 min on ice, samples were centrifuged at 10,000 x g for 30 min at 4 ºC. The supernatant was collected as the nuclear extract. A Bradford assay was done to confirm equal protein loading, and samples used immediately for Western blot.

Preparation and collection of conditioned media

For CAR^{Ex8} or CAR^{Ex7} extracellular domain shedding, 2 x 10^6 – 4 x 10^6 inducible MDCK (60) cells were seeded per well in 6-well plate. The following day, cells were washed with PBS containing calcium and magnesium and induced overnight with 50 µg/ml Dox. The day after, cells were washed with PBS and treated with Tat-peptides (final concentration 100 µM or as indicated in the text) in serum deprived media for 4-5 hrs. The conditioned media were collected in pre-chilled tubes, cleared of cell debris, and rotated at 4ºC for 2 hrs with mouse anti-Flag antibody (Fisher scientific, MA). Protein G Sepharose bead slurry (GE Healthcare) was prepared by washing 3 times with opti-MEM media, and 40 µL of washed beads was added to each sample tube with additional rotation at 4°C for overnight. The next day, beads were precipitated by centrifugation at 4°C then washed 3 times with Opti-MEM. Finally, precipitate was eluted with Laemmli/2-mercaptoethanol buffer and subjected to SDS-polyacrylamide gel electrophoresis (10% unless otherwise indicated). Proteins were transferred to a polyvinylidene difluoride (PVDF) membrane (Millipore, Bedford, MA), blocked with 5% BSA in TBS-T, probed with rabbit anti-Flag (Millipore, MA) to detect the shed CAR ECD. The membrane was also stained with Ponceau S stain to confirm equal loading.

Preventing AdV infection by the shed CAR ECD

Conditioned media from vehicle, TAT-scramble, TAT-NET1, or TAT-E6 treated MDCK epithelia was collected and incubated with AdV-GFP (MOI 100) for 30 min at 37 ºC with slight shaking. Hela cells were infected with the mixture for 1 hr after which media were replaced with complete media. To remove the CAR^{Ex8} ECD, conditioned media were pre-cleared using antibody specific for the ECD of CAR (mouse anti-Flag). 24 hrs post infection, cells were washed with PBS 3 times and images were taken at 20 x

magnification power. Image analysis was done using Metamorph software as previously described.

Ponceau S Stain

Ponceau S stain (Sigma-Aldrich, MO) was prepared in 0.1% (w/v) in 5% (v/v) acetic acid. A PVDF membrane was incubated with Ponceau S stain for 15 min at room temp. To destain, the membrane was placed in 10 ml of 10% (v/v) acetic acid solution for 10 min and scanned for imaging using ChemiDoc^{TM} MP imaging system (Bio-Rad, CA).

RNA extraction

RNA extraction was done using GeneJET RNA purification kit (Thermo scientific, MA), according to the manufacturer protocol. Epithelial cells ($5*10^6$) or lung tissue (30 mg) were lysed using lysis buffer containing β-mercaptoethanol on ice. The lung tissues were homogenized using mortar and pestle in 300 µL until suspension is uniform. Once homogenized, proteinase K (600 µl) was added to the mixture and vortex then incubated for 10 min at room temperature to insure homogenous solution. Mixture was then centrifuged at 4ºC for 10 min at 13,500 x g, and it was transferred to RNA free tube. Repeated administration of the lysate (up to 700 µl) was added into RNA purification column. Each time, the column was centrifuged at 13,500 x g for 1 min and the flow through was discarded. The column was washed twice with wash buffer 1, and wash buffer 2. Finally, the RNA was eluted with ribonuclease free water added to the center of column. Gloves were change between each steps and aseptic technique were taken in consideration to minimize RNA degradation. The RNA was directly used to make cDNA for further experiment.

Reverse PCR and cDNA synthesis

Freshly isolated RNA was subjected to cDNA using qSript^{TM} cDNA SuperMix, according to the manufacturer protocol. 1 µg of total RNA was incubated with 1x dilution of cDNA supermix in a total volume 20 µl using 0.2 ml micro tubes. After sealing each reaction properly, the tubes were vortexed and centrifuged briefly to collect the mixture at the bottom of the reaction tube. The mixture was loaded into 96 wells plate and sealed with plastic cover. All steps were performed on ice to minimize ice. The PCR setting was programmed for 40 cycles 5 min at 25ºC, 30 min at 42ºC, and 5 min at 85 º C, the plate was hold at 4ºC. After cDNA was completed, 1/10 of the first strand reactions were used for PCR amplification.

Immunocytochemistry

Cells were kept on ice for 5 min, washed 3 times with ice cold PBS supplemented with Mg^{2+} and Ca^{2+} (PBS +/+). The cells were then fixed with methanol containing 1% paraformaldehyde for 20 min at -20°C. Cells were rinsed with ice cold PBS, allowed to come to room temperature, and blocked with 2% bovine serum albumin (BSA) in SuperBlock (Pierce, Rockford, IL) for 45 min. Appropriate primary antibodies were added to cells for 2.5 hrs at 37°C or overnight at 4°C. Cells were rinsed 5 times with PBS with the last rinse greater than 10 min. Cells were blocked with 2% BSA in Superblock for 5 min and then incubated with appropriate Alexa-labeled secondary antibodies (Invitrogen) for 2 hrs at 37°C. The cells were rinsed 5 times with PBS and mounted onto glass slides using Vectashield mounting media with DAPI (Vector Laboratories Inc., Burlingame, CA). Staining was evaluated by laser scanning confocal microscopy

(Olympus FV1000) with a 60X oil immersion lens; images are shown as either single X-Y or X-Z sections.

Plasmid transfection

Cells were transfected with plasmids 24 hours after seeding, when cultures reached over 60% confluence with Xfect (COS-7) transfection reagent (Clontech). Transfected cells were used for immunoprecipitation, Western blot. GFP plasmid was transfected into separate wells, under the same conditions with the cloned domains to monitor transfection efficiency. All experiments included both positive and negative controls, as described in the text, and were repeated a minimum of three times unless otherwise indicated. COS7 cells were transfected with the cloned domain plasmids to confirm protein expression by immunocytochemistry and Western blotting. MDCK cells were transfected using GenJet transfection reagent (SignaGen Laboratories) at the time of seeding (reverse transfection) to give 56-60% confluency after 24 hrs.

SiRNA Transfection

SiRNA targeting different parts of MAGI-1 gene (Stealth^{TM}) were purchased from Invitrogen Custom Laboratory Services (Carlsbad, CA) as dry pellets. siRNA that targets different parts of ADAM17 gene were purchased from Dharmacon (Lafayette, CO). Each siRNA duplex was re-suspended in RNase-free water to make a 20 mM solution. siRNA duplex was transfected at the time of cell seeding at concentrations (20-30 μM) into MDCK cells (reverse transfection) using Dharmacon transfection reagent I. Cells were then seeded with the appropriate number of cells that would give 50-60% confluence 24 hours after plating. Cells were incubated at 37°C, 5% CO2 for 48-72 hrs.

Non-targeting siRNA sequence (ON-TARGET plus) were used as a control for siRNA transfection. Validation of the level of MAGI or ADAM17 knockdown was done by evaluation of WB.

ADAM17 activity assay

ADAM17 activity was performed as described before with slight modification (154). Briefly, 20 µg of protein lysate in assay buffer (50 mM Tris, 5 mM $ZnCl_2$, 150 mM NaCl, and 10 µg/ml TIMP1, pH 9) was pre-incubated with DMSO or ADAM17 inhibitor (TIMP3) for 30 min at 37ºC. Then, internally quenched fluorogenic substrate Mca-PLAQAV-Dpa-RSSSR-NH2 (Enzo Life Sciences) was added to the mixture (final concentration 50 µM) and incubated for 10 min. Fluorescence was measured at an excitation of 328 nm and emission of 393 nm using a Synergy H1 microplate reader (Biotek, VT). The enzyme activity calculation was done according to the manufacturer recommendation. Values were normalized to the protein concentration of each sample.

Cell polarization and TER measurement

For polarization studies, $2 \times 10^4 – 2 \times 10^6$ cells per well were seeded on 10 mm diameter polyester tissue-culture treated Millicell filters with a pore size of 0.4µm (Millipore, Bedford, MA). Media on the apical surface of cells was removed the next day and the apical surface was maintained dry in order to establish an air-liquid interface. Polarized cells actively transport fluid from the apical to the basolateral surface and thus maintain a defined apical surface fluid composition.

Transepithelial electrical resistance was measured with a chopstick ohmmeter (World Precision Instruments, Sarasota, FL) every other day (Figure 14). When this

measurement was taken, media was aspirated from the wells and replaced with 600 µL fresh media at the basolateral surface. 400 µL of PBS supplemented with Ca^{2+} and Mg^{2+} was applied to the apical surface. The background electrical resistance was determined by adding media to the basolateral chamber and PBS to the apical chamber of a blank Millicell filter. The TER measurements were recorded in mohm (mΩ).

FITC Dextran assay

Assessment of epithelial integrity after peptide treatment was done using FITC-dextran assay as described before (155). Briefly, primary human airway epithelial cells were seeded on millicells and allowed to polarize as described in the TER measurement section. FITC-Dextran 4 kD or FITC-Dextran 70 kD (Sigma-Aldrich, MO) were prepared as stock solution (10 mg/ml) in ultrapure water and sterilized by filtration through a 0.22 µM pore size filter. Cells were washed with PBS containing calcium and magnesium, from the apical and basolateral side. 150 µl of pre-warmed FITC-Dextran in PBS (final concentration= 0.5 mg/ml) were added to the apical surface and 450 µl of PBS were added to the basolateral (Figure 14). After incubation for 120 min at 37 ºC, basolateral medium was collected, cells were washed with PBS and TER measurement were taken again. Controls for this experiment included the calcium chelating agent (EDTA) as well as the detergent Triton X-100 treatment for 10 min prior to the FITC-Dextran addition. EDTA chelates the calcium required for cadherin based adhesion and transiently breaks the junctions. Triton X-100 destroys the epithelial integrity by membrane permeabilization and it is used to assess to what extent the tracer molecules bind to remaining cellular components and debris (155). TER measurement were taken before and after treatments to confirm disruption of the epithelial tight junctions.

By the end of the 2 hrs, 100 µl aliquots were taken from the basolateral chamber and transferred to a 96-well plate for determination of relative fluorescence intensity (RFU) in a pre-calibrated Synergy H1 microplate reader (Biotech, VT) using software Gen5 2.04. A standard curve of each FITC-Dextran was established using range of concentration 0-20 µg/ml. The RFU values of the standard curve samples were taken in triplicates with an excitation wavelength 490 ± 9 nm and an emission wavelength of 520 ± 9 nm. The standard curves were used to determine the unknown concentration of the FITC-Dextran diffused to the basolateral side. Each peptides treatment condition was done in triplicate.

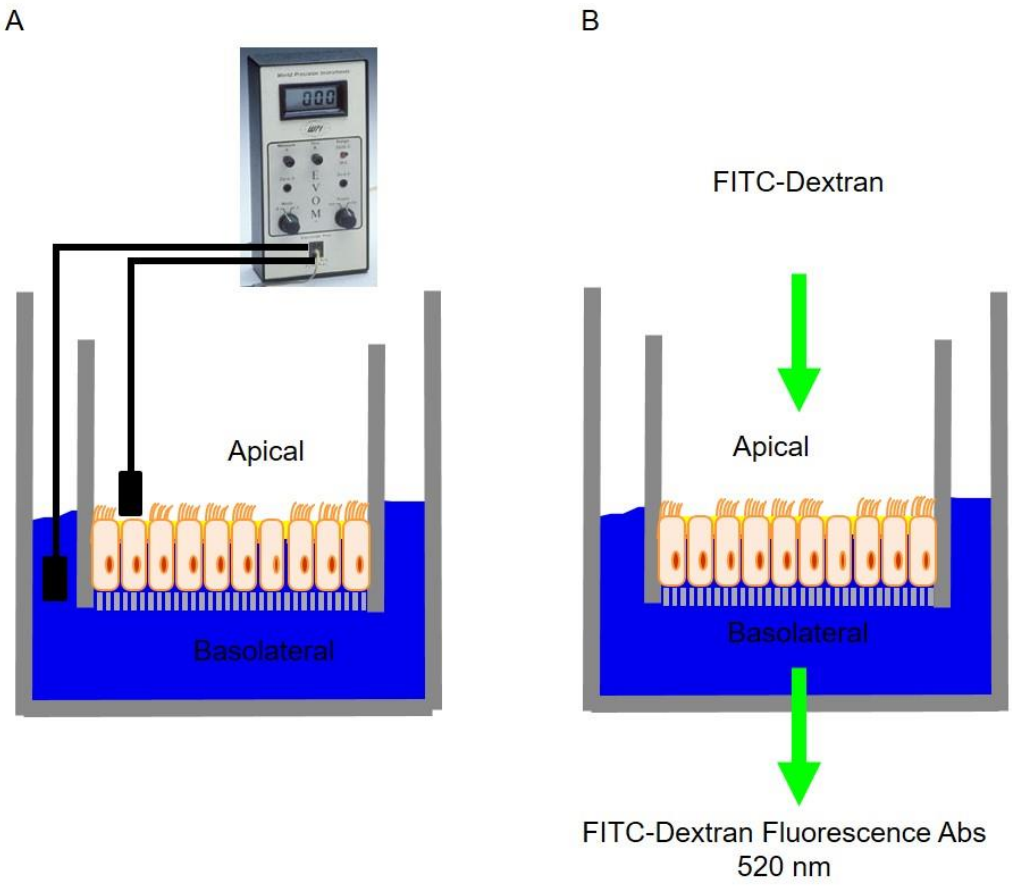

Figure 14. Schematic diagram of methods used to assess epithelial cells integrity.

(A) Model of TER measurement as an indicator of epithelial polarization. Transepithelial electrical resistance (TER) was determined by adding media to the apical and basolateral chambers. Electrical resistance was taken in mΩ using voltmeter with chopstick electrodes. (B) Schematic model of FITC-Dextran permeability assay across epithelial cells. FITC-labelled dextran was added to the apical surface. Dextran diffusion was assessed by collecting the basolateral media and measuring at the emission fluorescence of the FITC-dextran.

FITC-Dextran permeability assay is a good measure of epithelial integrity

In order to validate my approach in using FITC-Dextran as a measure of epithelial integrity, I optimized the conditions of FITC-Dextran assay in epithelia cells. First, epithelial cells were polarized on millicells until the TER reaches 1500-3000 Ohm. Then, the epithelia were treated with PBS, EDTA or Triton X-100 for 10 min at 37°C. In no treatment or PBS treatment condition, no significant change in the TER detected from baseline (Figure 15). In contrast, treatment with EDTA or Triton X-100 significantly dropped the TER (Figure 15), indicating that the measured TER was due to the tight junctions between epithelial cells. FITC-labelled Dextran permeability is another indicator of the epithelial integrity. To study the correlation between FITC-Dextran and the emission fluorescence, serial dilutions of standard concentration of the FITC-Dextran 4 kD and FITC-Dextran 70 kD were prepared. The fluorescence intensity was measured and standard curve was created for each Dextran. The standard curve of both FITC-Dextrans gave straight line with R^2=0.99 which indicates a linear correlation between the fluorescence intensity and the amount of FITC-Dextran in the solution (Figure 15).

I used this technology to assess the paracellular Dextran diffusion between epithelial cells. The procedure was done as explained above. FITC-Dextran 4 kD was used to assess paracellular flux of small molecules whereas Dextran 70 kD was used to assess the paracellular movement of large molecules. Under normal conditions (no treatment), there is traces of Dextran 4 kD that diffused across the epithelia but much less Dextran 70 kD, indicating intact tight junctions of the epithelia. PBS treatment slightly increased the diffusion of Dextran 4 kD but not Dextran 70 kD (Figure 15). Interestingly, treatment with EDTA (Ca^{+2} ion chelator) significantly increased the amount of Dextran 4

kD only, indicating partial disruption of the adherens junctions (Figure 15). Treatment with Triton X-100 significantly increased the diffusion of both Dextrans indicating complete perturbation of the cell junctions (cell lysis). This result further validates the applicability of the FITC Dextran diffusion assay as an indicator for epithelial integrity

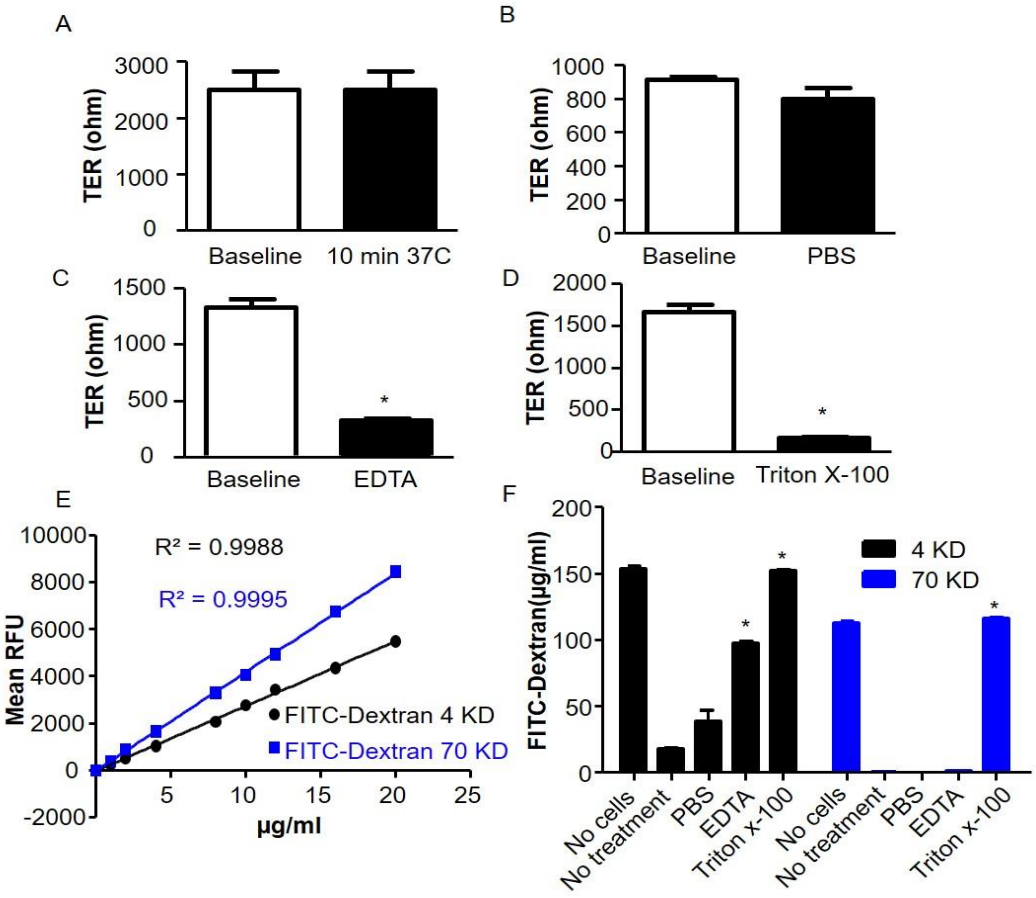

Figure 15. Optimization of FITC-Dextran permeability assay.

MDCK Epithelia were polarized and TER measurements were taken after 10 min of (A) no treatment (B) treatment with PBS (C) Treatment with 8 mM EDTA or (D) 1 % Triton, *$p < 0.05$ vs baseline. (E) FITC-dextran emission fluorescence correlated with the amount of FITC-dextran in solution. Serial dilution of FITC-dextran 4 kD and FITC-dextran 70 kD were prepared and excitation-emission fluorescence were measured at wavelength 490 ± 9 nm and 520 ± 9, respectively. (F) FITC-dextran permeability across polarized epithelial cells seeded on millicells. Cells were not treated, treated with PBS, EDTA, or Triton for 10 min at 37°C. *$p < 0.05$ compared to baseline or no treatment.

Vesicle trafficking by Rabs

The Rab Family antibody sampler kit (cell signaling, MA) was used to investigate the CAR^{Ex8} trafficking pathway. Polarized inducible MDCK cells were induced overnight with 500 ng/ml of dox. The next day, cells were incubated with protein synthesis inhibitor cycloheximide (100 mg/mL) for 4 h at 15-20°C to accumulate newly synthesized CAR^{Ex8} in the trans-Golgi network (TGN). By the end of the 4 hrs, TGN cargo was released by incubation at 37°C for 5-15 min (156). By the end of the release time, cells were washed with PBS and fixed immediately with 1% PFA in methanol. CAR^{Ex8} was stained with mouse anti-Flag and Rabs were probed with rabbit anti-Rab Ab. In some optimization conditions, FITC-labelled Wheat Germ Agglutinin (WGA) was used as a cell marker for the trans-Golgi compartment. Images were taken using FV1000 confocal microscopy (Olympus, NJ).

Animal handling and peptide administration

Animals (Tom/ CC10 and Tom/Spc background, JAX stock # 007576) were housed individually (male) or in groups (females) at 22°C under a 12-hour light/12-hour dark cycle with *ad libitum* access to water and standard mouse chow (3.0 kcal/g, 40.6% carbohydrate, 5.5% fat, and 22% protein; Harlan Teklad, Madison, WI). All experimental protocols were approved by the WSU Animal Care and Use Committee. Animal were 8-12 weeks old were originally purchased from Jackson laboratory and bred at the University of Iowa animal facility. Mice were anesthetized moderately using isoflurane in a closed chamber. Once the animal was knocked out, mice were removed quickly from the chamber and were held in 60° declined supine position by securing the fore and hind paws with the left hand. A sterile P_{200} pipette was used to deliver a volume of 50 µl in the

left nostril of the mouse during inhalation. Mice were given a dose of 500 µM of peptides dissolved in a volume of 50 µl of vehicle (PBS) via intranasal administration. Four hrs later, mice were infected intranasal (through the right nostril) with AdV-Cre (University of Iowa, IA). Virus dose $1.0*10^8$ PFU/50µl. After each intranasal administration, mice were held straight for few minutes to assure that all solution was inhaled. Then, they were returned to their cages for recovery to allow Cre-recombinase expression. Approximately 2 days later mice were euthanized by CO_2 inhalation. A 10 mm incision was made over the trachea of mice to visualize the insertion of tracheal intubation (size 60 - polyethylene (PE) tubing; Becton Dickenson and Co., MD, USA). Tube was moved down to the point of tracheal bifurcation and slid gently toward the left lung. At the point of left lung bifurcation, the distal trachea was tied but not secured along with the tracheal tube using (6-0 nylon; Ethicon). The right tracheal biforation was tied and secured. A solution contains 50% PBS and 50% tissue freezing media (Thermoscientifc, MA) was infused through the intratracheal tube using 20 ml syringe (Fix inflation). Once inflated, the knot was secured. Another knot was made in the proximal trachea and below the intubation site. The trachea and the left lung were then dissected, wrapped in foil and frozen in dry ice for 2 days. The right trachea was cut distal to the knot secured site. One lobe was submerged in RNA later (Thermofisher, MA) for RNA isolation. The other two lobes were dissected and frozen in liquid nitrogen for 2 hrs before they were transferred to dry ice. The left lung and trachea were fixed frozen in Tissue Freezing Medium (TFM) after removal of intubation tube. Lung lobes were cut sectioned in 25 micron sections using cryostat HM550 (Thermo scientific, MA). Sections were then vapor fixed in a chamber

containing 4% paraformaldehyde. After that they were visualized for red and green fluorescence expression using FV1000 (Olympus, NJ).

Statistics

All statistical analysis was done using Prism software (GraphPad, CA). Depending on the experimental condition, a T-test, one way or two-way Analysis of Variance (ANOVA) was performed. Tukey post hoc test was used to compare the all pairs of means. P value < 0.05 was considered as statistically significant.

CHAPTER 3: Investigation of the Effect and Molecular Mechanism of TAT-PDZ1 Peptides on CAR^{Ex8} and Adenovirus Infection

Rationale

Adenovirus (AdV) and coxsackievirus group B (CVB) infections can be severe and life threatening and no specific or effective therapeutics currently exist. Understanding the mechanisms leading to decreased susceptibility of the airway epithelium to viral infection will improve both therapeutic options and patient outcomes in the future. The discovery of the regulatory role of MAGI-1 on CAR^{Ex8} opened the door toward a clear and easy target for controlling AdV infection. CAR^{Ex8} contains a PDZ-binding motif that interacts with two MAGI-1 PDZ domains, PDZ1 and PDZ3, which regulate CAR^{Ex8} levels in opposing ways (Figure 8) (63). While an interaction with PDZ3 causes CAR^{Ex8} degradation and reduces AdV infection, interaction with the PDZ1 domain is able to rescue CAR^{Ex8} from degradation and increase AdV infection (63). This chapter is focused on identifying the mechanism behind MAGI-1 PDZ3-mediated CAR^{Ex8} downregulation using peptide-based molecules that block MAGI-1 PDZ1. The net result is CAR^{Ex8} degradation and the decreased apical AdV infection in polarized cells. Such therapeutics will be used for pre-clinical evaluation to suppress AdV infection *in vivo*

Results

Epithelial cells line most organs and form a strong barrier that protects organs from incoming microorganisms and environmental factors. My approach was to transduce epithelial cells with a peptide-based sequence that would alter CAR^{Ex8} level and AdV entry. The first challenge was to enhance peptide transduction in epithelial cells. Rapid transduction of proteins into cells can be facilitated by cell-permeable peptides (CPP; also called cell penetrating peptides and protein transduction domains) (115-117). The 11 aa cell permeable HIV-TAT sequence, which is able to facilitates peptide internalization, was conjugated to the C-terminal 9 aa sequence of the full length CAR^{Ex8}, to make TAT-CAR^{Ex8}-9c. While the last four amino acids of the full length CAR^{Ex8} are the residues responsible for the direct interaction with MAGI-1, the other residues provide extra PDZ domain specificity. I hypothesized that the designed peptide sequence would compete with the full length CAR^{Ex8} for MAGI-1 binding and release CAR^{Ex8} from MAGI-1 binding and degradation.

TAT- PDZ binding peptides enter epithelial and non epithelial cells

In order to test that the TAT-PDZ binding peptides are capable of entering polarized epithelial and non-epithelial cells, TAT-CAR^{Ex8}-9c peptide was synthesized as described in the materials and methods (Genscript). The entry of the TAT- peptide into CHO (non-polarized cells that do not express endogenous CAR) and MDCK cells (cells able to polarize and express endogenous CAR) was confirmed by two approaches. First,

using matrix assisted laser desorption ionization-mass spectrometry (MALDI-MS), TAT-CAR^{Ex8}-9c was detected in lysates from treated cells and spiked cell lysate but not lysates from untreated cells or cell medium. The synthesized peptide gave a unique and expected peak at *m/z* 2536 in the spectrum from both cell lines (Figure 16). The second approach was done by using fluorescently-labelled TAT-CAR^{Ex8}-9c. Peptides were synthesized and conjugated with the red fluorescence protein, Tamra. In both cell lines, the fluorescently labelled Tamra- TAT-CAR^{Ex8}-9c entered virtually all of the cells and localized throughout the cytoplasm with a higher density around the ER/golgi (arrow) and also, unexpectedly, within the nucleoli (Figure 17). These results validate my approach of using the TAT cell permeable peptides to facilitate peptide entry into epithelial and non-epithelial cells.

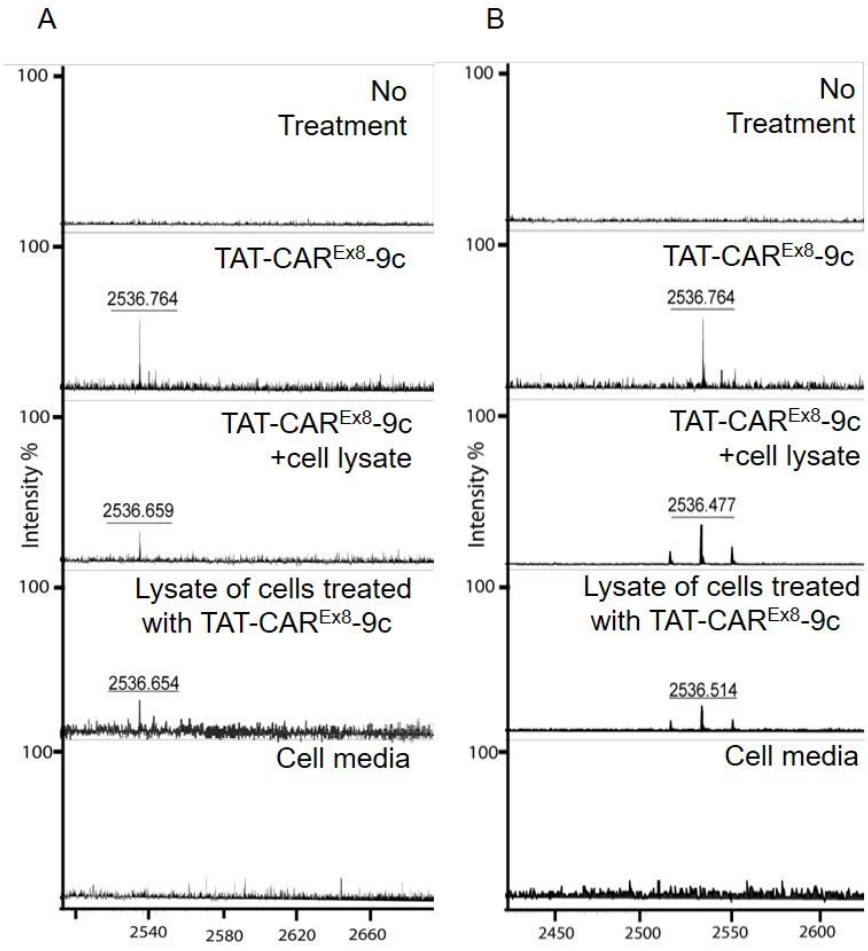

Figure 16. TAT-cell permeable peptides enter non-epithelial and epithelial cells.

MALDI-TOF analyses of TAT-CAREx8-9c peptides associate with (A) CHO cells (non-epithelial) and (B) MDCK epithelia. A peak at *m/z* 2536 showed in both cell lines corresponded to the m/z of TAT-CAR^{Ex8}-9c. CHO or MDCK were incubated with either TAT-CAR^{Ex8}-9c or vehicle for 1 hr at 37°C. Cell pellets obtained were used for MALDI-TOF mass spectrometric analysis as described under *Materials and Methods*. TAT-CAR^{Ex8}-9c enters cells and peaked at *m/z* 2536.

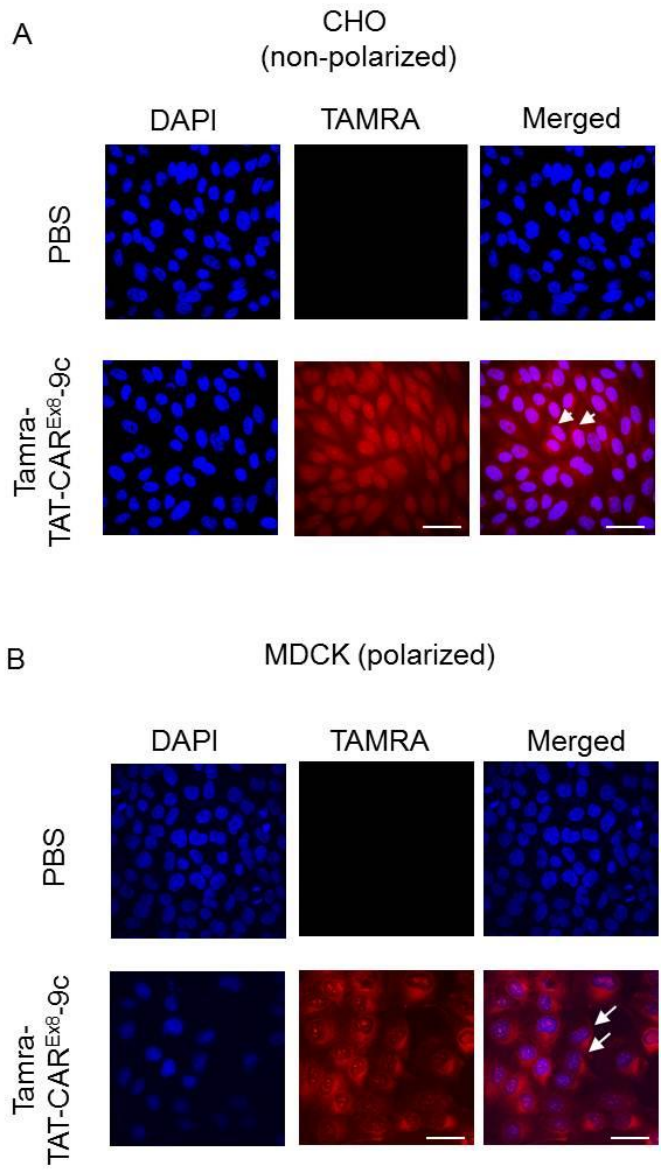

Figure 17. TAT-Cell permeable peptides enter non-epithelial and Slide epithelial cells.

(A) CHO or (B) MDCK cells were treated with either vehicle (PBS) or fluorescently labelled TAMRA-TAT-CAR^{Ex8}-9c. Peptide was detectable within 1 h after incubation inside cells. White arrows indicate ER/Golgi region of cell with intense TAMRA (red) fluorescence. Confocal 60x oil immersion lens, White line = 10 µm.

TAT- PDZ binding peptides perturb CAR^{Ex8} MAGI-1 interaction

Since the full length CAR^{Ex8} can interact with both MAGI-1 PDZ1 and PDZ3, I tested if the designed TAT-CAR^{Ex8}-9c would be able to perturb the interaction between MAGI-1 and CAR^{Ex8} in the epithelial cells. I used immunoprecipitation to reveal the physical uncoupling of CAR^{Ex8} and MAGI-1 upon treatment with TAT-CAR^{Ex8}-9c, using the advantage of inducible CAR^{Ex8} MDCK epithelial cells that express Flag-CAR^{Ex8} (60). As expected, MAGI-1 was co-immunoprecipitated with Flag-CAR^{Ex8} in the vehicle treatment condition. In contrast, co-immunoprecipitation of MAGI-1 with Flag-CAR^{Ex8} was markedly decreased in MDCK cells pre-treated with TAT-CAR^{Ex8}-9c. Interestingly, pre-treatment with TAT-CAR^{Ex8}-9c that contains mutated PDZ binding motif (TAT-CAR^{Ex8}- AA-9c), did not affect co-immunoprecipitation of MAGI-1 with Flag-CAR^{Ex8} (Figure 18). These results indicate that the TAT-CAR^{Ex8}-9c peptide, but not the mutated peptide, is able to disrupt the cellular interactions between the full length CAR^{Ex8} and MAGI-1 through the PDZ binding motif of CAR^{Ex8}.

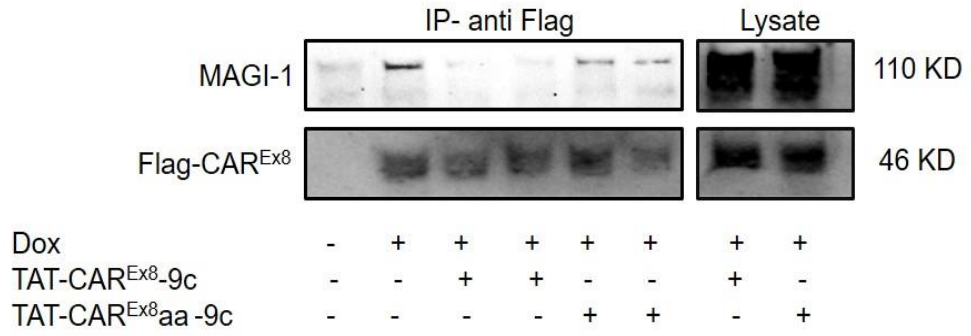

Figure 18. TAT-cell permeable peptides interrupt MAGI-1-CAR^{Ex8} interactions.

Western immunoblots showing immunoprecipitates (IP, left lanes) from inducible MDCK-CAR^{Ex8} epithelia pretreated with TAT-CAR^{Ex8}-9c or control TAT-CAR^{Ex8}-AA-9c. Stable MDCK-CAR^{Ex8} cells were induced with 200 ng/ml Dox for 24 hrs. After overnight induction, cells were treated with either TAT-CAR^{Ex8}-9c or TAT-CAR^{Ex8}- AA-9c (100µM). CAR^{Ex8} was immunoprecipitated using flag antibody. MAGI-1 was blotted to determine co-IP. Note the marked reduction in MAGI-1 coimmunoprecipitated with Flag-CAR^{Ex8} from MDCK pretreated with TAT- CAR^{Ex8}-9c. Right lanes show cell lysate with no immunoprecipitation, acting as positive controls. Note that there was no difference in CAR^{Ex8} protein level in the IP blot possibly due to the increased CAR^{Ex8} production induced by doxycycline.

TAT- PDZ1 peptides binds selectively to MAGI-1 PDZ1

In order to identify small molecules that could decrease apical CAR^{Ex8} protein expression, novel cell-permeable peptides that bind the PDZ1 domain of MAGI-1 were developed (Table 4). Target sequences were based on published interactions between cellular NET1 and viral HPV16 E6 with MAGI-1 PDZ1 (112, 144). I tested the specificity of my peptides to MAGI-1 PDZ domains by a fluorescence binding assay. The purified PDZ1 and PDZ3 domains were labelled with the Cy3 fluorophore and tested for interactions with the synthesized TAT-PDZ peptides. In contrast to TAT-scramble peptide which showed no interactions with either PDZ1 or PDZ3 (Table 4), TAT-CAR^{Ex8}-9c bound both domains, with higher affinity to PDZ3 than PDZ1 (Table 4). By contrast, TAT-NET1 showed an interaction with MAGI-1 PDZ1 (Kd=28 ± 11 nM) but not PDZ3 (Kd = N.I, No Interaction) (Figure 19). Similarly, TAT-E6 bound MAGI-1 PDZ1 (Kd = 15 ± 4 nM) but not PDZ3 (Kd = N.I, No Interaction) (Figure 20). These results indicate the selectivity of the designed TAT-PDZ1 selective peptides, TAT-NET1 and TAT-E6, toward the MAGI-1 PDZ1 domain.

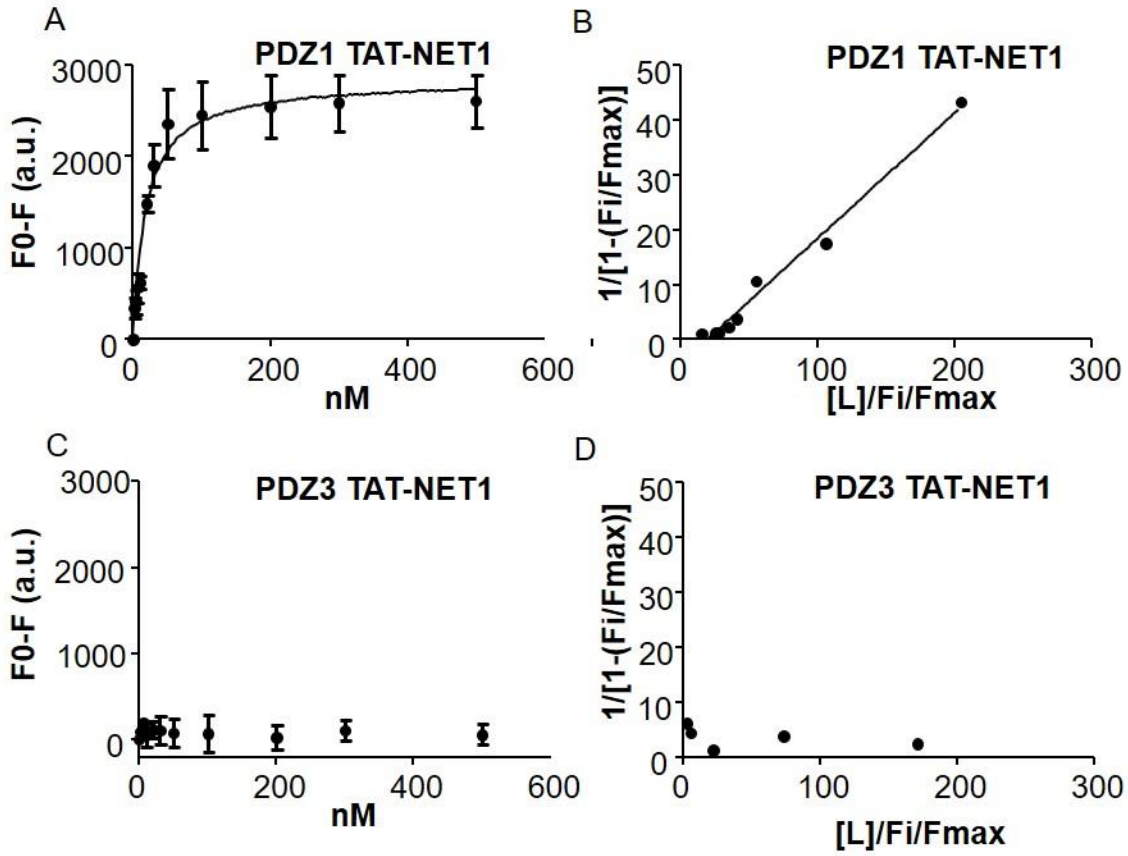

Figure 19. TAT-NET1 binding peptides bind selectively to MAGI-1 PDZ1 domain.

Ligand binding assay between TAT-NET1 peptide and purified MAGI-PDZ-1. MAGI-1 PDZ3 domain was used as a control. TAT-NET1 binds to MAGI-1 PDZ1 (A, B) but not PDZ3 (C, D) (TAT-NET1 Kd=28± 11). Double reciprocal plot (B) showed linear curve indicating a single binding site between TAT-NET1 and PDZ1 (B) but not PDZ3 domain (D).

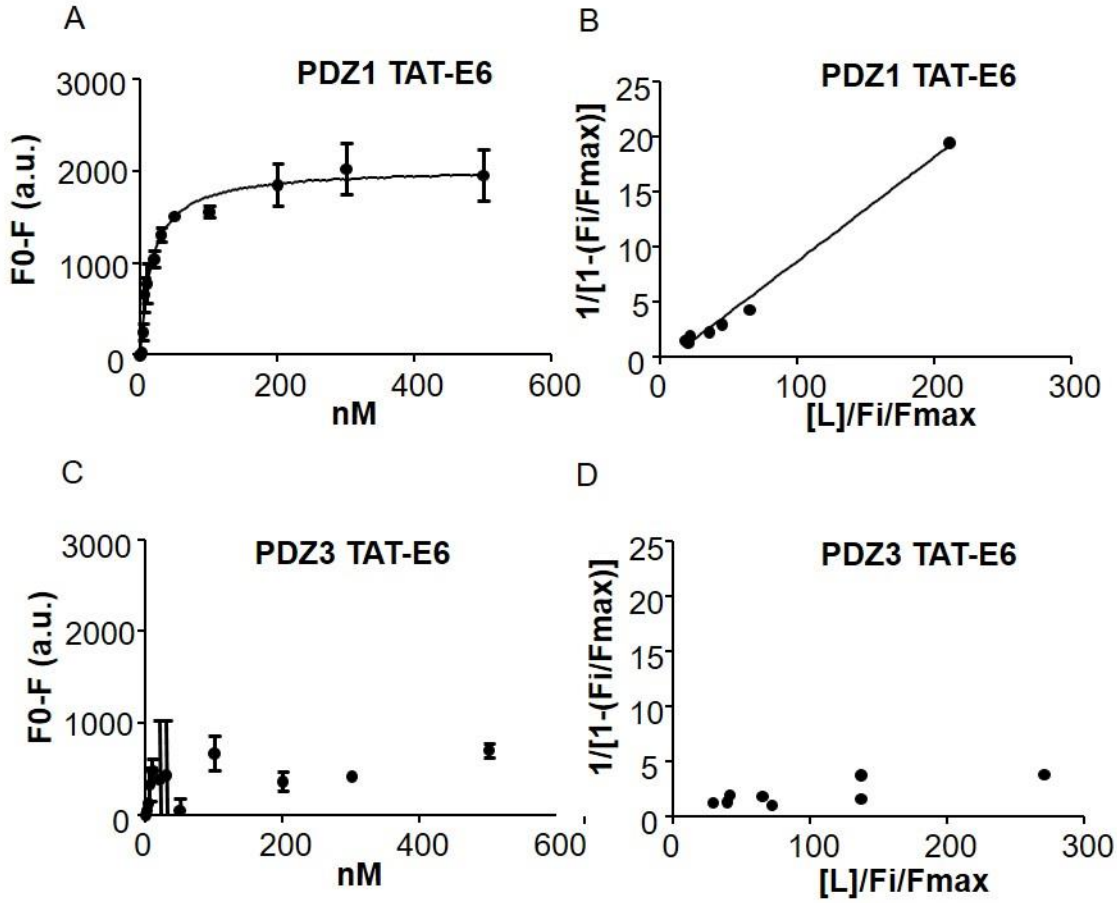

Figure 20. TAT-E6 binding peptides bind selectively to MAGI-1 PDZ1 domain.

Ligand binding assay between TAT-E6 and purified MAGI-PDZ-1. MAGI-1 PDZ3 domain was used as a control. TAT-E6 binds to MAGI-1 PDZ1 (A, B) but not PDZ3 (C, D) (TAT-E6 Kd=15± 4). Double reciprocal plot (B) showed linear curve indicating a single binding site between the ligand and PDZ1 (B) but not PDZ3 domain (D).

TAT-PDZ1 selective binding peptides diminish CAR^{Ex8} protein levels and suppress AdV transduction

As TAT-PDZ1 peptides interact selectively with the MAGI-1 PDZ1 domain, I tested whether the TAT-PDZ1 peptides were able to promote CAR^{Ex8} degradation**.** First, I tested the cancer epithelial cell line, MDCK. Treatment with TAT-NET1 or TAT-E6 significantly decreased the protein level of CAR^{Ex8} (Figure 21). To assess the effect of TAT-PDZ1 peptides on AdV transduction, MDCK epithelia were treated with vehicle, TAT-scramble, TAT-NET1, or TAT-E6. Both TAT-PDZ1 peptides significantly decreased AdV transduction compare to vehicle treatment as measured by qPCR for the number of AdV DNA genomes (Figure 21). This corresponded to a decrease in Ad-β-gal gene expression using the β-galactosidase assay, which indicated reduced viral transduction (Figure 21). I further tested the effect of TAT-PDZ1 peptides on CAR^{Ex8} in a more clinically relevant model, primary human airway epithelia (HAE). Similar to MDCK, the level of CAR^{Ex8} protein was significantly decreased in the TAT-PDZ1 treated conditions (Figure 22). This also corresponded to a suppression of AdV entry into the HAE (Figure 22). These data suggest that the TAT-PDZ1 peptides could efficiently reduce or prevent AdV entry in airway epithelia. I took a further advanced step and tested the efficacy of TAT-PDZ1 peptides in epithelia from an animal model of AdV pathogenicity. Using epithelial cells from cotton rats (a well-known animal model for AdV pathogenesis, (157)) both TAT-PDZ1 decreased the level of CAR^{Ex8} protein compared to TAT-scramble and control treated conditions (Figure 23). Similar to HAE, AdV transduction was significantly suppressed in the TAT-PDZ1 treated conditions

(Figure 23). Overall, these data indicate that TAT-PDZ1 binding peptides efficiently and reproducibly suppress AdV transduction by targeting CAR^{Ex8} level.

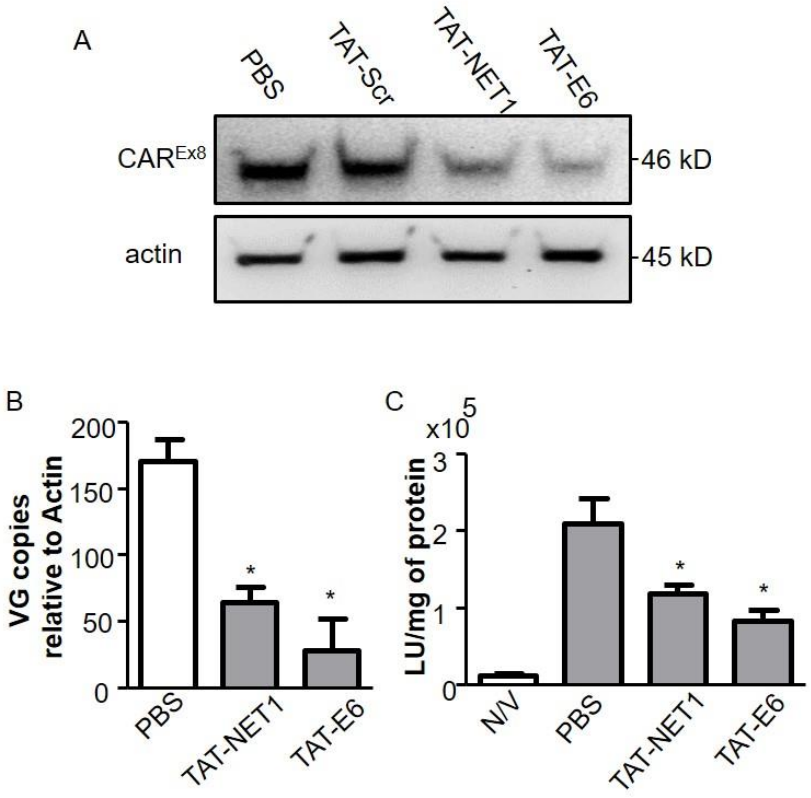

Figure 21. TAT-PDZ1 binding peptides decrease CAR^{Ex8} protein levels and AdV transduction in MDCK epithelia.

(A) Western Blotting from MDCK epithelia treated with either TAT-scramble or TAT-PDZ1 peptides (TAT-E6 or TAT-NET1). A marked decrease in CAR^{Ex8} protein level was seen in the TAT-PDZ1 treated conditions. Actin was used to confirm equal protein loading. (B) QPCR of the AdV viral genome showed a significant decrease in AdV entry into MDCK epithelia treated with the TAT-E6 or TAT-NET1 as compared to control. (C) B-galactosidase activity assay showed a significant suppression of AdV transduction in TAT-PDZ1 treated MDCK epithelia. * $P < 0.05$ compare to PBS.

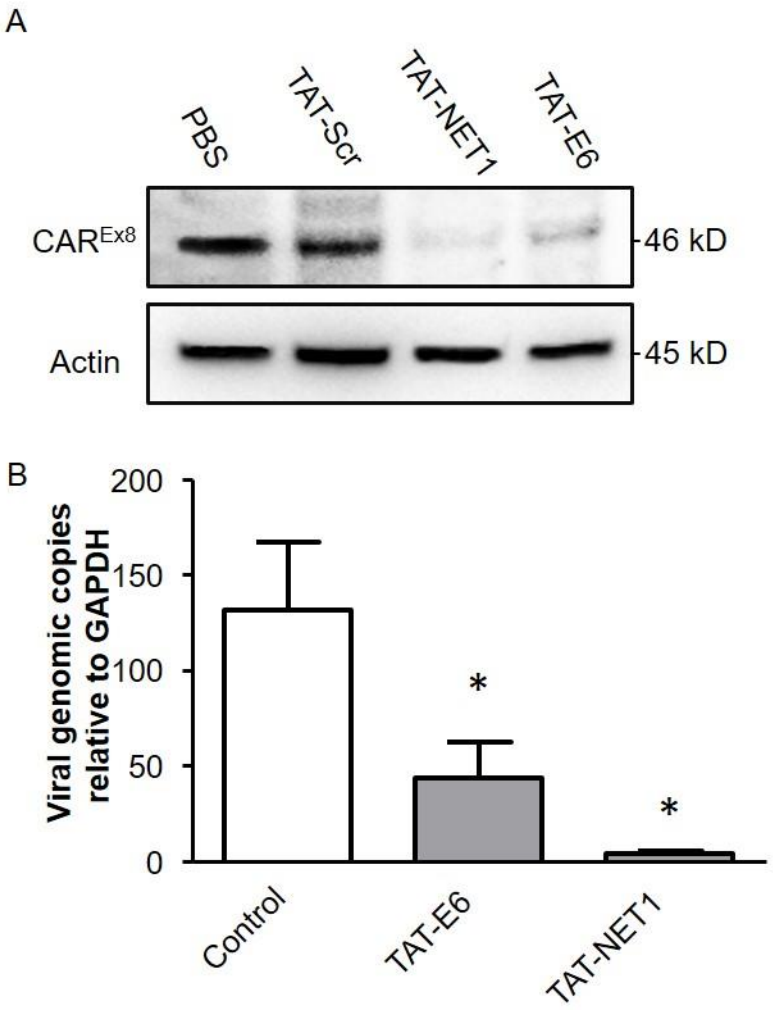

Figure 22. TAT-PDZ1 binding peptides decreased CAR^{Ex8} protein levels and AdV transduction.

(A) Western Blotting from Human Airway Epithelia (HAE) treated with either TAT-scramble or TAT-PDZ1 peptides (TAT-E6 or TAT-NET1). A marked decrease in CAR^{Ex8} protein level was seen in the TAT-PDZ1 treated conditions. Actin was used to confirm equal protein loading. (B) QPCR of the AdV viral genome showed a significant decrease in AdV entry into HAE treated with the TAT-E6 or TAT-NET1 as compared to control. * $p < 0.05$ compare to control.

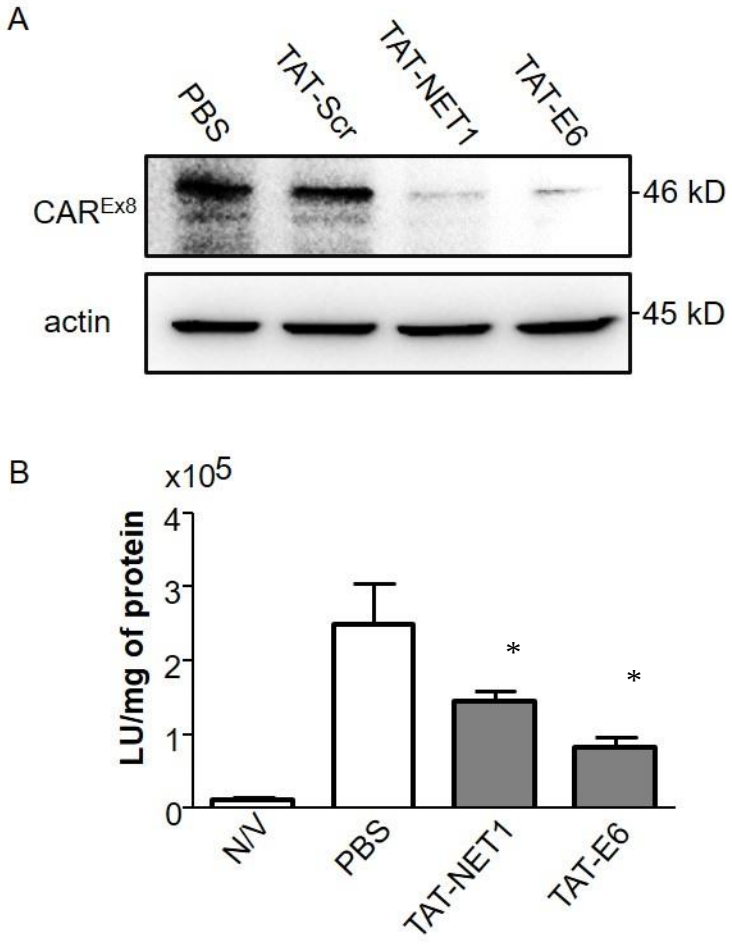

Figure 23. TAT-PDZ1 binding peptides decreased CAR^{Ex8} protein levels and AdV transduction in cotton rat epithelia.

(A) Western Blotting from cotton rat epithelia treated with either TAT-scramble or TAT-PDZ1 peptides (TAT-E6 or TAT-NET1). A marked decrease in CAREx8 protein level was seen in the TAT-PDZ1 treated conditions. Actin was used to confirm equal protein loading. (B) B-galactosidase assay showed a significant suppression of AdV transduction in TAT-PDZ1 treated cotton rat epithelia. *$p < 0.05$ compare to PBS.

TAT-PDZ1 binding peptides decreased CAR^{Ex8} by inducing degradation of the translated protein

I next investigated the mechanism by which TAT-PDZ1 peptides decrease CAR^{Ex8} protein. First, I tested if TAT-PDZ1 alters CAR^{Ex8} mRNA levels by qRT-PCR. As expected, there was no change in CAR^{Ex8} transcript level upon treatment with TAT-PDZ1 peptides (Figure 24A). I then tested if TAT-PDZ1 peptides alter CAR^{Ex8} protein degradation. Using the global proteasome and RIP inhibitor (MG-132), the effect of TAT-PDZ1 on CAR^{Ex8} peptides was completely reversed in the MG-132 pre-treated condition (Figure 24B), indicating that TAT-PDZ1 peptides decrease CAR^{Ex8} by inducing degradation of the full length protein.

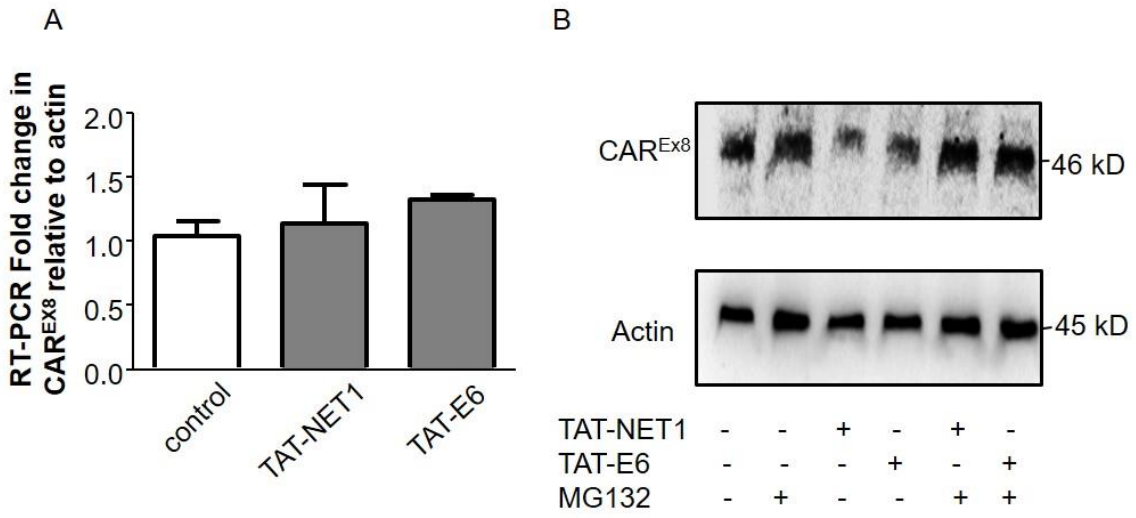

Figure 24. TAT-PDZ1 binding peptides decrease CAR^{Ex8} by inducing degradation of the translated protein.

(A) TAT-PDZ1 peptides do not change CAR^{Ex8} transcript levels. RT-PCR from TAT-PDZ1 pre-treated MDCK epithelia. No change in CAR^{Ex8} transcript level was seen among treated conditions. (B) Western Blotting of TAT-PDZ1 treated peptides in the presence or absence of the proteosomal and RIP inhibitor, MG-132. Pre-treatment with MG-132 rescued the full length CAR^{Ex8} from TAT-PDZ1 induced degradation.

Downregulation of CAR^{Ex8} protein levels by regulated intramembrane proteolysis (RIP)

To determine whether TAT-PDZ1 peptides exaggerate the normal cellular pathways that regulate CAR^{Ex8} degradation, I followed the fate of CAR^{Ex8} by ICC and confocal microscopy. In MDCK epithelia, most CAR^{Ex8} is at the apical surface while some is distributed in the cytoplasm (Figure 25A, red). Treatment with TAT-PDZ1 peptides dramatically altered the localization of CAR^{Ex8} to nuclear inclusions consistent with RIP (Figure 25B, C, red). To determine the nature of the CAR^{Ex8} nuclear inclusions after TAT-PDZ1 peptide treatment, the cytoplasmic and nuclear fractions were isolated from induced MDCK-CAR^{Ex8} cells after peptide or control treatment and cell lysis for Western blotting. The advantage of using inducible MDCK-CAR^{Ex8} cells is because that they express CAR^{Ex8} tagged with Flag epitope at the N-terminal extracellular domain upon induction with Dox (60). In that way, I was able to distinguish CAR^{Ex7} from CAR^{Ex8}, which otherwise would have identical extracellular domains. As expected, treatment with TAT-PDZ1-binding peptide decreased cytoplasmic CAR^{Ex8} as opposed to control TAT-scramble and PBS (dilutent) treatments (Figure 26). Moreover, the nuclear fraction showed a 14 kD fragment, which corresponds to the expected size of the CAR^{Ex8} C-terminus, only detectable with C-terminal CAR^{Ex8} Ab in the TAT-PDZ1 peptide treated cells (Figure 26). These results indicate that TAT-PDZ1 peptides target CAR^{Ex8} degradation and I hypothesized that this was by inducing regulated intramembrane proteolysis (RIP).

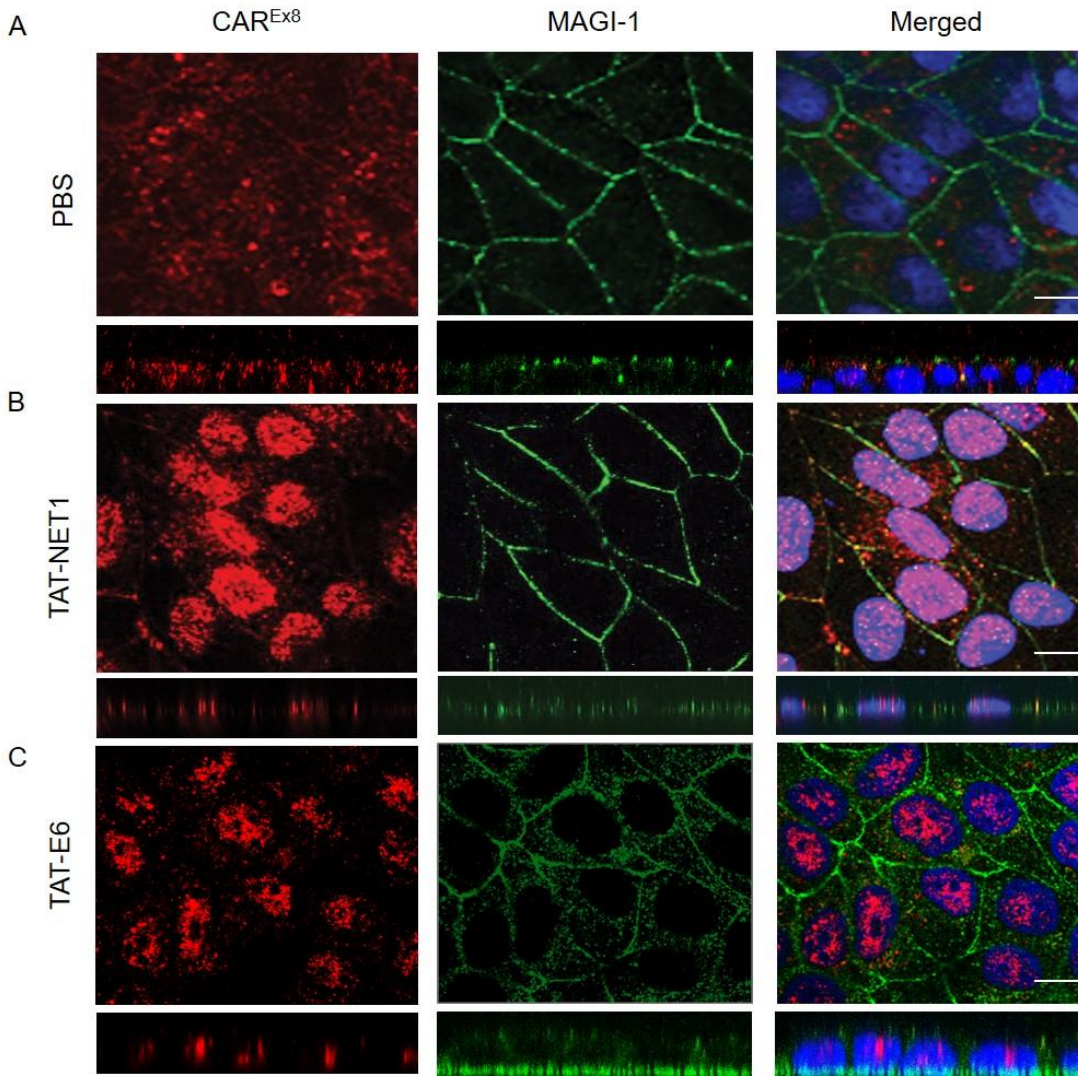

Figure 25. TAT-PDZ1 binding peptides change the immunolocalization of endogenous CAR^{Ex8}.

(A) CAR^{Ex8} (red) localizes mainly at the apical membrane of MDCK epithelial cells (see xz section). (B) Treatment with TAT-NET1 (50µM) or (C) TAT-E6 (50µM) causes delocalization of CAR^{Ex8} to the nuclear compartment but has minor to no effect on the junctional staining of MAGI-1 (green). Whit bar =10 µm

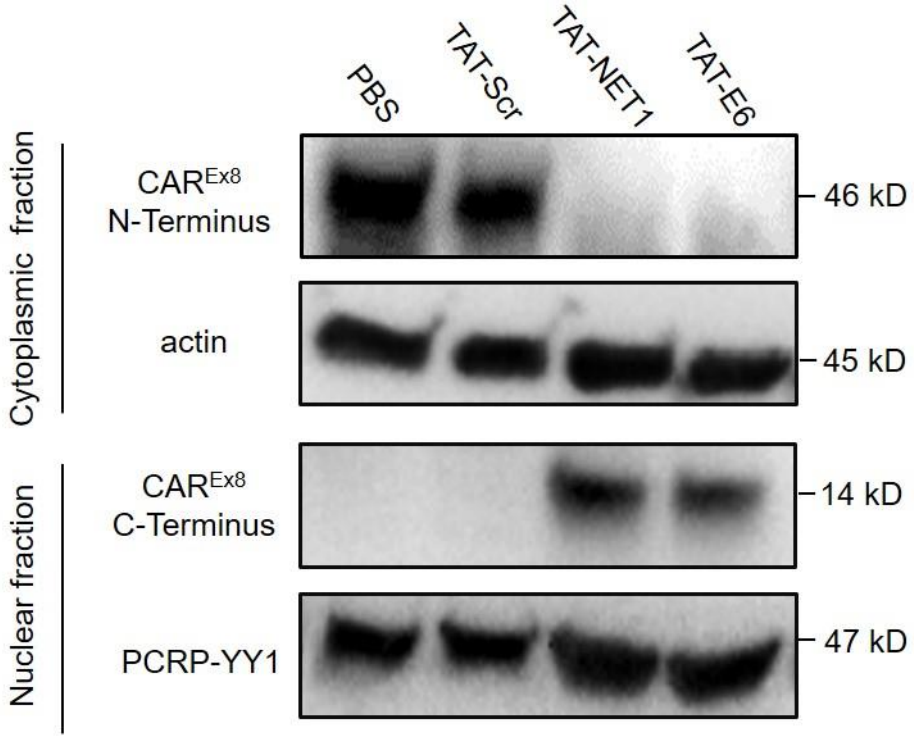

Figure 26. TAT-PDZ1 binding peptides translocate the CAR^{Ex8} cytoplasmic domain to the nucleus.

MDCK CAR^{Ex8} cells were induced with 50 ng/ml Dox after which they were treated with 100 µM of TAT-Scr, TAT-NET1, or TAT-E6. Immunoblotting from cellular fractionation of MDCK epithelia into cytoplasmic and nuclear fractions is shown. Treatment with TAT-PDZ1 markedly decreases CAR^{Ex8} in the cellular fraction. A 14 KD band corresponding to the cytoplasmic domain of CAR^{Ex8} was present in the nuclear fraction in the TAT-PDZ1 treated conditions. Actin (cytoplasmic) and PCRP-YY1 (nuclear) were used to confirm equal protein loading in the cytoplasmic and nuclear fraction, respectively.

Considering that most transmembrane proteins undergo RIP by secretases, I tested if γ-secretase inhibitor (compound E) would reverse the effect of TAT-PDZ1 peptides. Pretreatment with compound E prevented TAT-E6 induced nuclear translocation of the cytoplasmic domain of CAR^{Ex8} (Figure 27). I confirmed this result by immunoblotting which showed a decrease in the 14 KD fragment formed upon pre-treatment with γ-secretase inhibitor compound E (Figure 28). I further confirmed the effect of comp E on reversing TAT-PDZ1 peptide by cellular fractionation of the cytoplasmic and nuclear fraction. Pretreatment with comp E resulted in only a partial rescue of the full length CAR^{Ex8} from TAT-PDZ1 peptide but completely reversed nuclear translocation of the cytoplasmic domain of CAR^{Ex8} (Figure 29). Notably, some 14 KD band was detectable in the cytoplasmic fraction in the comp E pretreated conditions. This indicates that the TAT-PDZ1 peptides induce RIP of the cytoplasmic domain of CAR^{Ex8} by γ-secretase which causes the CAR^{Ex8} cytoplasmic domain to be translocated to the nucleus. This is consistent with a previous report of ripping the mouse CAR protein (homologous to human CAR^{Ex8} studied here) cytoplasmic domain by γ-secretase (158).

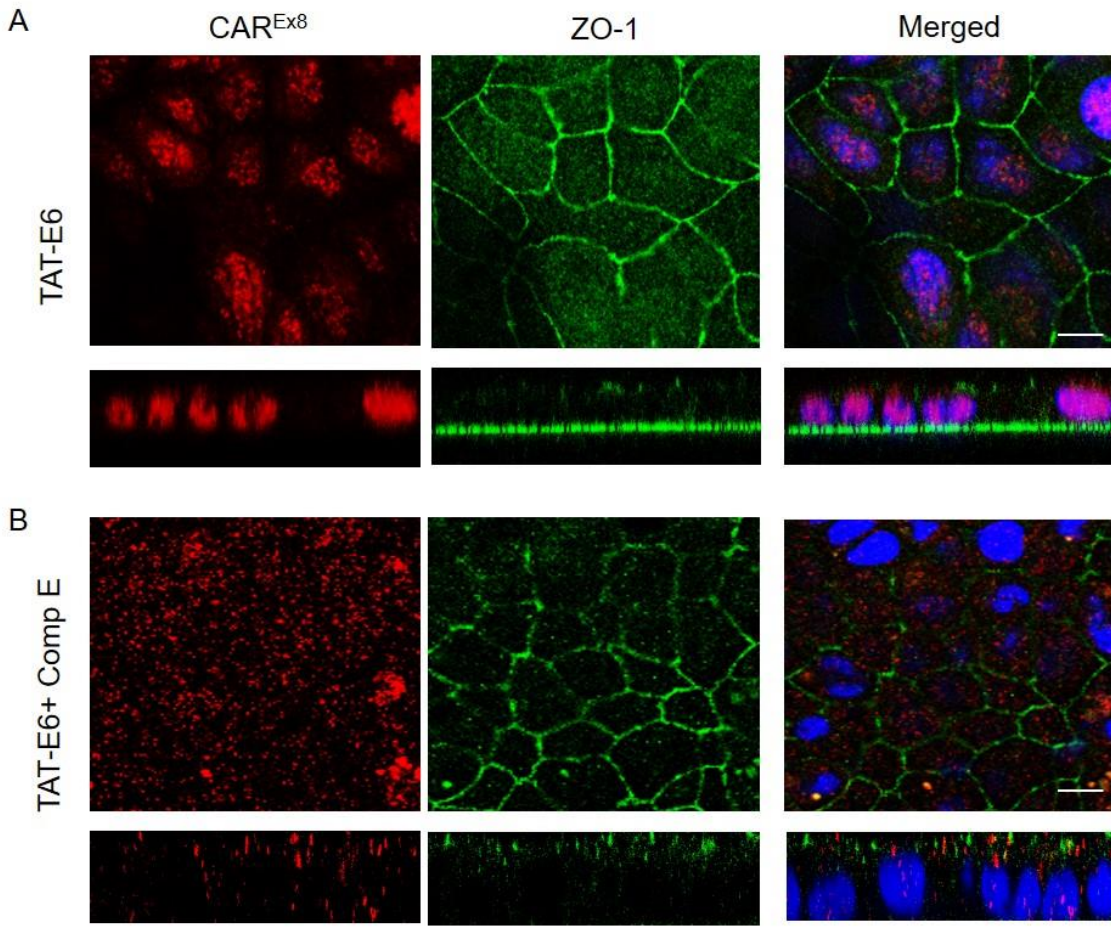

Figure 27. Selective gamma-secretase inhibitor (compound E) reverses TAT-E6 induced nuclear translocation of the cytoplasmic domain of CAR^{Ex8}.

(A) CAR^{Ex8} cytoplasmic domain is translocated into the nucleus upon TAT-E6 peptide treatment. (B) Pre-treatment with comp E reversed the effect of TAT-E6 and rescued the cytoplasmic domain of CAR^{Ex8} from nuclear translocation. White bar= 10 µm

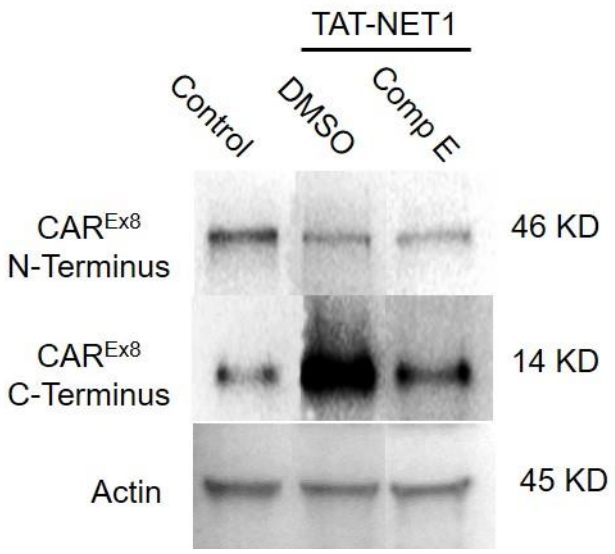

Figure 28. Selective γ-secretase inhibitor (compound E) reversed TAT-NET1 induced nuclear translocation of the cytoplasmic domain of CAR^{Ex8}.

Western immunoblotting from MDCK epithelia treated with TAT-NET1 in the presence or absence of the selective gamma-secretase inhibitor (compound E). Pre-treatment with comp E decreased cytoplasmic domain formation of CAR^{Ex8} (14 KD), but did not rescue the full length CAR^{Ex8} from TAT-NET1 induced degradation.

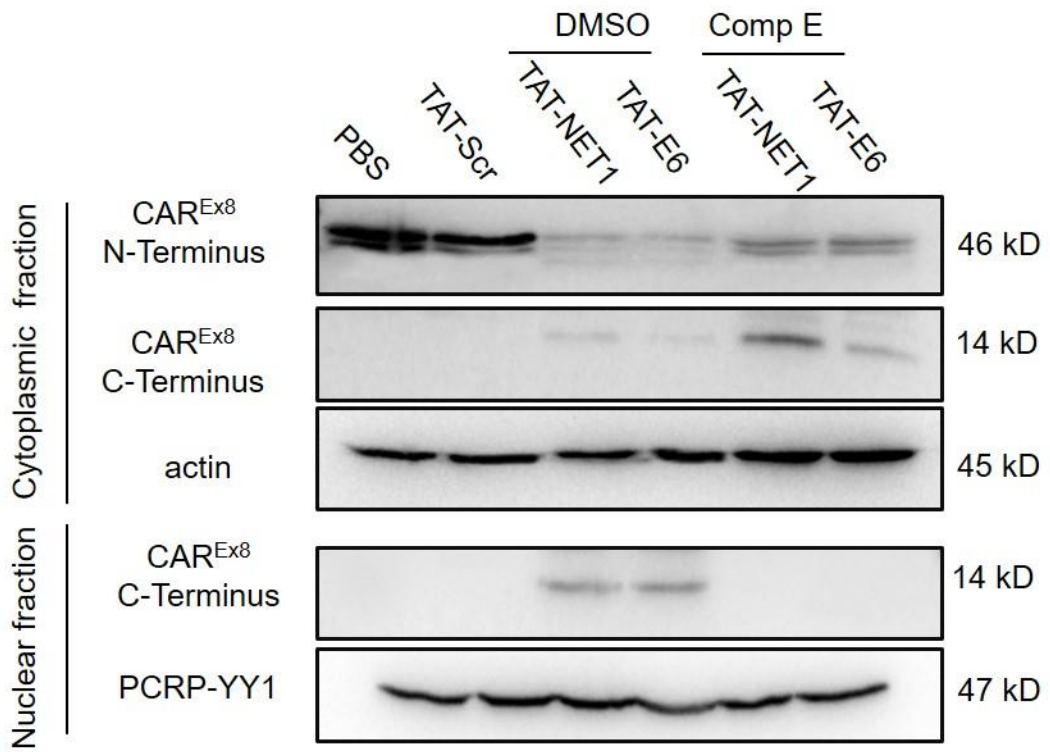

Figure 29. Selective gamma-secretase inhibitor (compound E) reverses TAT-PDZ1 induced nuclear translocation of the cytoplasmic domain of CAR^{Ex8}.

CAR^{Ex8} cytoplasmic domain is translocated into the nucleus upon TAT-E6 and TAT-NET1 peptide treatment. Pre-treatment with compound E reversed the effect of both peptides and rescued the cytoplasmic domain of CAR^{Ex8} from nuclear translocation. However, it did not rescue the full length CAR^{Ex8} from TAT-PDZ1 induced cleavage. Note that the 14 KD band detected in the cytoplasmic fraction is expected to be the transmembrane and the cytoplasmic domain of CAR^{Ex8}, however, no difference in M.wt was noticed possibly due to the small molecular weight (2 KD) of CAR^{Ex8} transmembrane domain.

TAT-PDZ1 peptides induce CAR^{Ex8} extracellular domain shedding

Because the mechanism of RIP is usually preceded by shedding of the extracellular domain (ECD), I tested if the widely expressed membrane metalloprotease ADAM17 would reverse the effect of TAT-PDZ1 peptides and restore the level of CAR^{Ex8}. First, I used nuclear fractionation to see if inhibition of ADAM17 would rescue ripping of CAR^{Ex8}. Strikingly, treatment with selective ADAM17 inhibitor (TIMP3) completely rescued the full length CAR^{Ex8} from TAT-PDZ1 induced CAR^{Ex8} degradation in the cytoplasmic fraction (Figure 30). As was the case with comp E treatments, treatment with TIMP3 ablated the nuclear translocation of the cytoplasmic domain of CAR^{Ex8} (Figure 30A). I further confirmed the role of ADAM17 in TAT-PDZ1 induced CAR^{Ex8} degradation using siRNA that selectively targeted the ADAM17 sequence. Silencing ADAM17 reversed the effect of TAT-E6 on CAR^{Ex8} degradation (Figure 30B). This revealed that ADAM17 and gamma-secretase are the two enzymes by which TAT-PDZ1 induce CAR^{Ex8} degradation.

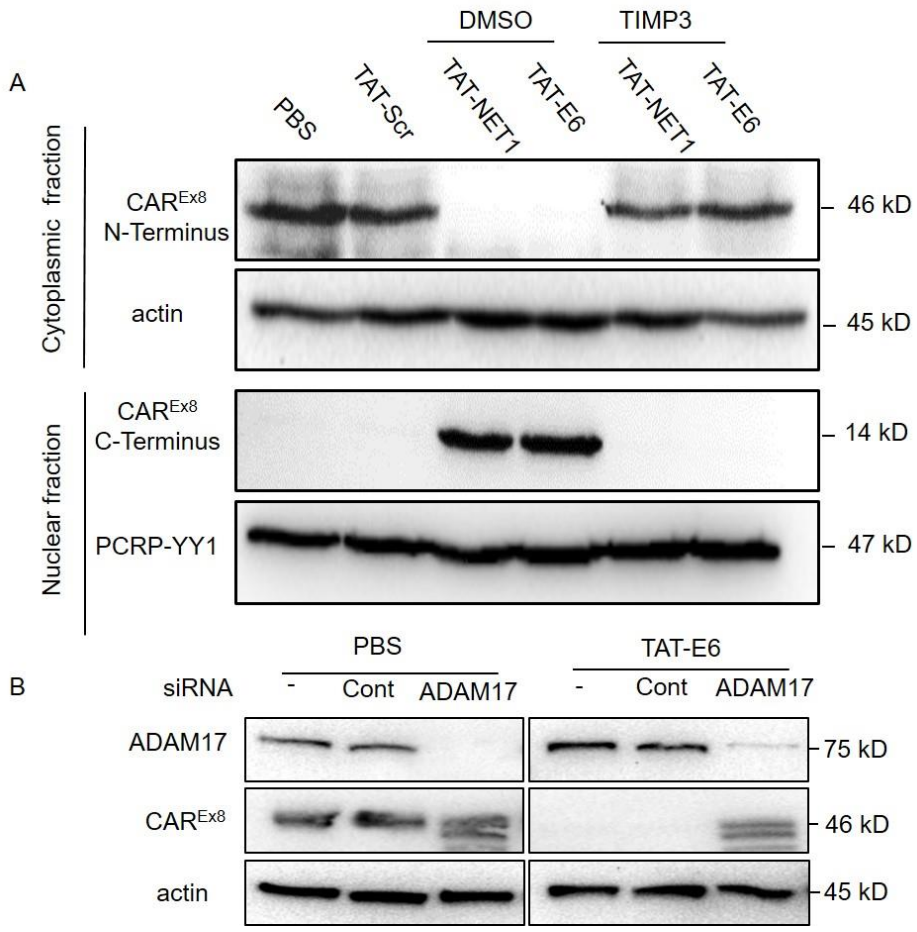

Figure 30. Silencing ADAM17 reverses TAT-PDZ1-induced CAR^{Ex8} degradation.

(A) Selective ADAM17 inhibitor (TIMP3) completely reversed the effect of TAT-PDZ1 peptides in both the cytoplasmic and nuclear fractions and rescued the full length CAR^{Ex8} from degradation. (B) Silencing ADAM17 did not change CAR^{Ex8} levels in the absence of TAT-PDZ1 peptide, but it completely reversed the effect of TAT-PDZ1 peptide compared to control siRNA. N-term Ab: antibody that detects CAR^{Ex8} N-terminal domain (Flag). C-term Ab: antibody that detects CAR^{Ex8} C-terminal domain (5678p). Actin and PCRP-YY1 were used to confirm equal protein loading in the cytoplasmic and nuclear fraction, respectively.

Since ADAM17 (also known as TACE) is required for the TAT-PDZ1 effect in decreasing CAR^{Ex8}, I tested whether TAT-PDZ1 peptides induced CAR^{Ex8} ECD shedding in the extracellular media (hereafter called conditioned media). As expected, TAT-E6 increased Flag- CAR^{Ex8} ECD shedding in the conditioned media of inducible MDCK cells in a dose dependent manner (Figure 31). This corresponded with a decrease in the full length CAR^{Ex8} protein expression in the cell lysate (Figure 31). Similarly, TAT-NET1 increased CAR^{Ex8} ECD shedding in the media, which was corresponded to a decrease in the full length protein level of CAR^{Ex8} in the cell lysate (Figure 32).

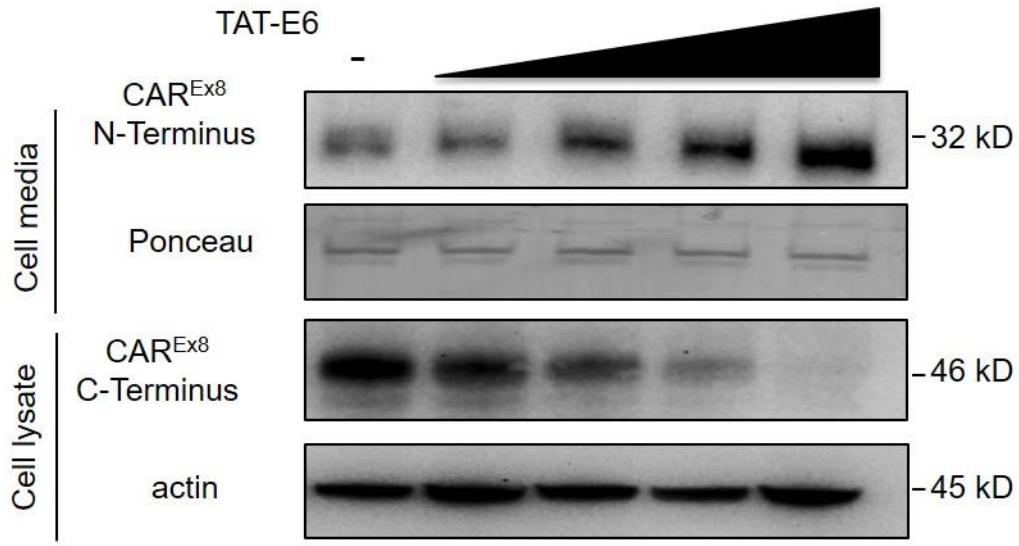

Figure 31. TAT-E6 peptides induce CAR^{Ex8} ectodomain shedding.

TAT-E6 increased CAR^{Ex8} ECD shedding in the cell media in a dose dependent manner. This was corresponded to a decrease in the full length CAR^{Ex8} in cell lysate. MDCK CAR^{Ex8} stable cells were induced with 50 ng/ml Dox after which they were treated with increasing concentrations of TAT-E6 (0-100 µM). N-term AB: antibody that detects CAR^{Ex8} N-terminal domain (Flag). C-term AB: antibody that detects CAR^{Ex8} C-terminal domain. Ponceau staining was used to confirm equal loading.

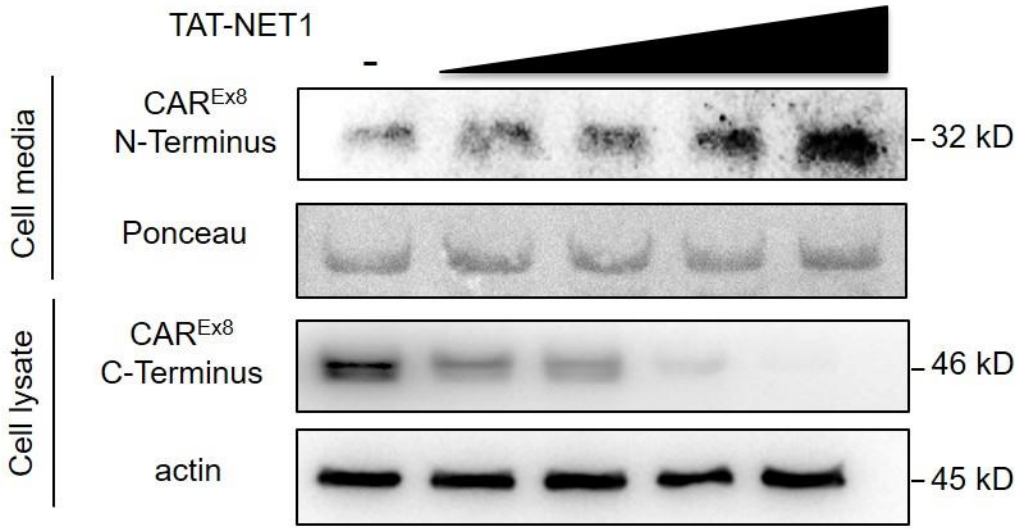

Figure 32. TAT-NET1 peptides induce CAR^{Ex8} ectodomain shedding.

TAT-NET1 increased CAR^{Ex8} ECD shedding in the cell media in a dose dependent manner. This was corresponded to a decrease in the full length CAR^{Ex8} in cell lysate. MDCK CAR^{Ex8} stable cells were induced with 50 ng/ml Dox after which they were treated with increasing concentrations of TAT-NET1 (0-200 μM). N-term AB: antibody that detects CAR^{Ex8} N-terminal domain (Flag). C-term AB: antibody that detects CAR^{Ex8} C-terminal domain. Ponceau staining was used to confirm equal loading.

ADAM17 inhibitor reversed the effect of TAT-PDZ1 peptide and rescued CAR^{Ex8} from degradation

To test the hypothesis that ADAM17 is responsible for CAR^{Ex8} ECD shedding induced by TAT-PDZ1 peptides, epithelial cells were pretreated with increasing concentration of ADAM17 inhibitor (TAPI-1) followed by treatment with TAT-E6. Treatment with TAPI-1 decreased CAR^{Ex8} ECD shedding and rescued the full length CAR^{Ex8} from TAT-PDZ1 mediated degradation (Figure 33). These data suggest that ADAM17 is the mediator through which TAT-PDZ1 peptides induce CAR^{Ex8} degradation.

TAT-PDZ1 peptides increased CAR^{Ex8} degradation is time dependent

I then tested the time course of TAT-PDZ1 action in epithelial cells. Treatment with a single dose (50 μM, 1hr) of TAT-E6 induces CAR^{Ex8} degradation which was terminated after 24 hrs (Figure 34). In the cell media, TAT-E6 increased CAR^{Ex8} ECD shedding which plateaus at 2-24 hrs post-treatment (Figure 34). This indicates that the effect of TAT-PDZ1 peptides on CAR^{Ex8} degradation is fast and lasts for 24 hrs. It also indicates that the CAR^{Ex8} ECD may be quite stable in the media which may imply a long lasting protection from AdV infection due to the shed CAR^{Ex8} ECD in the culture media (see section CAR^{Ex8} shed ECD reduced AdV transduction).

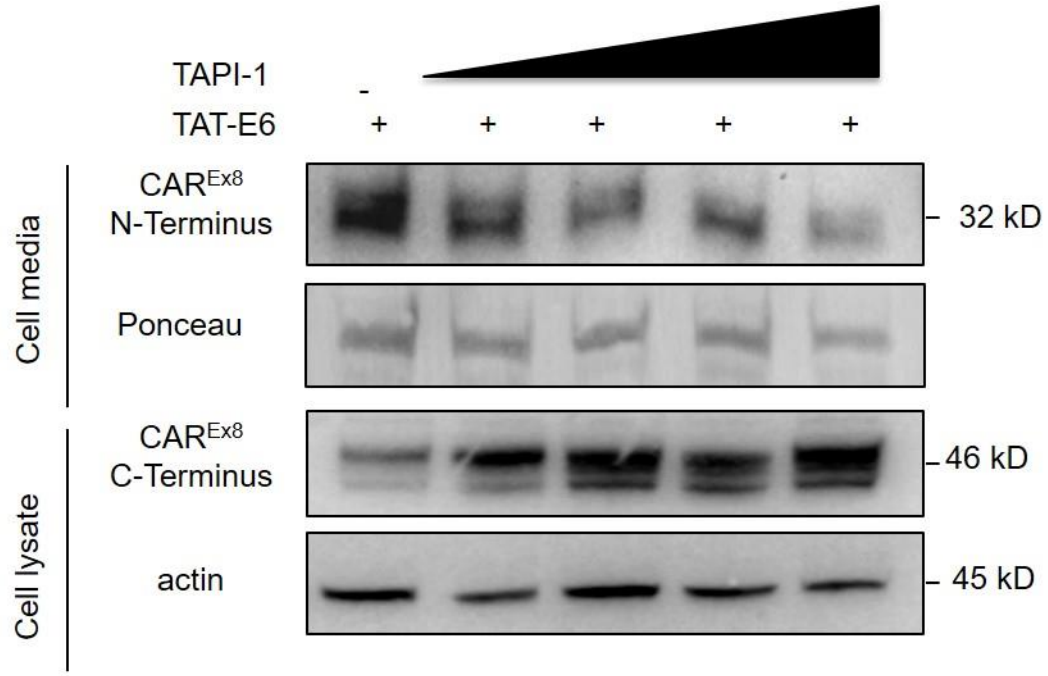

Figure 33. TAT-PDZ1 peptides induce CAR^{Ex8} ectodomain shedding by ADAM17.

ADAM17 inhibitor (TAPI-1) reversed the effect of TAT-PDZ1 on CAR^{Ex8} ECD shedding in a dose dependent manner. MDCK cells were induced with 50 ng/ml Dox and pre-treated with TAPI-1 (0-100 μM). Cells were then treated with TAT-E6 (100 μM).

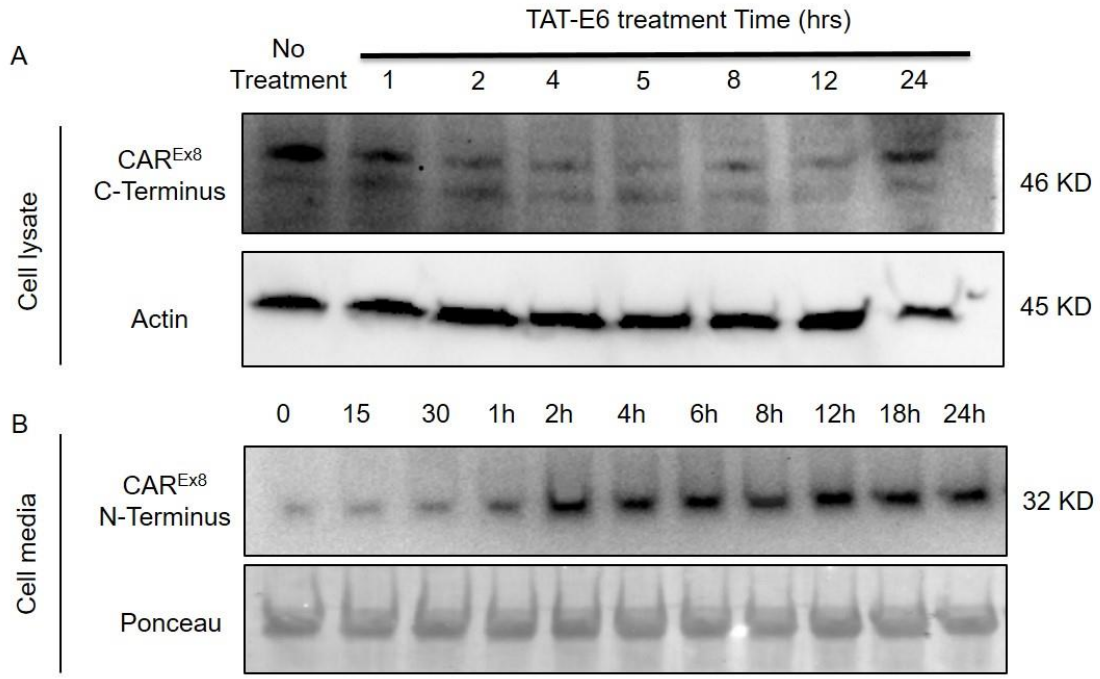

Figure 34. TAT-PDZ1 peptides induce CAR^{Ex8} degradation in a time dependent manner.

MDCK-CAR^{Ex8} epithelia were induced with 50 ng/ml of Dox for 24 hrs, after which Dox was removed. Cells were then treated with 100μM TAT-E6 peptide and cells lysed at different time points. (A) Western immunoblotting for CAR^{Ex8} protein expression in MDCK epithelia over time after single dose of TAT-E6 peptide treatment. CAR^{Ex8} degradation is time dependent and the effect of TAT-E6 was reversed by 24 hrs. (B) Western immunoblotting of CAR^{Ex8} ECD in the media after single dose of TAT-E6 peptides treated MDCK for different time point. CAR^{Ex8} ECD shedding is time dependent and plateau at 2-24 hrs.

TAT-PDZ1 peptides do not induce CAR^{Ex7} shedding

Due to the fact that CAR^{Ex7} and CAR^{Ex8} share the same transmembrane and extracellular domains, it is expected that ADAM17 would also be able to shed CAR^{Ex7} upon treatment with TAT-PDZ1 peptides. Moreover, CAR^{Ex7} has been shown to interact with MAGI-1-PDZ3 domain (150). To be able to differentiate and track the ECD of CAR^{Ex7}, I used inducible MDCK epithelia that overexpress Flag-CAR^{Ex7} upon treatment with Dox (60). In the inducible CAR^{Ex7} MDCK epithelia, TAT-PDZ1 peptides significantly decreased the endogenous protein level of CAR^{Ex8} but did not change the protein level of Flag-CAR^{Ex7} (Figure 35). Moreover, there was no change in the CAR^{Ex7} ECD shedding in the condition media (Figure 35). These data validated the selectivity of the TAT-PDZ1 peptides in targeting the CAR^{Ex8} isoform but not CAR^{Ex7}.

TAT PDZ1 peptides do not change ADAM17 activity

I hypothesized that TAT-PDZ1 peptides would activate ADAM17, which would mediate CAR^{Ex8} shedding followed by RIP. Using a fluorogenic ADAM17 enzyme assay (154), it was shown that there was no significant change in ADAM17 activity upon TAT-PDZ1 peptide treatment (Figure 36). Ionomycin was used as positive control for activating ADAM17 as reported before (159, 160). These data rule out the possibility that TAT-PDZ1 peptides specifically activate ADAM17 to degrade CAR^{Ex8}.

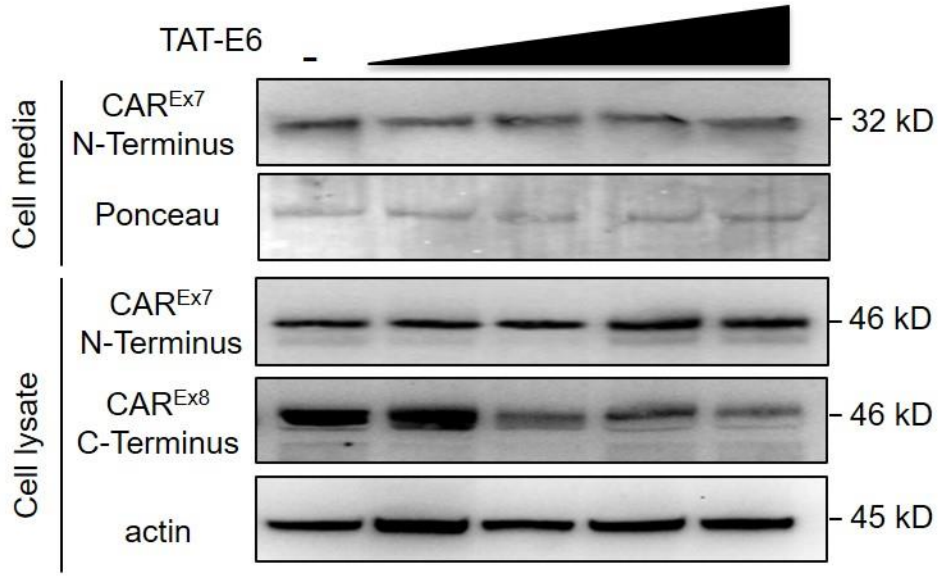

Figure 35. TAT-PDZ1 peptides do not affect CAR^{Ex7} shedding.

MDCK CAR^{Ex8} stable cells were induced with 50 ng/ml Dox after which they were treated with increasing concentrations of TAT-E6 (0-100 μM). No change in CAR^{Ex7} cellular level or ECD domain shedding was noticeable. However, CAR^{Ex8} protein is decreased slightly with increasing doses of the peptides. N-term Ab: antibody that detects CAR^{Ex8} N-terminal domain (Flag). C-term Ab: antibody that detects CAR^{Ex8} C-terminal domain. Ponceau staining was used to confirm equal loading of media.

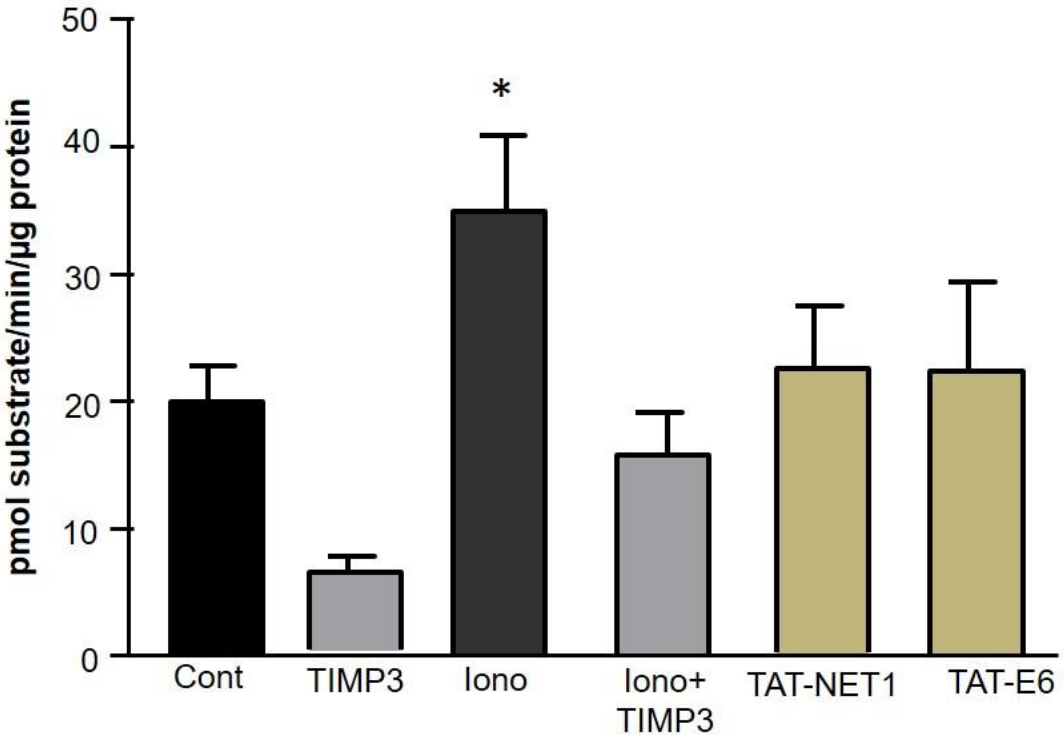

Figure 36. TAT-PDZ1 peptides do not change ADAM17 activity.

Fluorogenic ADAM17 enzyme assay was done as described in the materials and methods. Ionomycin was used as a positive control, and selective ADAM17 inhibitor, TIMP3, was used as a negative control. No significant change in the enzyme activity was observed upon treatment with TAT-PDZ1 peptides, TAT-NET1 or TAT-E6. *P<0.05 compare to control.

ADAM17 interacts with MAGI-1 PDZ2 domain

Another possible hypothesis and explanation of the effect of the peptides is that ADAM17 interacts with MAGI-1 at the same time as CAR^{Ex8}. I tested if ADAM17 and CAR^{Ex8} are present in a complex and whether treatment with TAT-PDZ1 peptides would enhance the affinity/interaction between enzyme and substrate. Cells were transfected with plasmids encoding empty pcDNA3.1 plasmid, ADAM17, and ADAM17 together with each of the isolated myc-tagged PDZ domains of MAGI-1 (PDZ0-5). Immunoprecipitation with a myc-tag specific Ab showed that ADAM17 was co-immunoprecipitated mainly with the MAGI-1 PDZ2 domain (Figure 37). I confirmed these interactions using the direct binding assay between the C-terminus of ADAM17 (TAT-ADAM17-9c) and the purified MAGI-1 PDZ domains. I tested the ability of the purified ADAM17 to interact with each MAGI-1 PDZ domain. A high affinity interaction (Kd = 35 ± 7nM) was detected between the ADAM17 C-term domain and MAGI-1 PDZ2 domain (Figure 38). No interactions were detectable between ADAM17 any other MAGI-1 PDZ domain by binding assay (data not shown). Therefore, MAGI-1 is an essential scaffold protein that can bring ADAM17 and CAR^{Ex8} into the same complex. It is likely that treatment with TAT-PDZ1 peptide enhances the close proximity between the enzyme-substrate complexes, i.e ADAM17-PDZ2 with CAR^{Ex8} -PDZ3 domain of MAGI-1.

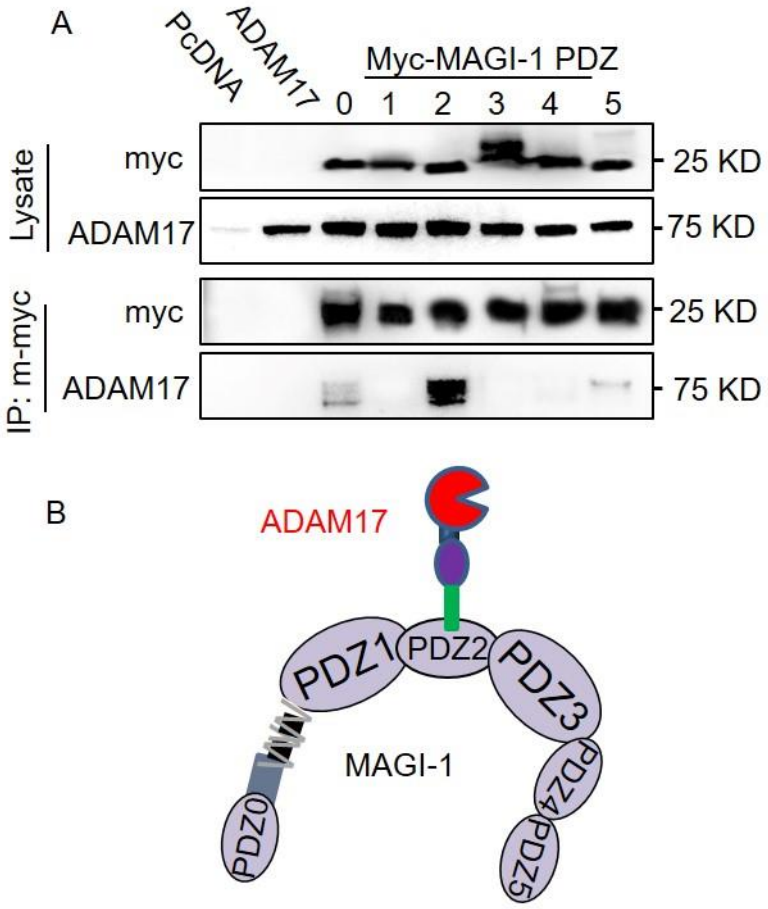

Figure 37. ADAM17 interacts with MAGI-1 PDZ2 domain.

(A) Western immunoblotting showing lysate (top two panels) and immunoprecipitate (bottom two panels) of COS7 cells co-transfected with ADAM17 alone or each myc-tagged MAGI-1 PDZ domain. Transfected cells were immunoprecipitated using myc antibody. ADAM17 was mainly co-immunoprecipitated with MAGI-1 PDZ2 domain. (B) Schematic model of the interaction between MAGI-1 PDZ2 domain and ADAM17.

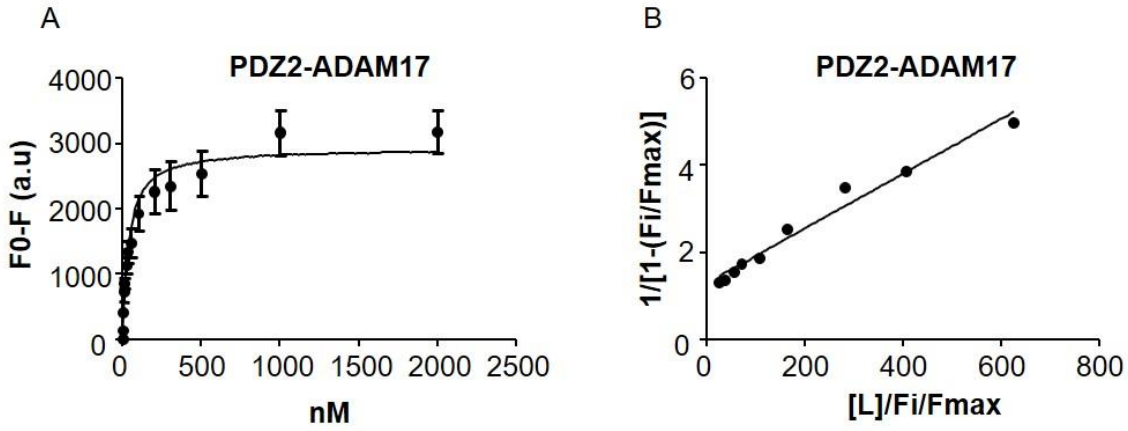

Figure 38. ADAM17 has high affinity interactions with MAGI-1 PDZ2 domain.

(A) Direct binding assay between Cy3 PDZ2 and an ADAM17 C-terminal domain showed a high affinity interaction with Kd= 35±8 nM. (B) Double reciprocal plots showed a linear line demonstrating a single binding site.

TAT-ADAM17-9c reversed the effect of TAT-E6 on CAR^{Ex8} and AdV infection

To further validate the ternary complex hypothesis between MAGI-1, ADAM17, and CAR^{Ex8}, TAT-peptides were designed to target the MAGI-1 PDZ2 domain. Due to of the high affinity interactions between ADAM17 and MAGI-1 PDZ2 domain, the last 9 aa sequence of ADAM17 was synthesized and tagged to TAT (TAT-ADAM17-9c). The effect of TAT-ADAM17-9c on rescuing CAR^{Ex8} from TAT-E6 mediated degradation was tested in MDCK epithelia. Treatment with TAT-ADAM17-9c in the absence of TAT-PDZ1 peptide did not change the level of CAR^{Ex8}, However, TAT-ADAM17-9c rescued the full length CAR^{Ex8} from degradation upon exposure to TAT-E6 in a dose dependent manner (Figure 39). These data further confirmed the hypothesis of ADAM17 binding to MAGI-1 PDZ2 domain is important for CAR^{Ex8} degradation.

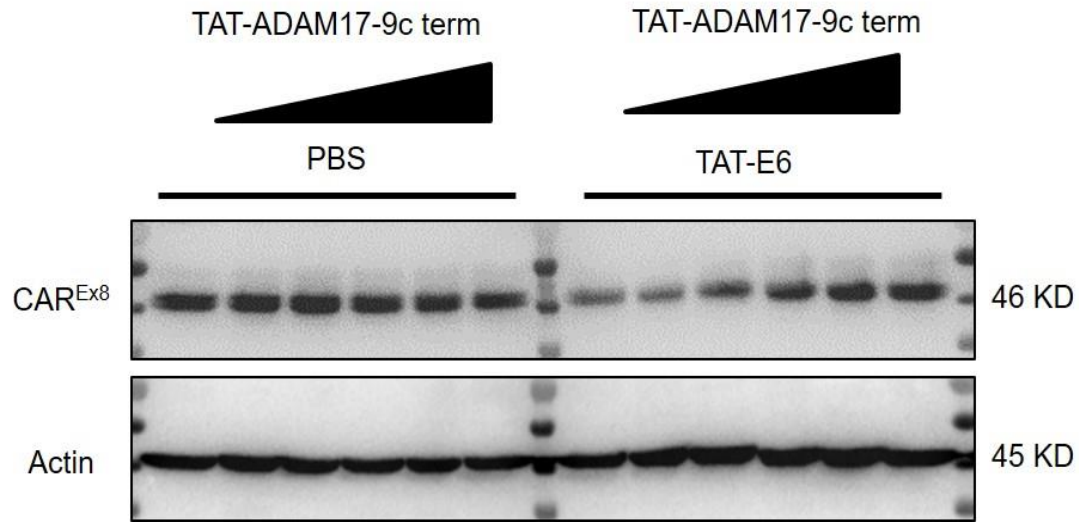

Figure 39. TAT-ADAM17-9c rescues CAR^{Ex8} from TAT-PDZ1 induced degradation.

TAT-ADAM17-9c peptides do not change CAR^{Ex8} under control (basal) conditions. However, it rescues the full length CAR^{Ex8} from TAT-E6 induced degradation in a dose dependent manner. MDCK epithelia were treated with 50µM TAT-ADAM17-9c for 1hr prior to 4hrs treatment with 50µM TAT-E6.

MAGI-1 is an important scaffold protein that brings CAR^{Ex8} in close proximity to ADAM17

To verify the role of MAGI-1 in mediating the effect of CAR^{Ex8} degradation by TAT-PDZ1 peptides, I silenced MAGI-1 by specific siRNA and looked for CAR^{Ex8} expression in the absence or in the presence of TAT-PDZ1 peptides. As shown in Figure 40, the MAGI-1 protein was successfully silenced in both the PBS and the TAT-E6 treated condition. I had expected a potential increase in CAR^{Ex8} proteins upon MAGI-1 silencing, however, CAR^{Ex8} protein expression was not affected by MAGI-1 silencing. As expected, CAR^{Ex8} protein expression was significantly decreased in the TAT-E6 treated conditions and silencing MAGI-1 rescued the full length CAR^{Ex8} from TAT-E6 induced degradation (Figure 40). This shows that MAGI-1 is an important mediator for CAR^{Ex8} degradation by TAT-E6 and supports the ternary complex hypothesis between MAGI-1, CAR^{Ex8}, and ADAM17.

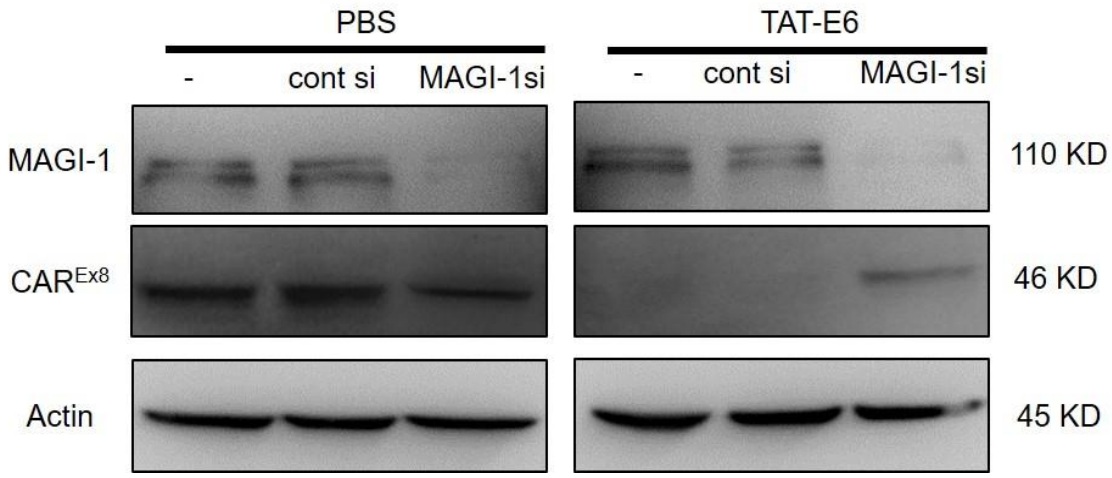

Figure 40. Silencing MAGI-1 reverses the effect of TAT-E6 on CAR^{Ex8} degradation.

SiRNA designed to specifically target MAGI-1 protein were transfected into MDCK epithelia for 72 hrs. Epithelia were treated with either PBS or TAT-E6 for 4-5 hrs before lysing the cells.

CAR^{Ex8} shed ECD reduced AdV infection

It is plausible that the biological significance of the shed CAR^{Ex8} ECD is to act as protective mechanism against AdV entry. Soluble CAR^{Ex8} ECD has been successfully used by many authors to prevent AdV and CVB infection *in vitro* and *in vivo* (161, 162). Conditioned media from Dox-induced MDCK-CAR^{Ex8} epithelia treated with TAT-PDZ1 or scramble peptides was collected and incubated with AdV-GFP before the mixture was added to HeLa cells. HeLa cells are non-polarized, express high levels of CAR^{Ex7} protein that is not susceptible to TAT-PDZ1 peptide, and are readily susceptible to adenovirus infection (See material and methods). Conditioned media from TAT-E6 and TAT-NET1, but not TAT-scramble exposed cells, significantly reduced GFP expression in AdV-GFP infected HeLa cells (Figure 41). To confirm that the decreased AdV transduction was mediated by the shed CAR^{Ex8} ECD, conditioned media from the assigned treated conditions were cleared by immunoprecipitation using Flag antibody prior incubation with AdV-GFP. The mixture was transferred to infect HeLa cells, and AdV transduction was quantitated based on GFP expression. Interestingly, removal of CAR^{Ex8} ECD restored AdV infection in HeLa cells and reversed the effect of the TAT-PDZ1 peptides in the cell media (Figure 41). These data illustrated that TAT-PDZ1 peptides have an indirect long-term therapeutic effect of abolishing AdV by shedding CAR^{Ex8} ECD which acts as decoys, binding to AdV fiber-knob, to prevent AdV entry. To verify the involvement of ADAM17 in the protective CAR^{Ex8} ECD shedding, cells were pre-incubated with either comp E or TIMP3 before treatment with the peptides, and conditioned media was collected and tested for its ability to abolish AdV transduction. Consistent with only a partial inhibition of RIP of the cytoplasmic domain by gamma-

secretase, pre-incubation with comp E did not affect AdV transduction. By contrast, the ADAM17 inhibitor TIMP3 completely reversed the effect of TAT-PDZ1 peptides and restored AdV infection (Figure 41).

To further confirm the ability of CAR ECD to abolish AdV infection, CAR-FC protein (which is a purified form of CAR ECD) was incubated with different MOI of AdV in cell culture media before infecting HeLa cells. Whereas conditioned media from cells treated with PBS demonstrated a dose dependent increase in AdV-GFP infection, addition of CAR-FC to PSB-pre-incubation media could partially block the increase of infection. Conditioned media from cells treated TAT-E6 significantly decreased AdV-GFP transduction but could be partially overcome by high doses of AdV (MOI 100) (Figure 42). Consistent with previous results, ADAM17 inhibition reversed the effect of TAT-E6 and restored the AdV infection (Figure 42). This suggests that the shed CAR^{Ex8} ECD can act as decoy to bind AdV and protect epithelia from AdV infection.

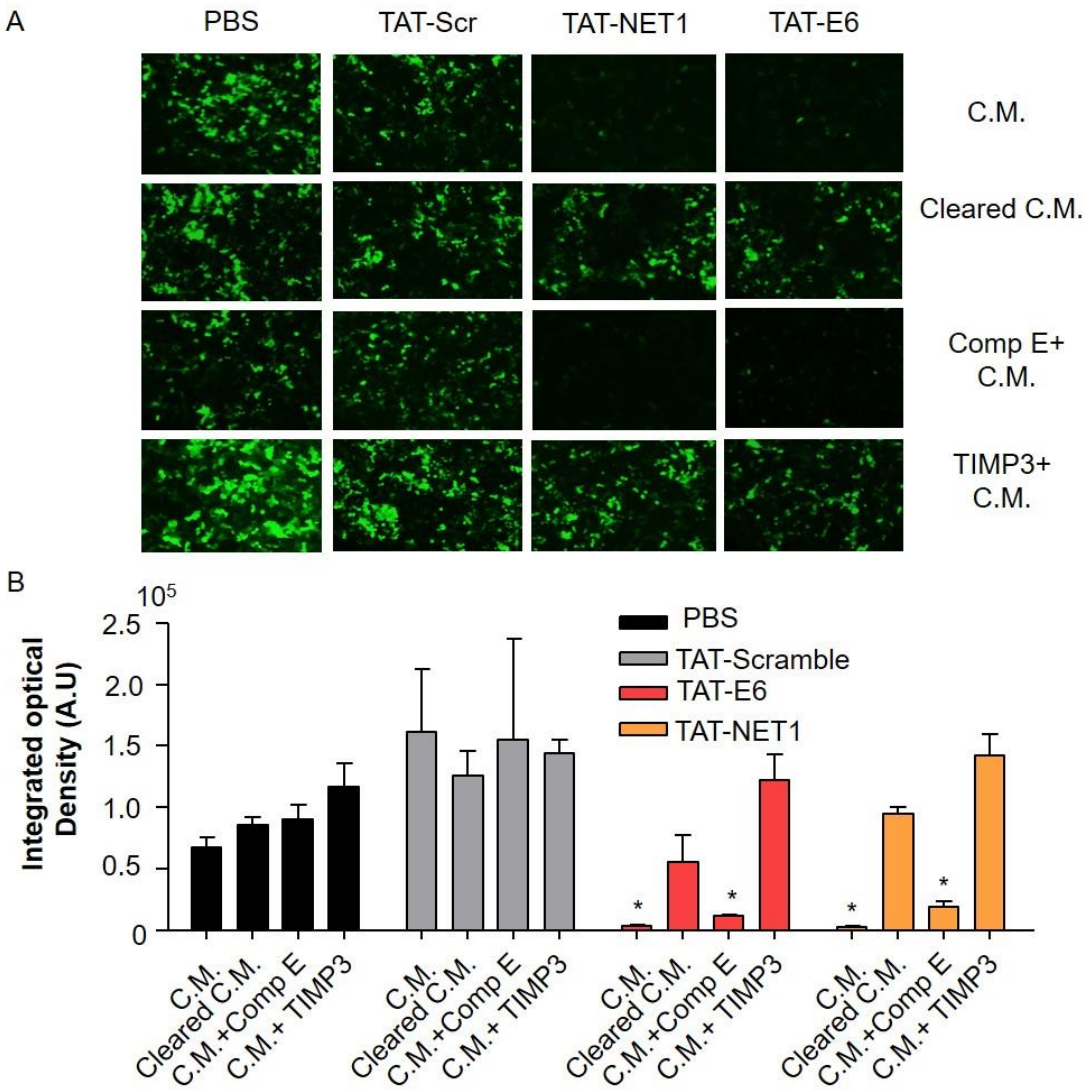

Figure 41. Shed CAR^{Ex8} Extracellular domain (ECD) decreases AdV infection.

MDCK-CAR^{Ex8} cells were induced with 50 ng/ml Dox O/N. Cells were treated with vehicle, TAT-Scr, or TAT-PDZ1 peptide for 4 hrs after which the C.M. were collected, precleared, and incubated with AdV-GFP (MOI 100) for 30 min at 37ºC. HeLa cells were then infected with the mixture for 1 hr at 37 ºC. (A) GFP-expression in HeLa cells infected with AdV-GFP incubated with conditioned media (C.M.) of MDCK cells treated with either TAT-Scr or TAT-PDZ1 peptides. Notice the decrease in AdV entry

with C.M media from TAT-PDZ1 peptides (first row). Pre-clearing CAR^{Ex8} ECD from C.M. by IP (second row), restored the AdV infection in HeLa cells. Pretreatment of inducible MDCK cells with gamma-secretase inhibitor (Compound E, Comp E; third row) did not reverse the effect of TAT-PDZ1 treatment, however, pre-treatment with ADAM17 inhibitor (TIMP3; forth row) did reverse the effect of C.M. from TAT-PDZ1. (B) Quantitation of the GFP expression in HeLa cells. Quantitation was done by Metamorph® 24 hrs post infection as described in the materials and methods, $*p < 0.05$ compared to PBS.

A

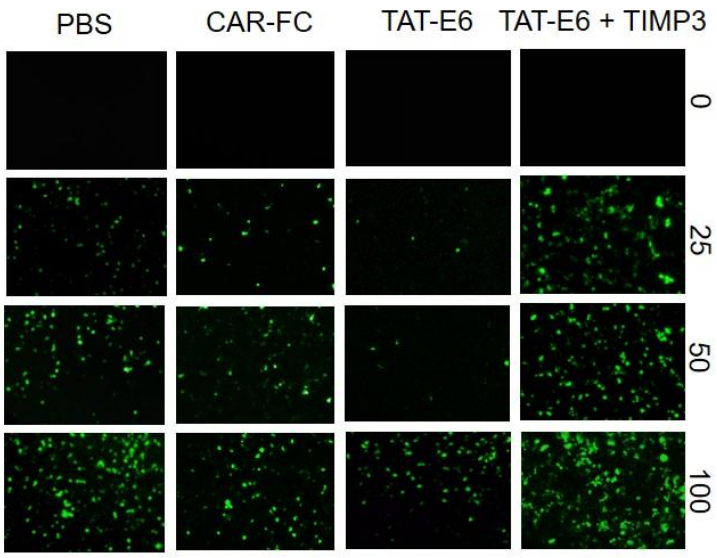
PBS
CAR-FC
TAT-E6
TAT-E6 + TIMP3
0
25
50
100

B

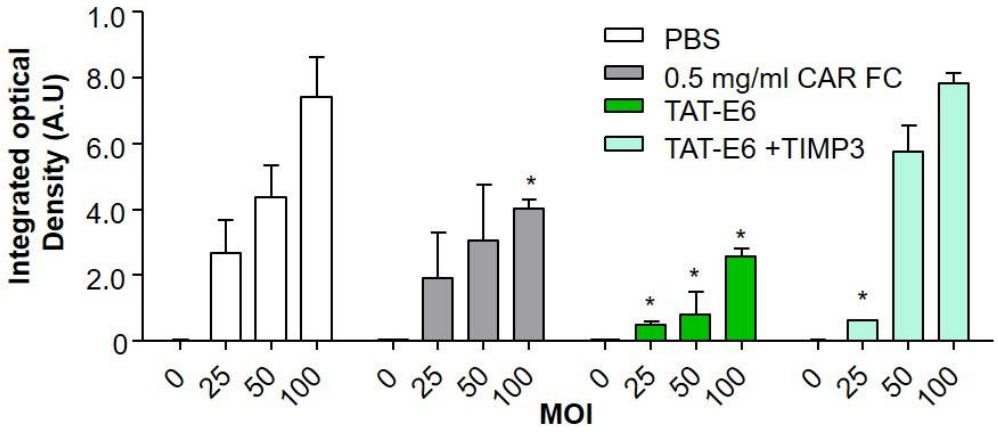
Integrated optical Density (A.U)
1.0
8.0
6.0
4.0
2.0
0
PBS
0.5 mg/ml CAR FC
TAT-E6
TAT-E6 +TIMP3
*
0
25
50
100
MOI

Figure 42. CAR^{Ex8} ECD decreases AdV infection.

Stable MDCK CAR^{Ex8} cells were induced with 50 ng/ml Dox O/N prior to treatment with vehicle, TAT-Scr, TAT-PDZ1-E6 peptide, or a combination of TAT-E6 and ADAM17 inhibitor TIMP3, for 4 hrs. Conditioned media (C.M.) was collected, precleared, and incubated with AdV-GFP (MOI 100) for 30 min at 37 ºC. HeLa cells were then infected with the mixture for 1 hr at 37 ºC. (A) GFP-expression in HeLa cells infected with AdV-GFP incubated with C.M. taken from MDCK cells or soluble CAR EDC (CAR-Fc, 1 mg/ml). AdV-GFP infection was done at MOI 0, 25, 50, 100. (B) Quantitation of GFP expression in HeLa cells infected in (A). Quantitation was done by Metamorph® 24 hrs post infection as described in the materials and methods, *$p < 0.05$ compared to PBS.

TAT-PDZ1 peptides do not change epithelial integrity

I tested if TAT-PDZ1 binding peptides alter epithelial integrity by two approaches. First, epithelial cells were seeded onto millicells and treated with a 50 μM dose of TAT-PDZ1 peptides, TAT-scramble, or vehicle (PBS) every day over a period of 14 days. Trans-epithelial resistance (TER) measurements were taken every other day to determine if TER reading would increase. An increase in TER indicates the formation of tight junctions and an epithelium. Continuous treatment with PDZ1 peptides did not alter the formation of an epithelium and epithelial integrity as showed by TER measurements (Figure 43). The second approach involved measuring the epithelial integrity by a FITC-dextran diffusion assay. FITC-dextran was added to the apical surface of the epithelia and basolateral media collected and measured for FITC-dextran an hour later. No difference in the permeability of FITC-Dextran 70 KD was noticed between treated and untreated conditions (Figure 44). Similarly, no difference in the diffusion of FITC dextran 4 KD (Figure 45A) across the epithelial cells was observed upon TAT-PDZ1 treatment as compared to control treatment. To further confirm that this effect was due to intact tight junctions, cells were treated with 8 mM EDTA for 10 min, followed by peptide treatment and FITC-Dextran 4 KD diffusion assay. As expected, pretreatment with EDTA increased FITC-Dextran 4 KD diffusion in all conditions equally (Figure 45). Taken together, these data illustrate the safety of the TAT-PDZ1 peptide in reducing AdV transduction without changing the epithelial integrity.

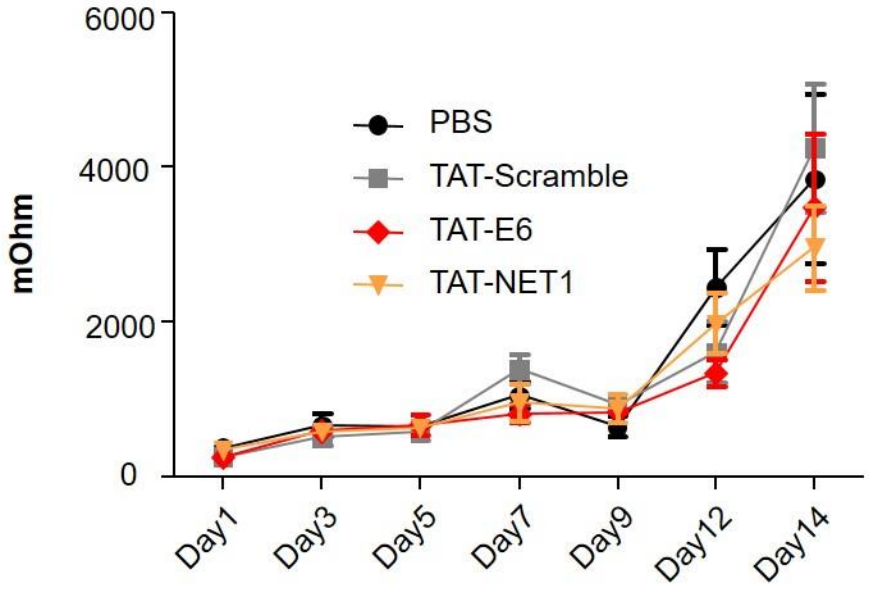

Figure 43. TAT-PDZ1 peptides do not change Transepithelial resistance.

HAE cells were treated apically with single dose of PBS, TAT-scramble (50µM; for 4hrs) or TAT-PDZ1 peptides (50µM; for 4hrs) daily for 14 days. Transepithelial resistance (TER) was taken every other day for 14 days. No change in TER was noticeable upon treatment with TAT-PDZ1 peptides. Each condition represents the average of 4 replicates.

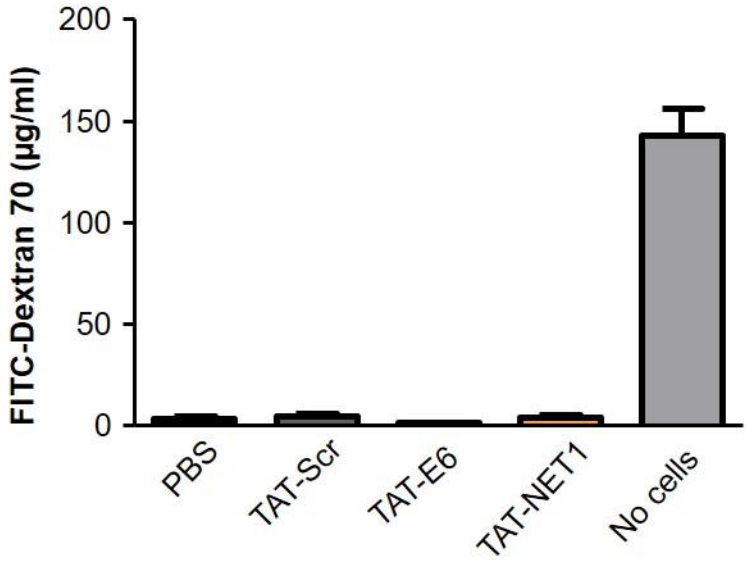

Figure 44. TAT-PDZ1 peptides do not change FITC-Dextran 70 KD permeability across epithelia.

HAE cells were treated with single dose of PBS, TAT-scramble (50µM; for 4hrs) or TAT-PDZ1 peptides (50µM; for 4hrs) daily for 14 days. FITC-Dextran 70 diffusion across treated epithelia in the presence or absence of EDTA. There was no difference in Dextran 70 KD diffusion among treatments. FITC-Dextran 70 was added from the apical membrane and the diffused Dextran was collected from the basolateral media, measured and quantified as described in the material and methods. Assay was performed by the 14^{th} day of peptide treatment.

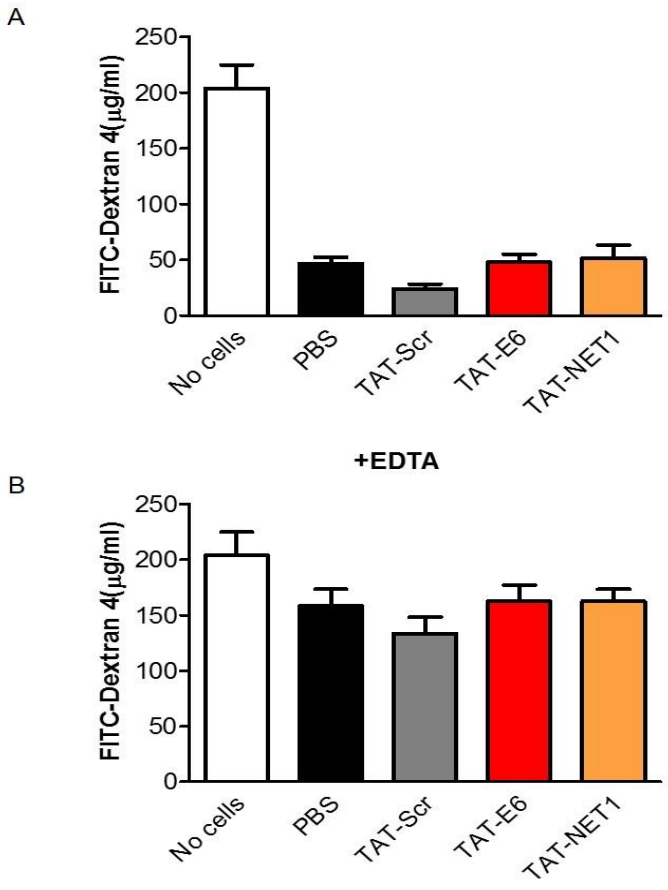

Figure 45. TAT-PDZ1 peptides do not change FITC-Dextran 4 kD permeability across epithelia.

HAE cells were treated apically with single dose of PBS, TAT-scramble (50µM; for 4hrs) or TAT-PDZ1 peptides (50µM; for 4hrs) daily for 14 days. FITC-Dextran 4 diffusion across treated epithelia in the presence or absence of EDTA. There was no difference in Dextran 4 kD diffusion among treatments. Pre-treatment with EDTA increased Dextran 4 kD permeability in all conditions. FITC-Dextran 4 kD was added from the apical membrane and the diffused Dextran was collected from the basolateral media, measured and quantified as described in the material and methods. Assay was performed at the 14th day of peptide treatment.

Conclusions

The data presented elucidate new potential therapeutics that protect polarized epithelia from AdV infection. The newly proposed MAGI-1 PDZ1 domain blockers resulted in decreased CAR^{Ex8} and suppression of AdV infection. Moreover, the results illustrated the mechanism by which the PDZ1 peptides degrade CAR^{Ex8} and decrease AdV infection. Regulated intramembrane proteolysis (RIP) was implicated as the mechanism involved in decreasing the level of CAR^{Ex8} and also induction of extracellular domain (ECD) shedding of CAR^{Ex8} followed by localization of the cytoplasmic domain to the cell nucleus. Furthermore, I described a new novel interaction mechanism between ADAM17 and MAGI-1 PDZ2 domain. This interaction can be used to regulate ADAM17 expression and activity, which can potentially be exploited to treat many disease conditions. A model figure of the proposed molecular mechanism of action of TAT-PDZ1 peptides is shown in (Figure 46). TAT-PDZ1 peptides bind the MAGI-1 PDZ1 domain, shifting more CAR^{Ex8} to interact with MAGI-1 PDZ3 domain. ADAM17, which interacts mainly with MAGI-1 PDZ2 domain, cleaves the CAR^{Ex8} ECD. The γ- secretase then cleaves CAR^{Ex8} from the cytoplasmic domain which is translocated to the nucleus. CAR^{Ex8} extracellular domain is trafficked to the apical membrane where it is shed or released to the extracellular compartment and acts as decoys that bind and neutralize AdV.

My data showed that treatment with TAT-PDZ1 peptides but not TAT-PDZ3 (see next section) caused cleavage of CAR^{Ex8} by ADAM17 (resides in MAGI-1 PDZ2

domain). The exact reason for that is not currently known but one possibility is that that distance between MAGI-1 PDZ2 and PDZ3 is shorter than that between MAGI-1 PDZ1 and PDZ2. The three dimensional orientation of each MAGI-1 PDZ domain as well as the active site of ADAM17 is also an important factor to consider, especially with the presence of the hinge region in the extracellular domain within ADAM17 structure. Further experiments needed to clearly elucidate the exact mechanism. My data also showed that ADAM17 cleavage is CAR^{Ex8} specific and did not affect the level of CAR^{Ex7}. This could be due to the different localization of the two isoforms in polarized epithelia. Also the two isoforms differ only in the extreme C-term domain with CAR^{Ex7} contains 13 aa more. This may have caused different mode of interactions between the two isoforms and MAGI-1.

The mechanism of protection of TAT-PDZ1 against AdV infection is shown in another model (Figure 47). In the absence of CAR^{Ex8}, the airway epithelia are resistant to AdV entry (Figure 47A). If CAR^{Ex8} is present at the apical surface, it increases AdV entry which can accelerate AdV replication by having more AdV per cell (Figure 47B). Treatment with TAT-PDZ1 peptides decreased the level of CAR^{Ex8} and prevents AdV entry thereby protecting the cells from AdV infection (Figure 47C). In addition, the shed CAR^{Ex8} ECD generated upon TAT-PDZ1 peptides can act as decoys and decrease the deleterious effect of AdV on the epithelium (Figure 47D).

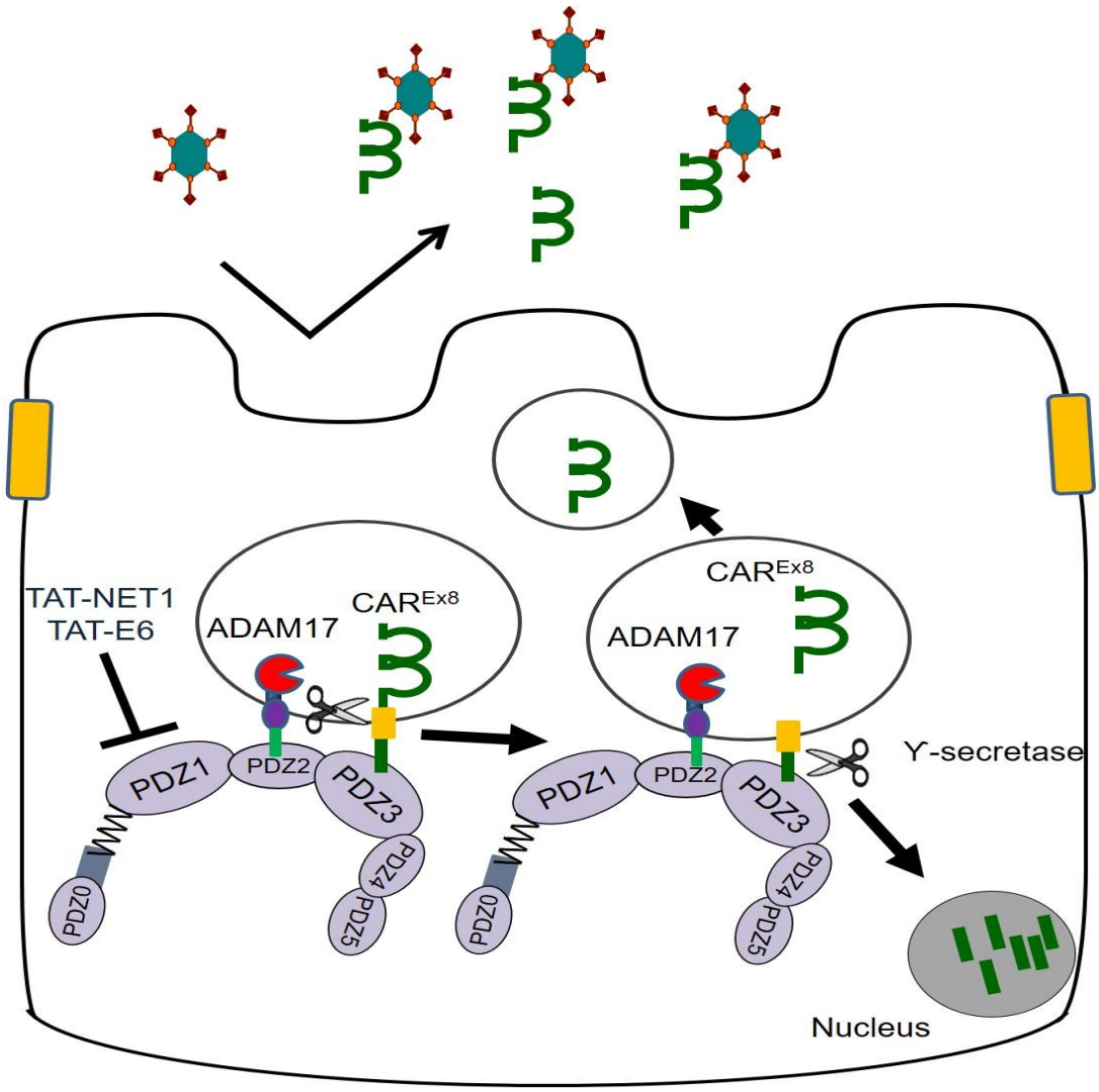

Figure 46. Schematic of TAT-PDZ1 peptide mediated decrease of AdV entry into polarized epithelia.

TAT-E6 and TAT-NET1 block MAGI-1 PDZ1 shifting CAR^{Ex8} to interact with MAGI-1 PDZ3 domain. ADAM17 interacts with MAGI-1 PDZ2 domain and cleaves CAR^{Ex8} ECD. The shed CAR^{Ex8} ECD interacts with and prevents incoming AdV from entry. Gamma secretase cleaves the CAR^{Ex8} from the cytoplasmic domain region which translocate into the nucleus.

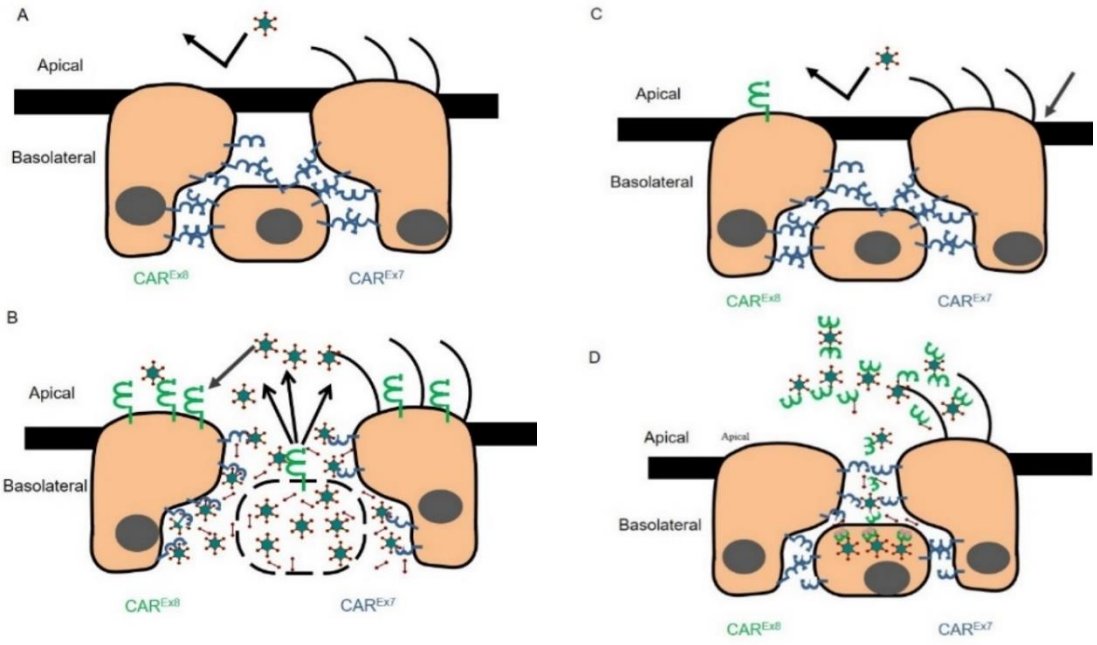

Figure 47. Model of protective mechanism of the TAT-PDZ1 peptides against AdV infection in human epithelium.

(A) In the absence of CAR^{Ex8}, epithelia are protected from AdV entry by the tight junctions which separate the apical and basolateral membrane. (B) In the presence of CAR^{Ex8} AdV enters and replicates in the epithelium, which disrupts the adherent and the tight junctions. (C) TAT-PDZ1 peptides decrease the number of CAR^{Ex8} in the cells which decreases the possibility of AdV entry. (D) TAT-PDZ1 peptides also induce CAR^{Ex8} ECD shedding which acts as a decoy to protect epithelium from AdV infection.

CHAPTER 4: Investigation of the effect and molecular mechanism of TAT-PDZ3 peptides on CAR^{Ex8} stability and Adenovirus infection

Rationale

Many of the steps that regulate the pathway through which newly synthesized CAR^{Ex8} reaches the apical membrane remain unclear. By contrast, basolateral localization of CAR^{Ex7} is known to require interactions with the clathrin adaptor proteins AP-1A and AP-1B (61, 163). The discovery of MAGI-1 as a master regulator of CAR^{Ex8} protein levels prompted screening for drug therapeutics that could enhance AdV mediated gene therapy by enhancing AdV binding and entry into epithelia. Such therapeutics could also be used to diminish the possibility of side effects mediated by high AdV dose required for therapeutic gene expression. The interactions between CAR^{Ex8} and MAGI-1 are mediated by the PDZ binding domain found at the extreme C-terminus of CAR^{Ex8} and the PDZ domains within MAGI-1 that can be modulated by cell permeable peptides.

The Rab family of small G proteins plays an important role in protein trafficking, including defining vesicular cargo destined for apical localization (164, 165). Individual Rabs can serve as markers for intracellular trafficking (164), which can be used to determine the pathway responsible for CAR^{Ex8} trafficking. Such knowledge would allow us to broaden our strategies by developing therapeutics that target CAR^{Ex8} at a specific cellular compartment in order to enhance AdV mediated gene therapy.

The main objective of this chapter is to test the hypothesis that cell permeable peptides that bind the MAGI-1 PDZ3 domain can act as decoys and rescue full length CAR^{Ex8} from MAGI-1 PDZ3 domain-mediated degradation. Increased CAR^{Ex8} at the apical surface of polarized human epithelia can potentially enhance AdV-mediated gene delivery in patients with genetic and acquired diseases such as cystic fibrosis, chronic obstructive pulmonary disease (COPD), and cancer. These peptides might also behave effectively as adjuvants to improve AdV-mediated vaccination strategies.

Results

TAT-PDZ3 peptides bind selectively to MAGI-1 PDZ3

We have previously shown that CAR^{Ex8} interacts with both the MAGI-1 PDZ3 and PDZ1 domains, however, CAR^{Ex8} has higher affinity for PDZ3 (63). I hypothesized that blocking the interactions between both MAGI-1 domains may be equivalent to blocking only the PDZ3 domain. To test this hypothesis and to design blockers that are specific for MAGI-1 PDZ3, we searched for interacting partners with the MAGI-1 PDZ3 domain, and no other MAGI-1 domains. ESAM is a protein that is known to selectively interact with only the MAGI-1 PDZ3 domain through its PDZ binding domain (139). The last 9 amino acids of both CAR^{Ex8} and ESAM proteins were synthesized and tagged with TAT cell permeable peptides as described in methods and chapter 3. The selectivity of TAT-CAR^{Ex8}-9c and TAT-ESAM toward the MAGI-1 PDZ3 domain was tested by direct binding assay using purified peptide and Cy3-labeled MAGI-1 PDZ domains. As shown in Figure 48, and as expected, TAT-CAR^{Ex8}-9c interacts with MAGI-1 PDZ1 domain (Kd = 23 ± 10 nM), however, it interacts with higher affinity with MAGI-PDZ3 (Kd = 4 ± 2 nM). Both interactions were confirmed to be single point interactions by the double reciprocal plot which showed a linear correlation (Figure 48). TAT-ESAM does not interact with MAGI-PDZ1 domain (Figure 49) but it interacts with MAGI-1 PDZ3 domain (Kd = 17 ± 5 nM) (Figure 49). These data show the high affinity binding of the TAT-PDZ3 peptides toward MAGI-1 PDZ3 domain.

The PDZ binding domain of TAT-CAR^{Ex8}-9c is required to rescue CAR^{Ex8} protein from degradation

In order to test the specificity of TAT-CAR^{Ex8}-9c toward MAGI-1 induced CAR^{Ex8} degradation and its effect on AdV transduction, TAT-CAR^{Ex8}-9c peptides with mutated PDZ binding domain (TAT-CAR^{Ex8}AA-9c) were synthesized. MDCK epithelia were treated with either TAT-CAR^{Ex8}-9c or TAT-CAR^{Ex8}AA-9c. In contrast to TAT-CAR^{Ex8}AA-9c, which did not change the protein level of CAR^{Ex8}, TAT-CAR^{Ex8}-9c peptides increased CAR^{Ex8} compared to control (Figure 50). The increase in CAR^{Ex8} corresponded to an increase in AdV genome transduction (Figure 50) as well as AdV gene expression as assessed by Ad-β-gal assay (Figure 50).

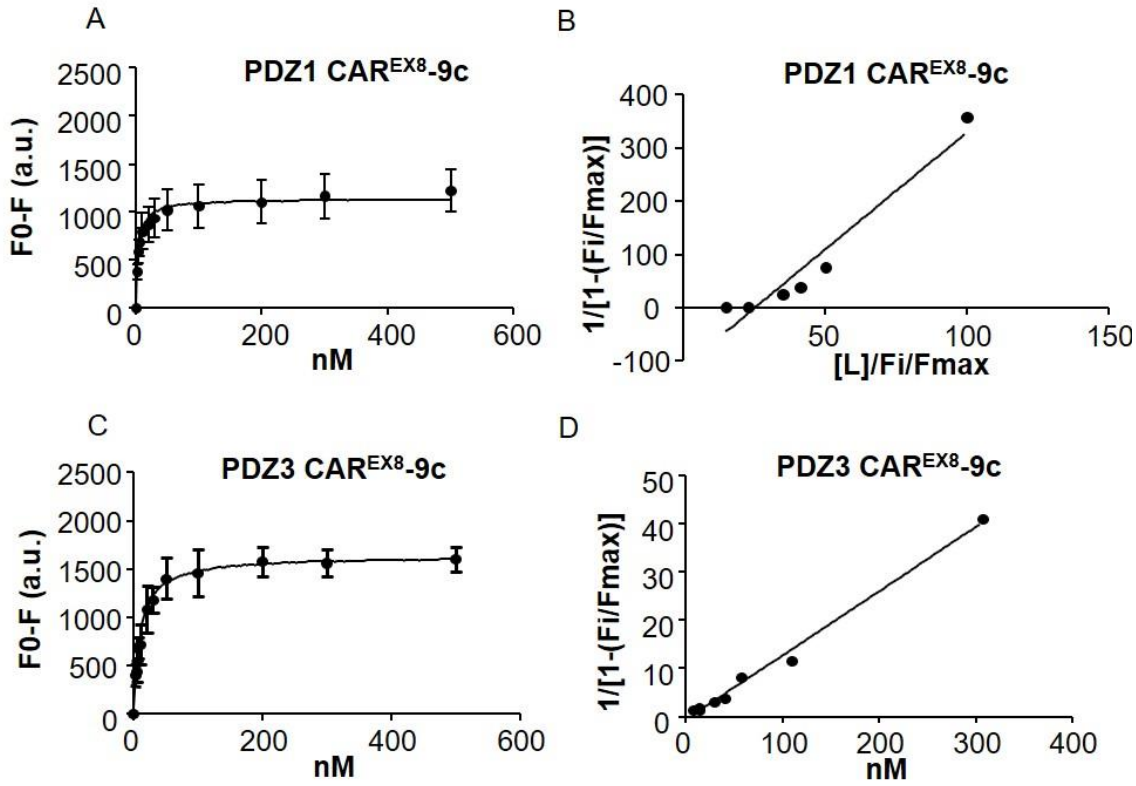

Figure 48. TAT-CAR^{Ex8}-9c binds to both MAGI-1 PDZ1 and PDZ3 domains.

Ligand binding assay between TAT-CAR^{Ex8}-9c and the purified MAGI-1 PDZ1 or PDZ-3. MAGI-1 PDZ2 domain was used as a control. TAT-CAR^{Ex8}-9c peptides binds to MAGI-1 PDZ1 (A, B; Kd= 23 ±9), and binds PDZ3 with higher affinity (C, D; Kd= 4± 2). B, D) Double reciprocal plot is linear indicating a single binding site between the ligand and PDZ3 (D) but not PDZ1 domain (B)

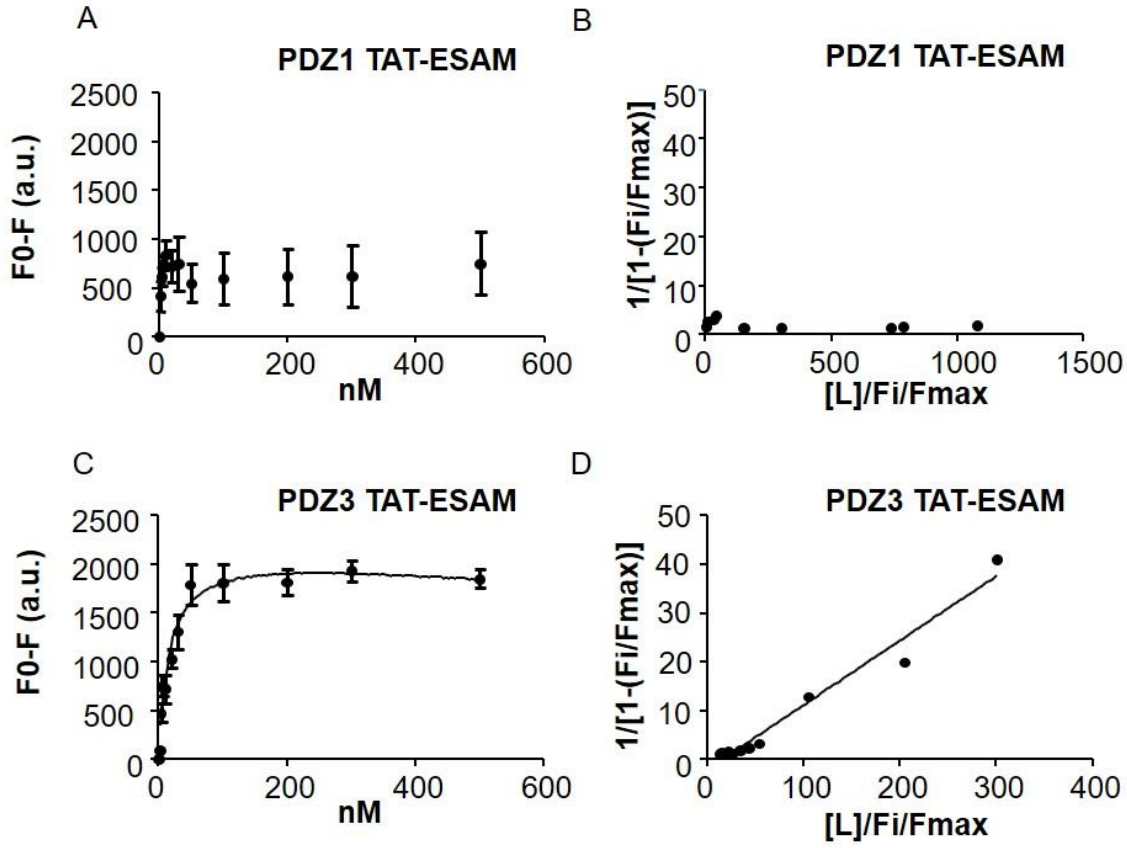

Figure 49. TAT-ESAM, a PDZ3 binding peptide, binds selectively to the MAGI-1 PDZ3 domain.

Ligand binding assay between TAT-ESAM and purified MAGI-1 PDZ1 or PDZ-3. TAT-ESAM peptide does not bind to MAGI-1 PDZ1 (A, B) but does binds PDZ3 (C, D; Kd= 17± 5). Double reciprocal plot shows (B) no curve indicating no binding to PDZ1 or (D) is linear indicating a single binding site between the ligand and PDZ3.

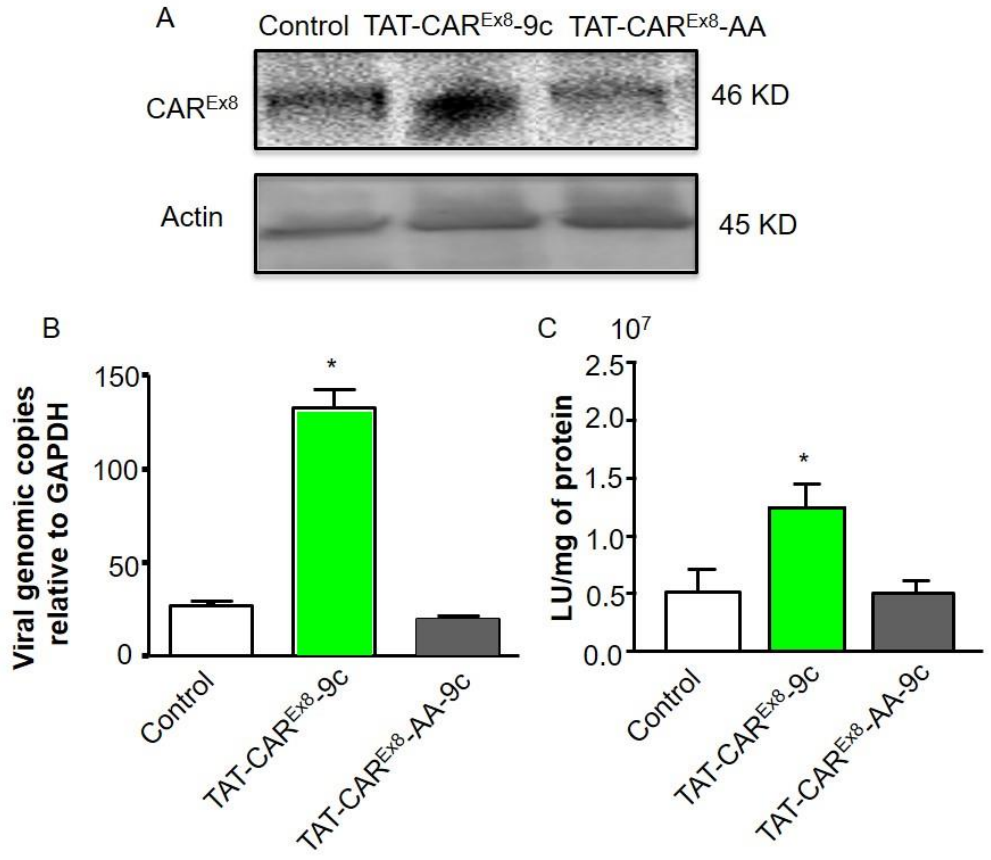

Figure 50. TAT-CAR^{Ex8}-9c increases apical CAR^{Ex8} and AdV transduction.

(A) Western blotting of MDCK cells treated with either TAT-CAR^{Ex8}-9c or control TAT-CAR^{Ex8}AA-9c. A marked increase in CAR^{Ex8} protein level was seen in the TAT-CAR^{Ex8}-9c treatment but not the mutated peptides. (B) QPCR of the AdV viral genome showed a significant increase in the AdV genomic transduction after TAT-CAR^{Ex8}-9c treatment condition as compared to controls. (C) AdV-β-gal assay of MDCK epithelia treated with TAT-CAR^{Ex8}-9c or control peptides. TAT-CAR^{Ex8} -9c treatment significantly increased the AdV-β-gal transduction compared to control peptide. *P<0.05 compared to control or TAT-CAR^{Ex8}AA-9c.

To further confirm that the increased CAR^{Ex8} is mainly due to blocking the MAGI-1 PDZ3 domain, MDCK epithelia were treated with TAT-ESAM which binds solely to MAGI-1 PDZ3. Interestingly, CAR^{Ex8} protein level was markedly and similarly increased in TAT-CAR^{Ex8}-9c and TAT-ESAM treated conditions (Figure 51), indicating that the effect is mediated by peptides binding to MAGI-1 PDZ3 domain. Consistent with the previous data, the increase in CAR^{Ex8} corresponded to an increase in the AdV genome entry and transduction as measured by AdV-β-gal gene expression (Figure 51). The same experimental approach was done in primary HAE and cotton rat epithelial cells (an animal model for AdV pathogenicity). In HAE, CAR^{Ex8} was increased in TAT-ESAM and TAT-CAR^{Ex8}-9c treated conditions. This corresponded to an increase in AdV entry (viral genomes) and transduction (AdV-β-Gal assay) (Figure 52). Consistent with the HAE, TAT-PDZ3 peptide treatment also increased CAR^{Ex8} protein as well as AdV-β-gal transduction in cotton rat epithelium as compared to control peptides (Figure 53). These data suggest that TAT-PDZ3 peptides bind MAGI-1 PDZ3 which increases apical CAR^{Ex8} protein and promotes AdV transduction.

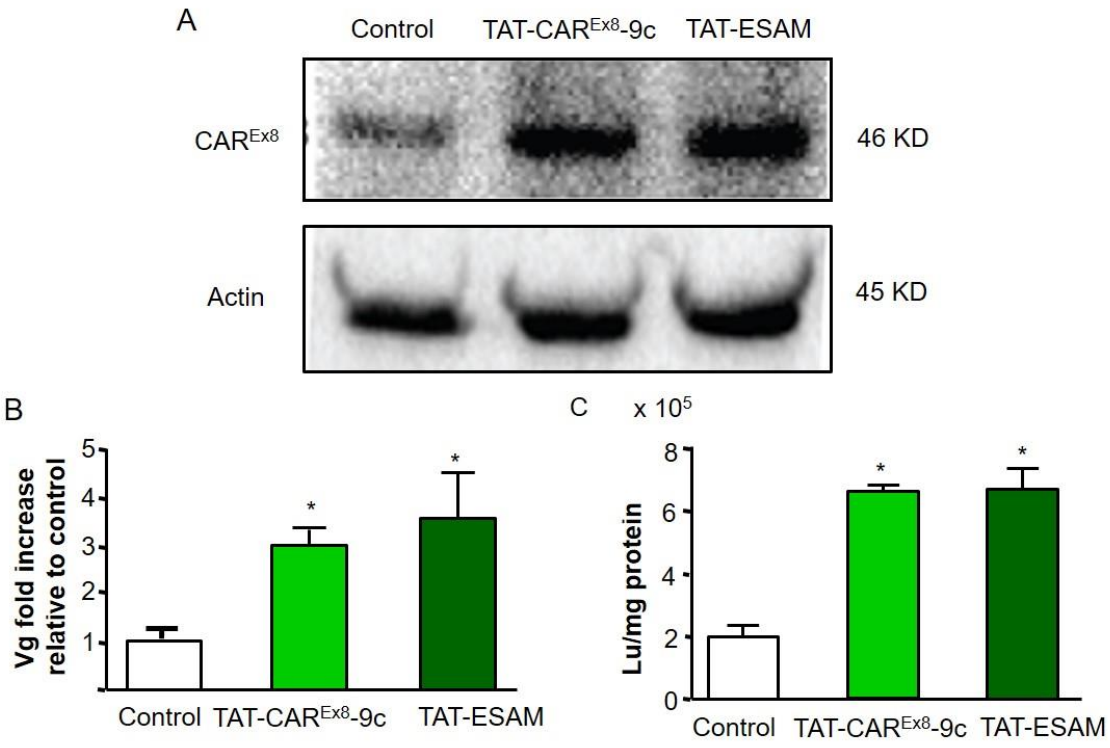

Figure 51. TAT-CAR^{Ex8}-9c and TAT-ESAM increase apical CAR^{Ex8} and AdV transduction.

(A) Polarized MDCK cells were treated with either TAT-CAR^{Ex8}-9c or TAT-ESAM and subjected to western blotting for CAR^{Ex8} protein. Actin was used to confirm equal protein loading. (B) QPCR for Ad viral genome showed a significant increase in the AdV genomic transduction in the TAT-CAR^{Ex8}-9c and TAT-ESAM treatment condition as compared to control (PBS). (C) AdV-β-gal assay of MDCK epithelia treated with TAT-CAR^{Ex8}-9c, TAT-ESAM, or control peptides. Both TAT-CAR^{Ex8} -9c and TAT-ESAM treatment significantly increased the AdV-β-gal transduction compared to control peptide. *$p < 0.05$ compare to control.

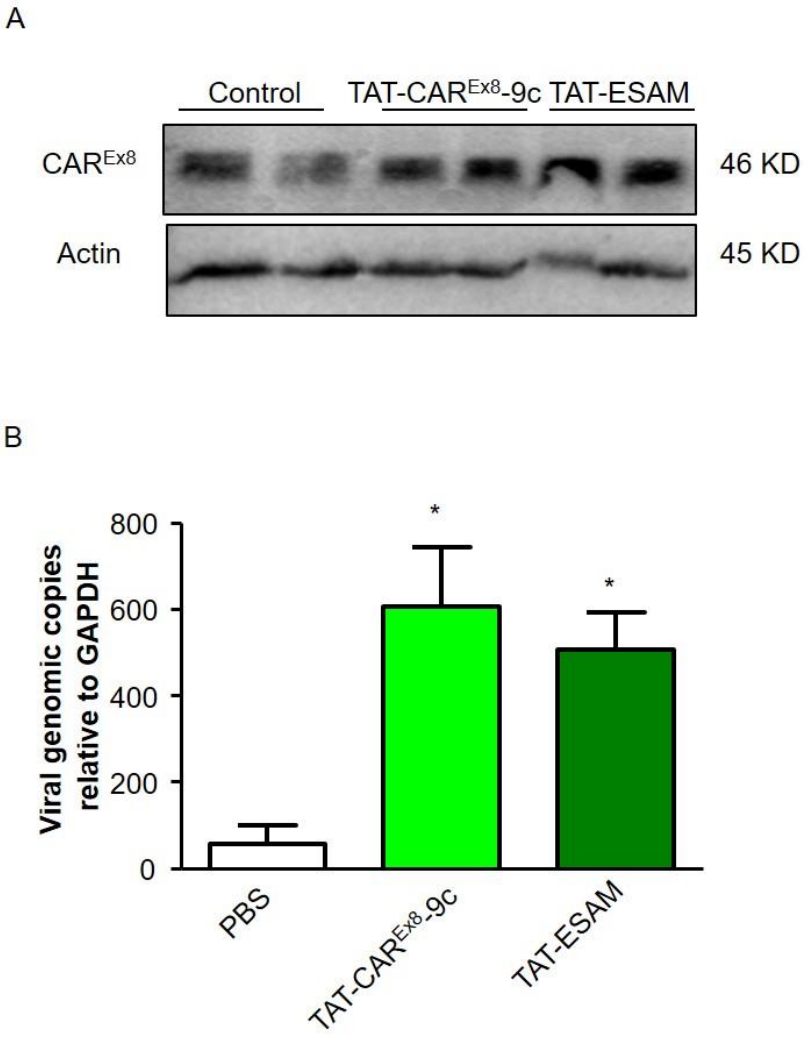

Figure 52. TAT-CAR^{Ex8}-9c and TAT-ESAM increase CAR^{Ex8} and AdV transduction in human airway epithelia (HAE).

(A) Polarized cotton rats epithelial cells were treated with either TAT-CAR^{Ex8}-9c or TAT-ESAM and subjected to western blotting for CAR^{Ex8} protein. Actin was used to confirm equal protein loading. (B) QPCR for Ad viral genome showed a significant increase in the AdV genomic transduction in the TAT-CAR^{Ex8}-9c and TAT-ESAM treatment condition as compared to control (PBS). *$p < 0.05$ compare to control (PBS).

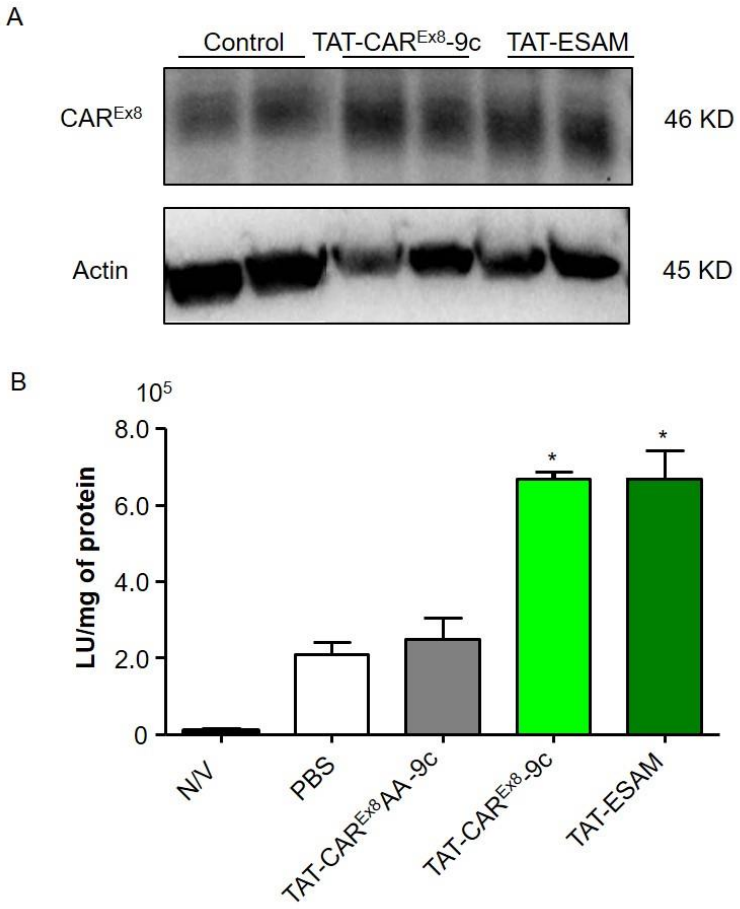

Figure 53. TAT-CAR^{Ex8}-9c and TAT-ESAM increase CAR^{Ex8} and AdV transduction in cotton rats epithelia.

(A) Polarized cotton rats epithelial cells were treated with either TAT-CAR^{Ex8}-9c or TAT-ESAM and subjected to western blotting for CAR^{Ex8} protein. Actin was used to confirm equal protein loading. (B) AdV-β-gal assay of MDCK epithelia treated with TAT-CAR^{Ex8}-9c, TAT-ESAM, or control peptides. Both TAT-CAR^{Ex8} -9c and TAT-ESAM treatment significantly increased the AdV-β-gal transduction compared to control peptide. *$p < 0.05$ compare to control.

TAT-PDZ3 peptides did not change CAR^{Ex8} transcript levels

To confirm that the increase in CAR^{Ex8} was post-translational, I then tested if TAT-PDZ3 peptides increase CAR^{Ex8} by promoting CAR^{Ex8} gene expression. Treatment with TAT-CAR^{Ex8}-9c and TAT-ESAM did not change the transcript level of CAR^{Ex8} compared to control (Figure 54). Interestingly, pretreatment with the protein synthesis inhibitor (CHX) partially reversed the effect of TAT-PDZ3 peptides (Figure 55). These data show that TAT-PDZ3 peptides increase CAR^{Ex8} levels by interfering with either newly translated protein or protein stability.

CAR^{Ex8} degrades rapidly in polarized epithelia

In order to determine the effect of TAT-PDZ3 peptides on CAR^{Ex8} protein stability, I first determined the half-life of CAR^{Ex8} protein in the cell. Stable MDCK-Flag-CAR^{Ex8} epithelia were used and CAR^{Ex8} protein synthesis was slightly induced by a low dose of Dox (50 ng/ml) overnight. Then, Dox-containing media was removed and replaced with media containing the protein synthesis inhibitor CHX in order to arrest protein synthesis, and the decrease in CAR^{Ex8} protein was tracked at different time points by Western blot. Using the one exponential decay approach, the half-life of CAR^{Ex8} protein was estimated to be 4.2 hrs (Figure 56). These data showed the fast turnover rate of CAR^{Ex8} protein in cells. To determine the effect of TAT-ESAM on CAR^{Ex8} stability, I used the same approach in the presence or absence of TAT-ESAM. Treatment with TAT-ESAM significantly increased the half-life of CAR^{Ex8} and caused a right shift of the degradation curve of CAR^{Ex8} (Figure 57). The experiment was not carried out long enough to clearly determine the new half-life; however, estimation suggested that it was extended to approximately >100 hours. Although future experiments will be used to evaluate protein

concentration at later time points, these data validate that TAT-ESAM increases CAR^{Ex8} stability.

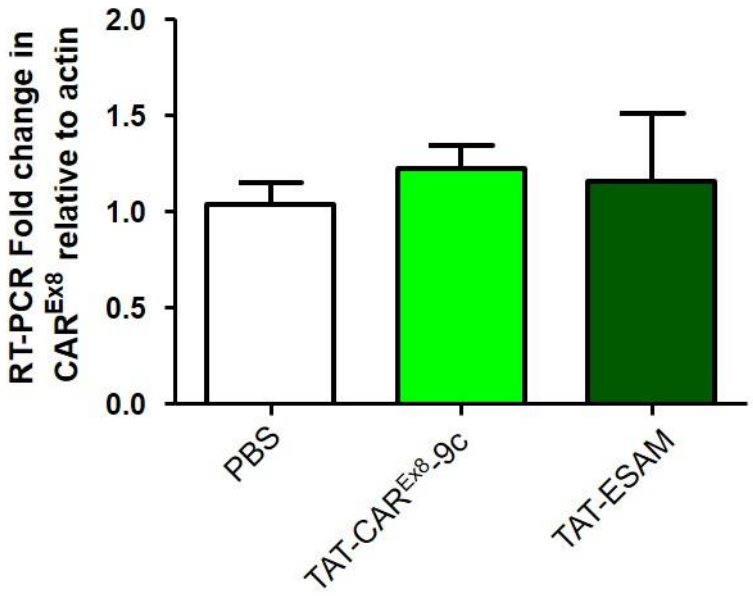

Figure 54. TAT-PDZ3 peptides do not change CAR^{Ex8} transcript levels.

RT-PCR specifically for CAR^{Ex8} transcripts after treatment with TAT-PDZ3 binding peptides or mock treatment (PBS).

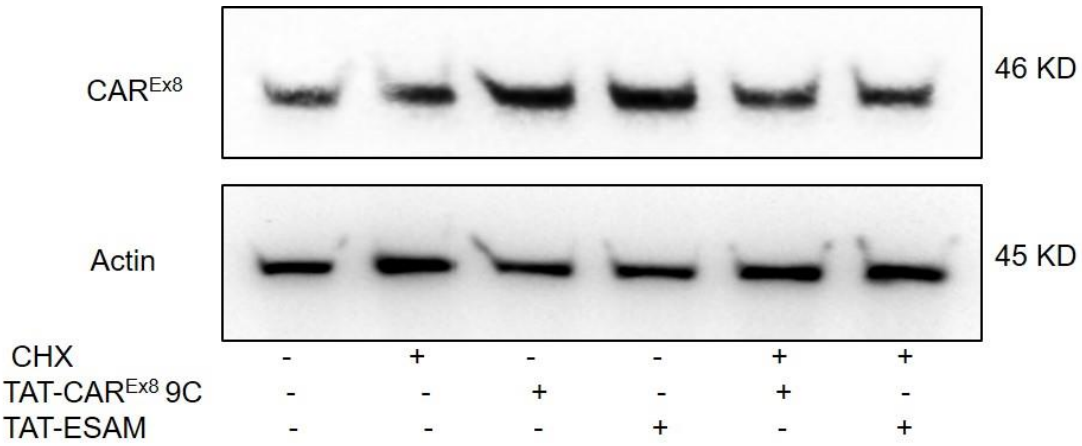

Figure 55. TAT-CAR^{Ex8}-9c and TAT-ESAM-mediated increase of apical CAR^{Ex8} is reduced by the protein synthesis inhibitor cycloheximide (CHX).

Western immunoblotting of CAR^{Ex8} in MDCK epithelia treated with either TAT-CAR^{Ex8} or TAT-ESAM in the presence or absence of the protein synthesis inhibitor CHX. Both TAT-PDZ3 binding peptides increase CAR^{Ex8} protein level, the effect was reduced upon pre-treatment with CHX.

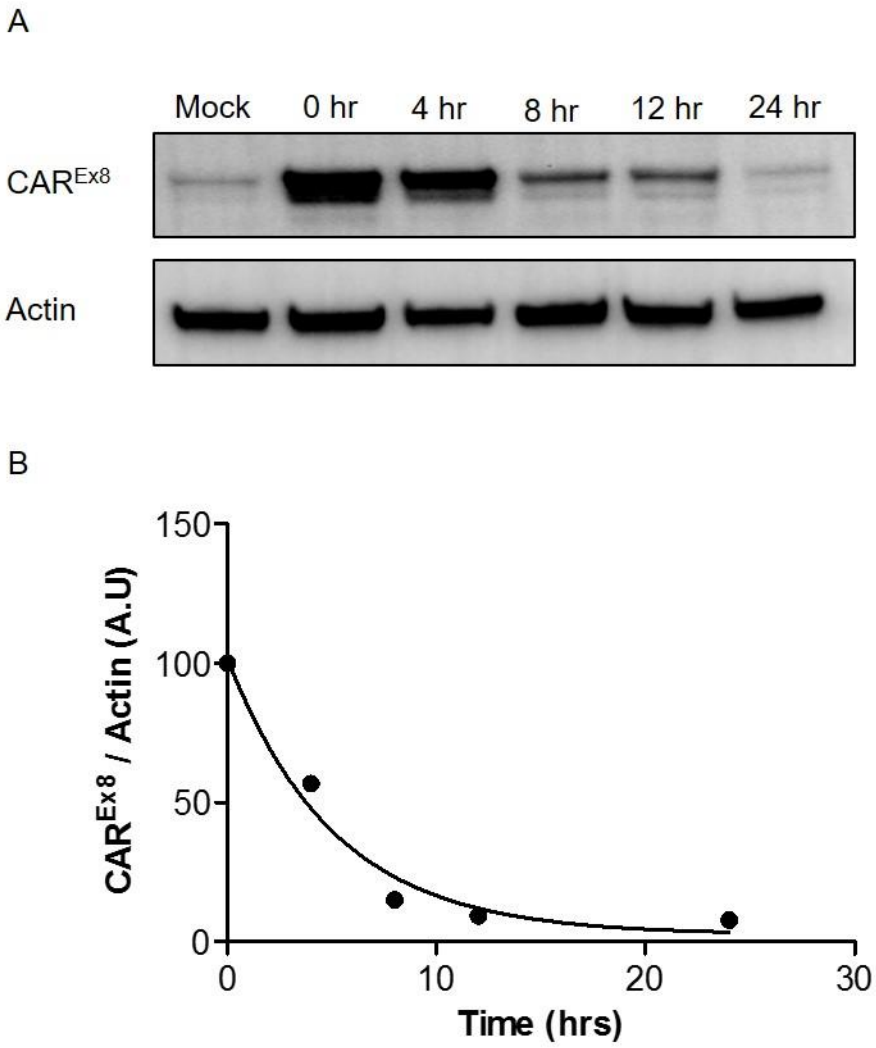

Figure 56. CAR^{Ex8} degrades rapidly in polarized epithelia.

MDCK cells stably expressing CAR^{Ex8} under a doxycycline-inducible promoter were induced for different time points. By the end of each induction period, Dox was removed and protein synthesis inhibitor (CHX) was used to stop further protein synthesis. (A) Western immunoblotting of CAR^{Ex8} protein over time. (B) XY plot represents the quantitation of the band intensity of CAR^{Ex8}/actin from (A). The half-life of CAR^{Ex8} was determined to be 4.2 hrs.

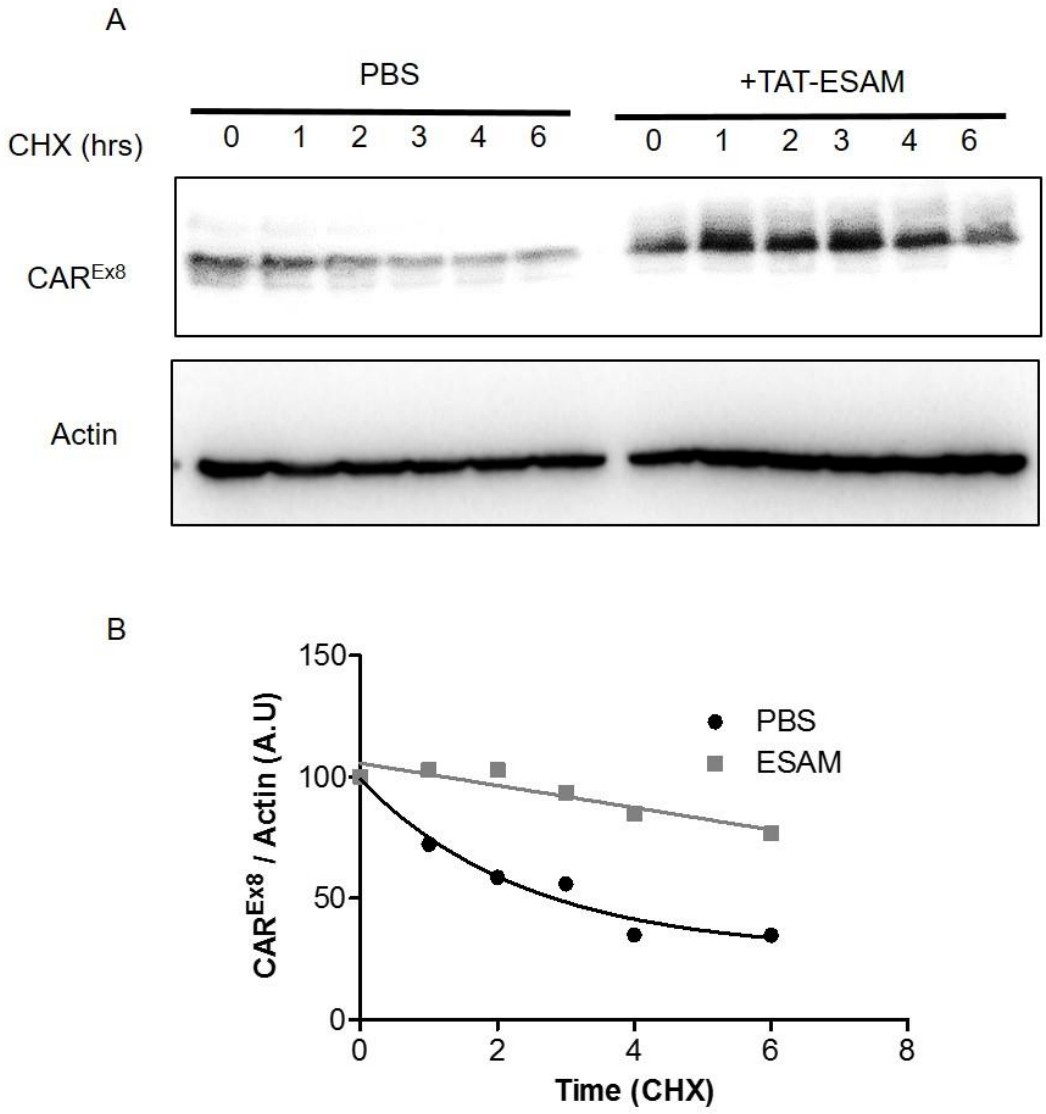

Figure 57. TAT-PDZ3 peptides increase the stability of CAR^{Ex8} protein.

(A) Western immunoblotting of CAR^{Ex8} protein degradation profile over time in the presence or absence of TAT-ESAM. Treatment with TAT-ESAM increases the stability of CAR^{Ex8} protein. (B) XY plot represents the quantitation of the band intensity of CAR^{Ex8}/actin from (A). TAT-ESAM shifts CAR^{Ex8} protein degradation profile and increases CAR^{Ex8} half-life.

TAT-PDZ3 peptides increase CAR^{Ex8} protein at the apical membrane and in a vesicular pattern within the cytoplasm

I tracked the change in level and cellular localization of CAR^{Ex8} after TAT-PDZ3 peptide treatment using ICC. Treatment with both peptides showed a dense speckled appearance of CAR^{Ex8} localized mainly at the apical membrane (Figure 58, see xz view) as well as within the cytoplasmic compartment of polarized epithelia (Figure 58). This pattern of distribution is consistent with vesicular transport of CAR^{Ex8} protein to the apical surface.

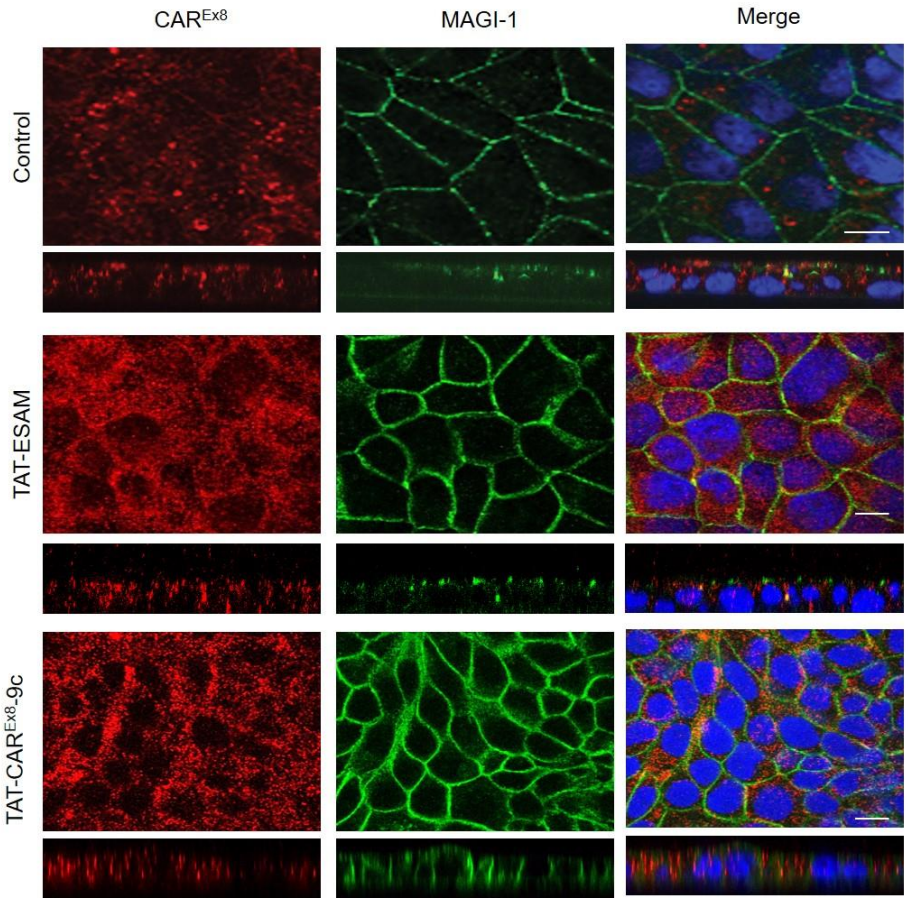

Figure 58. TAT-PDZ3 peptides increase CAR^{Ex8} protein at the apical membrane and in vesicular pattern within the cytoplasm.

Immunocytochemistry of polarized MDCK treated with TAT-ESAM or TAT-CAR^{Ex8}-9c shows upregulation of the cellular CAR^{Ex8} protein level. CAR^{Ex8} is localized mainly at the apical surface of polarized MDCK cells. After treatment with TAT-ESAM or TAT-CAR^{Ex8}-9c, CAR^{Ex8} is upregulated in a vesicular pattern within the apical surface and the cytoplasm of treated cells. Red (CAR^{Ex8}), Green (MAGI-1, a junctional protein), Blue (nucleus, DAPI). 60x oil immersion confocal microscopy, scale bar= 10µm

Trafficking of apical CAR^{Ex8} protein levels via Rabs

I hypothesized that CAR^{Ex8} is trafficked to the apical membrane of polarized epithelia via a regulated endosomal pathway. Rabs, small G-proteins that belongs to the Ras family, were used to delineate the trafficking pathway through which CAR^{Ex8} is localized apically. The Rab families of small G proteins play an important role in protein trafficking, including defining vesicular cargo destined for distinct localizations within a polarized cell, including apical localization (164, 165). They serve as markers for intracellular protein trafficking (164). I hypothesized that newly synthesized CAR^{Ex8} could be accumulated in the ER/Golgi by chilling the cells at 15-20ºC for 4 h and then released in bulk into the endosomal pathway, and subsequent trafficking followed. My first challenge was to determine the optimal cargo accumulation/release time in MDCK epithelia. I used inducible MDCK-Flag-CAR^{Ex8} cells that were induced with Dox to induce CAR^{Ex8} expression overnight. Cells were then incubated at 15-20°C for 4 hrs to allow newly synthesized CAR^{Ex8} to accumulate in the ER and Golgi. Then cells were incubated at 37°C at different time points for 5-20 min to allow trafficking towards the apical membrane. Fluorescently labelled Wheat Germ Agglutinin (WGA), which binds to sialic acid glycosylated molecules, was used as a marker for the plasma membrane as well as trans-Golgi apparatus. At early releasing times of 5-10 min, CAR^{Ex8} was localized mainly at the nuclear compartment, probably due to insufficient releasing time (Figure 59). However, at 10-15 min, CAR^{Ex8} could be seen leaving the ER/Golgi and entering the cytoplasm in a vesicular pattern (Figure 59). Given the vesicle-associated distribution at 15-20 min post-release, this time point was chosen for subsequent experiments.

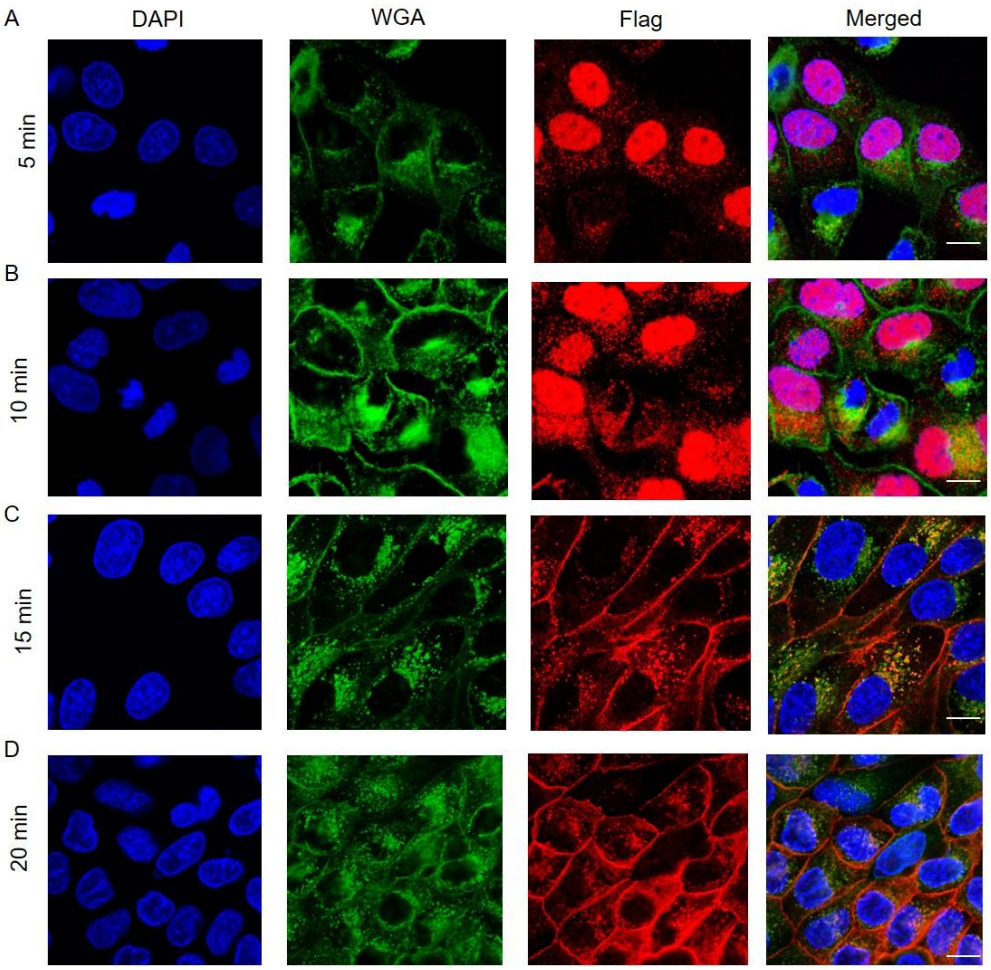

Figure 59. The Golgi-ER cargo is released within 15-20 min in MDCK epithelia.

Polarized MDCK-CAR^{Ex8} epithelia were induced with 500 ng/ml Dox overnight. ER-Golgi cargo was accumulated by incubation at 15-20ºC for 4hrs in the presence of protein synthesis inhibitor (CHX). To determine the optimal releasing time from the cargo, cargo was released at different time points (A) 5 min, (B) 10 min, (C) 15 min, and (D) 20 min followed by immunocytochemistry. Red (CAR^{Ex8}), Green (Wheat Germ Agglutinin, WGA, marker for cell membrane and late Golgi apparatus), Blue (nucleus, DAPI). 60x oil immersion confocal microscopy, scale bar= 10µm

CAR^{Ex8} partially co-localized with Rab4, but not Rab5

Rab4 is a marker for recycling endosomes within the apical sorting compartment whereas Rab5 is a marker for the clathrin coated vesicles and acts as a sorting signal to the basolateral membrane. Data showed that CAR^{Ex8} partially co-localized with Rab4 but not with Rab5 (Figure 60). This is consistent with the apical trafficking of CAR^{Ex8} in polarized airway epithelia and suggests that CAR^{Ex8} may alternate between the apical membrane and recycling endosomes in polarized epithelia.

CAR^{Ex8} does not co-localize with Rab7 but partially co-localizes with Rab9

Both Rab7 and Rab9 are late endosomal markers. Rab7 goes to the lysosome to deliver proteins destined to be degraded by the lysosomal pathway. However, Rab9 marks the vesicles that are recycled from the late endosome back to the Golgi apparatus. Results showed that Rab7 does not co-localize with CAR^{Ex8} (Figure 61). Consistent with the proposed mechanism of CAR^{Ex8} degradation, these data show that lysosomal degradation is not the main pathway for CAR^{Ex8} degradation. However, there was a partial co-localization between Rab9 and CAR^{Ex8} (Figure 62), indicating that some CAR^{Ex8} may be recycled back to the Golgi.

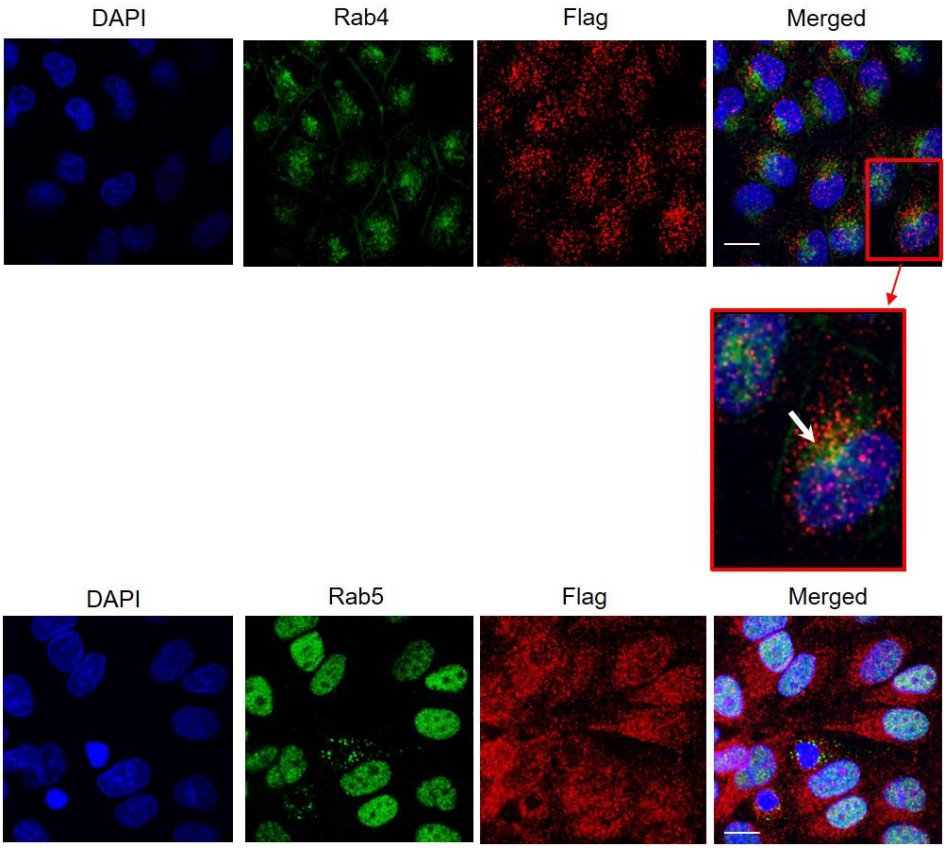

Figure 60. CAR^{Ex8} partially co-localizes with the Rab4, recycling endosomal marker, but not Rab5.

Polarized MDCK epithelia were induced with 500 ng/ml Dox overnight. ER-Golgi cargo was accumulated by incubation at 15-20ºC for 4hrs in the presence of CHX and release by incubation at 37°C for 15-20 min followed by fixation and immunocytochemistry. Red (CAR^{Ex8}), Green (Rab4 or Rab5), Blue (nucleus, DAPI). White arrow (inset) shows co-localization between CAR^{Ex8} and Rab4 shown in yellow/orange. 60x oil immersion confocal microscopy, scale bar= 10µm

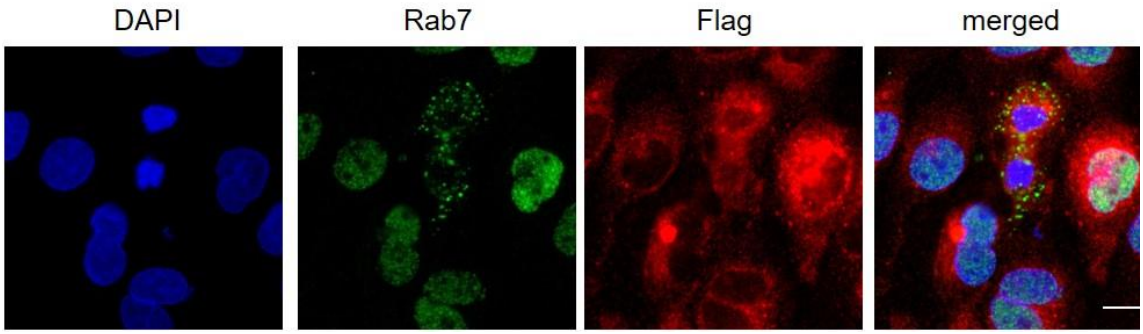

Figure 61. CAR^{Ex8} does not co-localize with Rab7, a late endosomal marker.

Polarized MDCK-CAR^{Ex8} epithelia were induced with 500 ng/ml Dox overnight. ER-Golgi cargo was accumulated by incubation at 15-20ºC for 4 hrs in the presence of CHX and it was released by incubation at 37°C for 15-20 min. CAR^{Ex8} did not co-localize with Rab7, a late endosomal marker. This suggests that newly synthesized CAR^{Ex8} does not go to degradation pathway. Red (CAR^{Ex8}), Green (Rab7), Blue (nucleus, DAPI). 60x oil immersion confocal microscopy, scale bar= 10µm

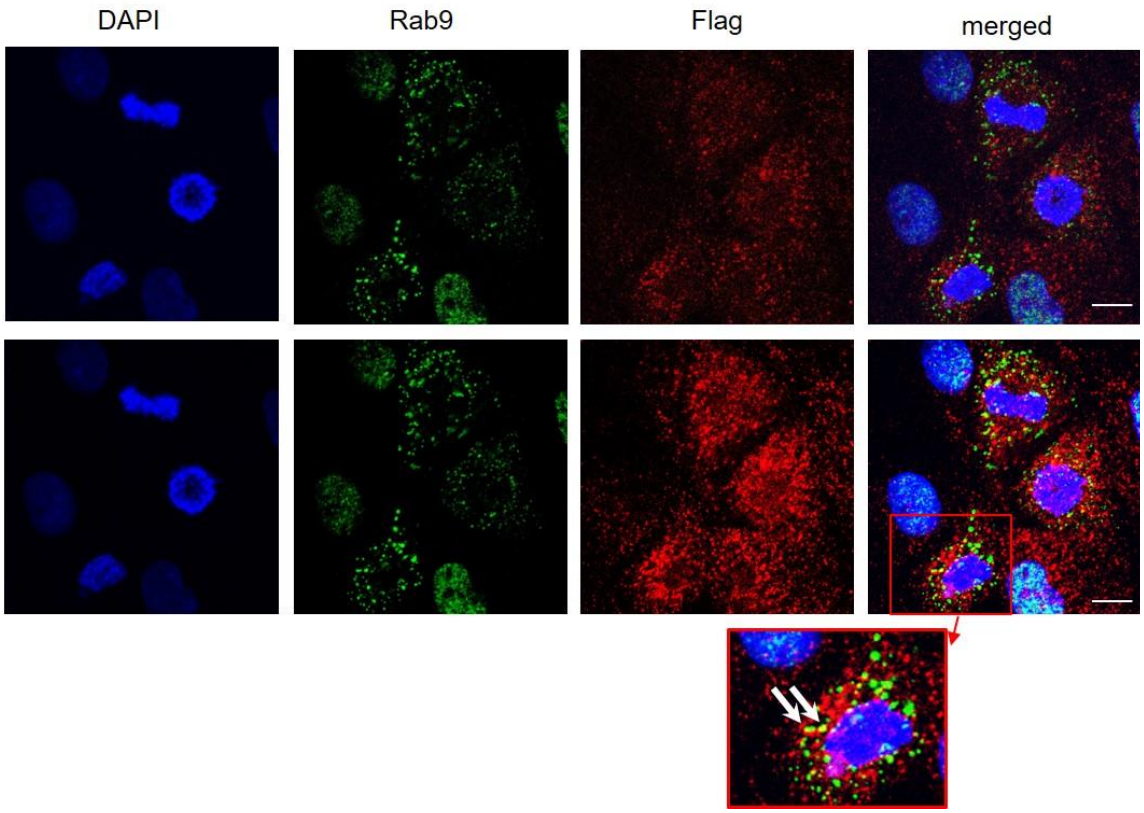

Figure 62. CAR^{Ex8} partially co-localized with the Rab9, late Endosomal-Golgi recycling marker.

Polarized MDCK-CAR^{Ex8} epithelia were induced with 500 ng/ml Dox overnight. ER-Golgi cargo was accumulated by incubation at 15-20ºC for 4 hrs in the presence of CHX and it was released by incubation at 37°C for 15-20 min. Red (CAR^{Ex8}), Green (Rab9), Blue (nucleus, DAPI). White arrow (inset) show colocalization between CAR^{Ex8} and Rab9 shown in yellow/orange. 60x oil immersion confocal microscopy, scale bar= 10µm

CAR^{Ex8} almost totally co-localized with Rab11, an early endosomal marker

One of the most significant co-localizations observed was between CAR^{Ex8} and Rab11, an early endosomal marker (Figure 63). The early endosome is an important compartment that receives and sorts vesicles from the Golgi, recycling endosome, and plasma membrane. Overall, these data showed that CAR^{Ex8} is trafficked through three main pathways: 1) From the ER-Golgi to the early endosome and/or to the recycling endosome. 2) From early endosome to late endosome or to recycling endosome. 3) From the late endosome to back to Golgi apparatus. Future experiments will test additional later time points and Rab inhibitors to confirm these findings.

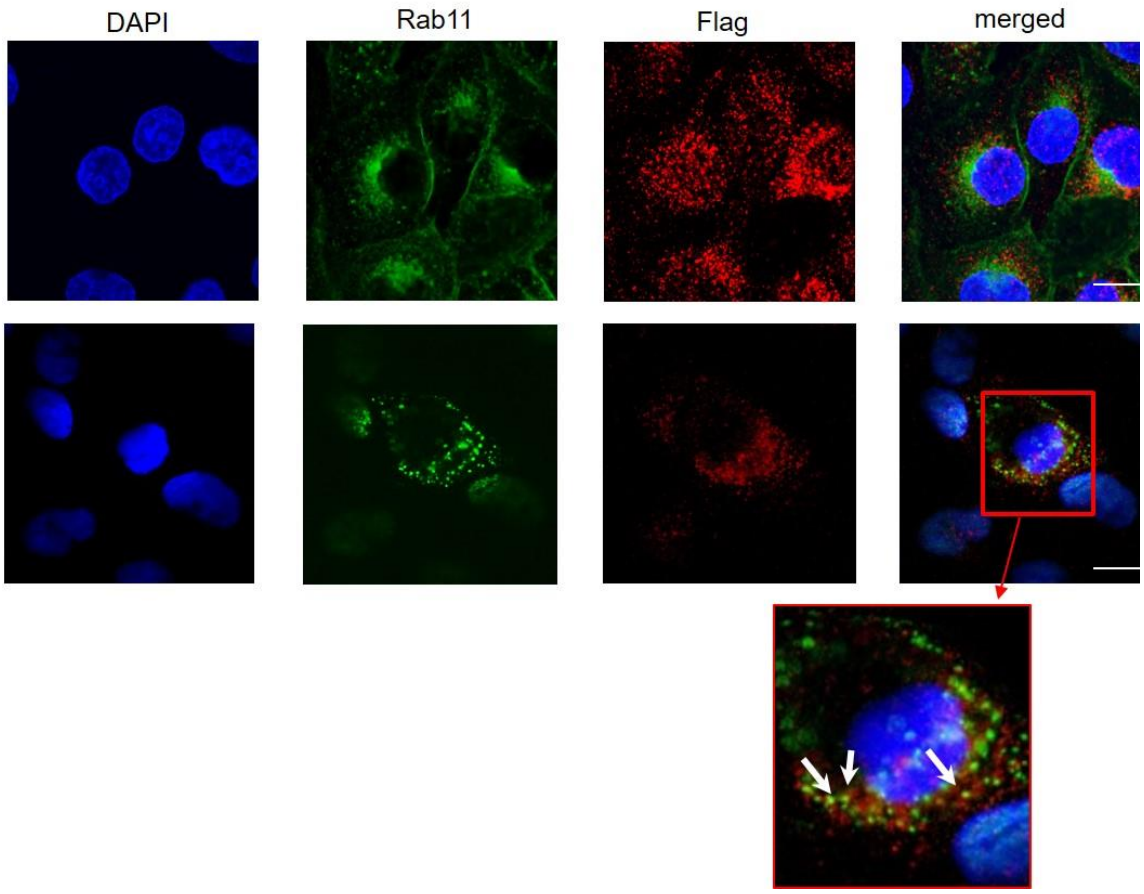

Figure 63. CAR^{Ex8} almost totally co-localized with the Rab11, an early endosomal marker.

Polarized MDCK-CAR^{Ex8} epithelia were induced with 500 ng/ml Dox overnight. ER-Golgi cargo was accumulated by incubation at 15-20ºC for 4 hrs in the presence of CHX and it was released by incubation at 37°C for 15-20 min. Localization is consistent with ICC of CAR^{Ex8} at the sub-apical membrane of polarized epithelia. Red (CAR^{Ex8}), Green (Rab11), Blue (nucleus, DAPI). White arrows (inset) show co-localization between CAR^{Ex8} and Rab11 shown in yellow. 60x oil immersion confocal microscopy, scale bar=10µm

TAT-PDZ3 peptides do not change epithelial integrity

I tested if TAT-PDZ3 binding peptides alter epithelial integrity by two approaches. First, polarized epithelial cells were treated with a dose of 50 µM of TAT-PDZ3 peptides, TAT-scramble, or vehicle (PBS) daily over a period of 16 days. Trans-epithelial resistance (TER) measurements were taken every other day. Continuous treatment with TAT-PDZ3 peptides did not alter the transepithelial integrity as shown by TER measurements (Figure 64). The second approach involves measuring the epithelial integrity by FITC-dextran diffusion assay. Consistent with TER data, no difference in the diffusion of FITC dextran 70 kD FITC-Dextran diffusion assay showed no change in the permeability of 70 kD Dextran permeability between treated and untreated conditions (Figure 66). Similarly, no difference in FITC Dextran 4 kD permeability was seen between the treatment conditions after 14 days of continuous treatment (Figure 65). To further confirm that the limited FITC-dextran diffusion effect was due to the formation tight junctions, cells were treated with EDTA for 10 min, followed by FITC-Dextran 4 kD diffusion assay. As expected, pretreatment with EDTA increased FITC-Dextran 4 kD diffusion in all conditions equally (Figure 66). This illustrates that TAT-PDZ3 peptides can promote AdV transduction without altering epithelial integrity.

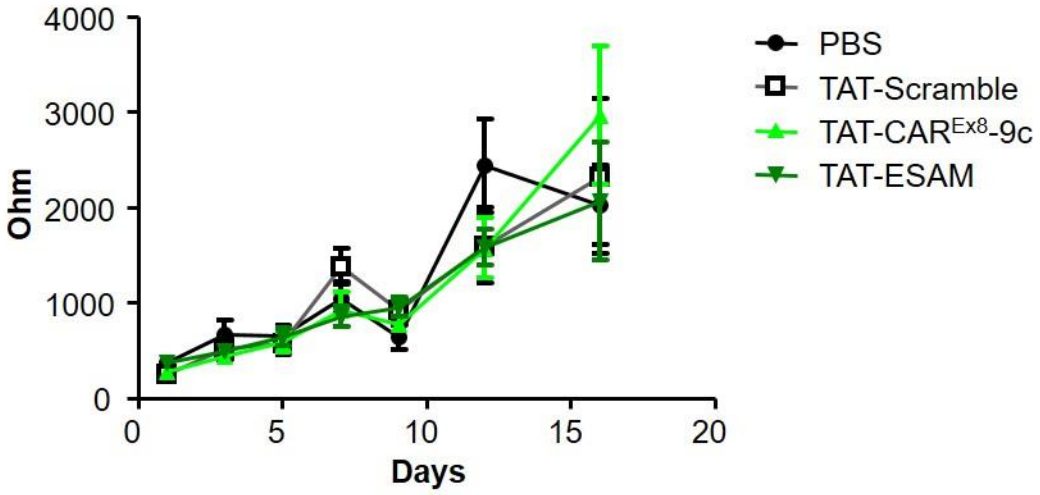

Figure 64. TAT-PDZ3 peptides do not change epithelial integrity.

HAE cells were treated apically with single dose of PBS, TAT-scramble or TAT-PDZ3 peptides (50µM; for 4hrs) daily for 16 days. Transepithelial resistance (TER) was measured every other day for 16 days. No change in TER was noticeable upon treatment with TAT-PDZ3 peptides. Each condition represents the average of 4 replicates.

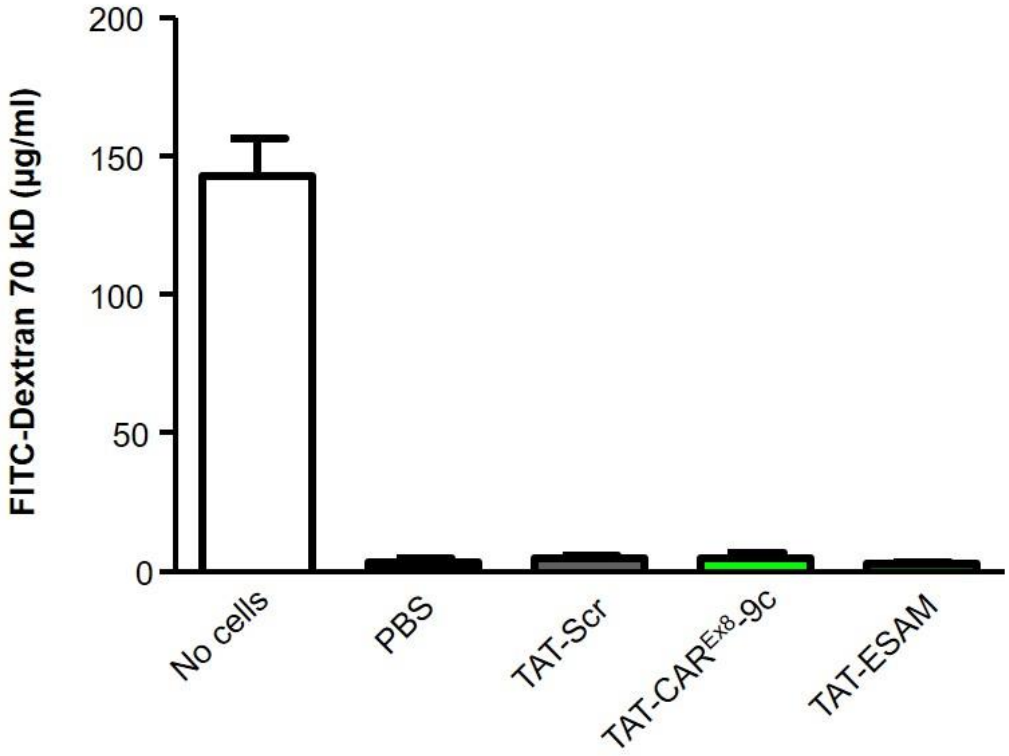

Figure 65. TAT-PDZ3 peptides do not change epithelial integrity.

HAE cells were treated apically with a single dose of PBS, TAT-scramble (50µM; for 4hrs) or TAT-PDZ3 peptides (50µM; for 4hrs) daily for 14 days. There was no difference in FITC-Dextran 70 kD diffusion across treated epithelia among treatments. FITC-Dextran 70 kD was added to the apical membrane compartment and Dextran in the basolateral media was measured and quantified as described in the material and methods. Assay was performed after the 14th day of peptide treatment.

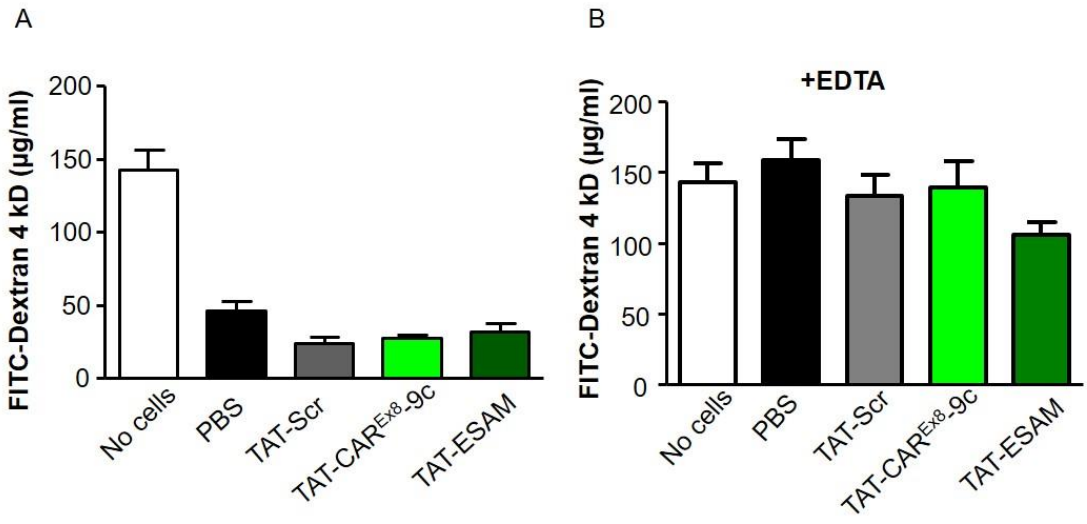

Figure 66. TAT-PDZ3 peptides do not change epithelial integrity.

HAE cells were treated apically with a single dose of PBS, TAT-scramble (50µM; for 4hrs) or TAT-PDZ3 peptides (50µM; for 4hrs) daily for 14 days. (A) FITC-Dextran 4 kD diffusion across treated epithelia in the absence of EDTA. There was no difference in Dextran 4 kD diffusion among treatments. (B) Pre-treatment with EDTA increased Dextran 4 kD permeability in all conditions. FITC-Dextran 4 kD was added to the apical membrane compartment and Dextran present in the basolateral media was measured and quantified as described in the material and methods. Assay performed on the 14^{th} day of peptide treatment.

Conclusions

The presented data validate new potential therapeutics that can be used to promote AdV-mediated gene therapy. Results illustrate the mechanism by which the PDZ3 peptides promote CAR^{Ex8} protein and increase AdV infection. My data showed that CAR^{Ex8} and AdV were increased upon TAT-PDZ3 peptide treatment in three different cell lines, including well-differentiated primary airway epithelia. This illustrates the reproducibility as well as the widespread application of TAT-PDZ3 peptides in promoting AdV transduction and enhancing AdV mediated gene therapy. I also discovered a possible mechanism of TAT-PDZ3 peptide action. The mechanism involved increasing CAR^{Ex8} stability by reducing MAGI-1 mediated CAR^{Ex8} degradation. However, the exact mechanism is yet to be fully elucidated. In addition, I have shown that there was right shift in the CAR^{Ex8} degradation curve in the TAT-ESAM treated condition; suggesting an increase in the half-life of CAR^{Ex8} protein. Further studies are needed to determine the fold increase in CAR^{Ex8} stability upon TAT-PDZ3 peptides treatment. Moreover, the proposed work illustrated possible trafficking pathways of CAR^{Ex8} to the apical membrane of polarized epithelia. Although further studies are needed, CAR^{Ex8} is suggested to be recycled between three main pathways. First, from the ER-Golgi to the early endosome and/or to the recycling endosome. Second, from early endosome to late endosome or to recycling endosome, and finally, from the late endosome to back to Golgi apparatus. The significance of the data in this chapter is that TAT-PDZ3 peptides can be exploited to enhance AdV mediated gene therapy by overexpression of CAR^{Ex8} in order to treat a wide variety of genetic diseases and disorders such as cystic fibrosis (Figure 67). It is also can be used to decrease the possible

side effects by lowering the viral load given to a patient in current clinical trials where AdV is used as vector for gene therapy.

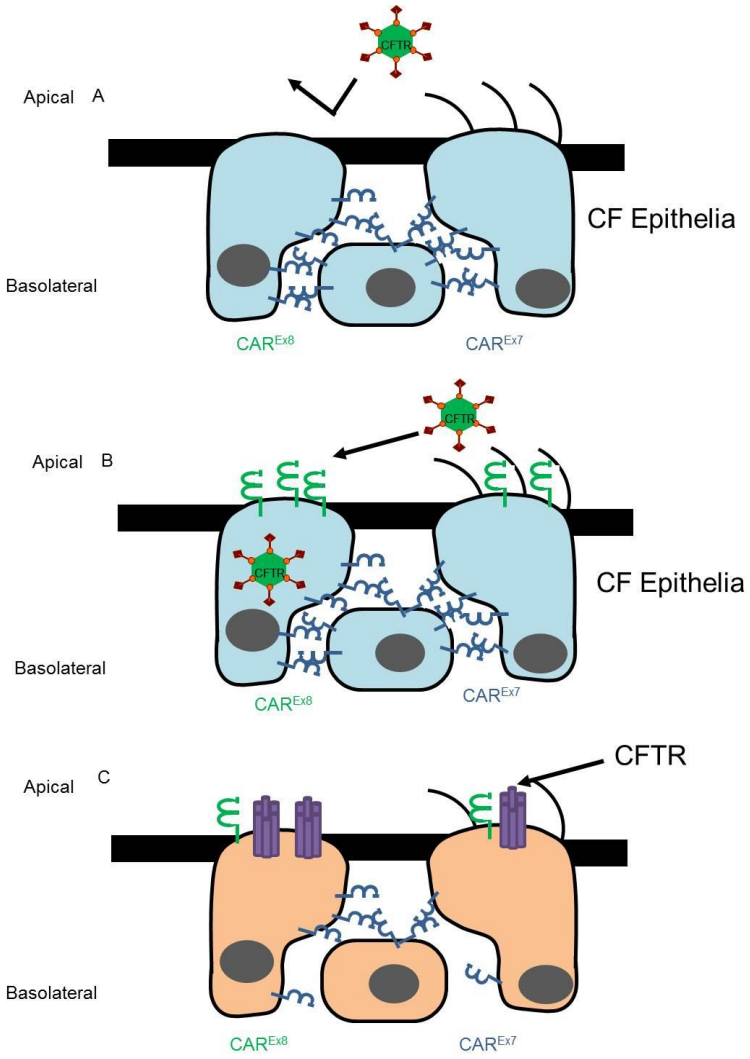

Figure 67. Model of enhancing AdV mediated gene therapy in cystic fibrosis (CF) epithelium by TAT-PDZ3 peptides.

(A) In the absence of CAR^{Ex8}, CF epithelia are devoid of the CFTR protein and resistant to AdV-CFTR transduction due to low levels of apical CAR^{Ex8}. (B) In the presence of TAT-PDZ3 peptides, CAR^{Ex8} level is significantly increase which would enhance AdV-CFTR transduction and (C) restore CFTR in the CF epithelium. CF: cystic fibrosis, CFTR: cystic fibrosis transmembrane conductance regulator.

CHAPTER 5: Biological evaluation of the effect of MAGI-1 TAT-PDZ peptides on Adenovirus infection *in vivo*

Rationale

AdV infection is common and can be life threatening (7). Currently there are no specific therapies to prevent or treat AdV infections and supportive care is the most common intervention. On the other hand, AdV remains the most commonly used vector for gene therapy (29). The objective of this chapter is the evaluation of a novel strategy to decrease or increase airway epithelial apical CAR^{Ex8} in order to decrease or increase AdV infection *in vivo,* respectively. My overall hypothesis is that decreasing apical CAR^{Ex8} will decrease AdV infection by decreasing viral entry while increasing CAR^{Ex8} in cells can be used to enhance the efficacy of AdV mediated gene therapy.

The lung is an initial portal for infection by many wild type AdV, such as AdV5, and is also a major target for gene therapy. Recombinant AdV-mediated gene delivery to the airway of mice via intranasal (IN) administration has been well studied (166-169). Low level AdV transduction in the lungs can be overcome by very high viral inoculums ($\sim 10^{10}$ IU) which can be lethal and causes profound side effects (44).

In the previous chapters, I demonstrated that cell permeable peptides that disrupt CAR^{Ex8} interactions with MAGI-1 were able to modulate CAR^{Ex8} levels and AdV transduction *in vitro*. In this chapter, I used the novel transgenic mouse model "td-Tomato" and recombinant AdV that carries cre-recombinase gene (AdV-Cre) to test the efficacy of TAT-PDZ peptides in modulation of AdV infection *in vivo*.

Results

To test the effect of the TAT-PDZ peptides on AdV infection *in vivo*, transgenic mice td-Tomato (JAX stock # 007576) were used. All mouse cells have a double fluorescent Cre reporter gene that expresses membrane-targeted tandem Tomato (tdT, RFP variant) prior to Cre mediated excision (*lox p*) and membrane-targeted green fluorescent protein (mG) after excision (170). That is, upon cre- recombinase expression, RFP-expressing cells will be converted to GFP-expressing cells (Figure 68). The genetic change is permanent and allows AdV transduction to be quantified based on the cell-by-cell or total GFP expression lung tissue.

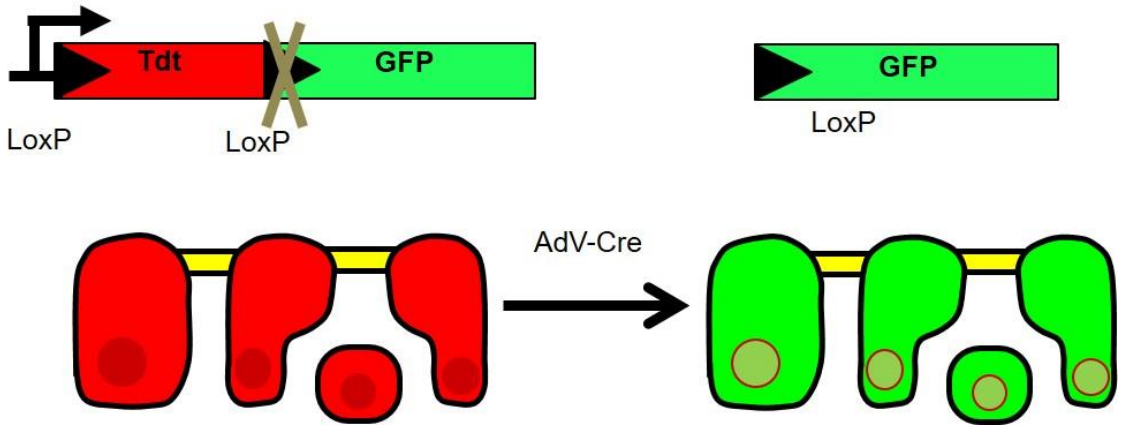

Figure 68. Red-tomato mice tdT-mouse model.

All cells express a transmembrane-bound form of RFP and fluoresce red. Upon expression of Cre re-combinase via AdV5-Cre, the tdT gene is cut out allowing transcription and translation of transmembrane-bound eGFP. This irreversibly turns the cells from red to green.

TAT-PDZ1 peptides suppressed AdV entry whereas TAT-PDZ3 promoted AdV transduction in lung tissue

Mice were anesthetized moderately by isoflurane after which they were treated intranasally (IN) with vehicle (PBS), TAT-CAR^{Ex8}-AA-9c, TAT-PDZ1 (TAT-NET1), or TAT-PDZ3 (TAT-CAR^{Ex8}-9c or TAT-ESAM) for 4 hrs. After which they were infected IN with AdV-Cre and 48 hrs later, lung tissues were investigated for GFP expression. As shown in Figure 69A, animals receiving no virus showed only RFP without GFP expression. Vehicle treated mice showed uniform distribution of the number of infected cells (shown in green) among the lung sections. Pre-treatment with TAT-PDZ1 peptides decreased the number of infected cells in contrast to TAT-PDZ3 peptides which increased the number of GFP infected cells. Quantitation of the number of GFP expressing cells showed a significant increase in TAT-PDZ3 treated mice and a decrease in TAT-PDZ1 treated mice (Figure 70). Similarly, the ratio between GFP to RFP intensity showed a similar trend of increased and decreased infection in TAT-PDZ3 and TAT-PDZ1 treatment, respectively.

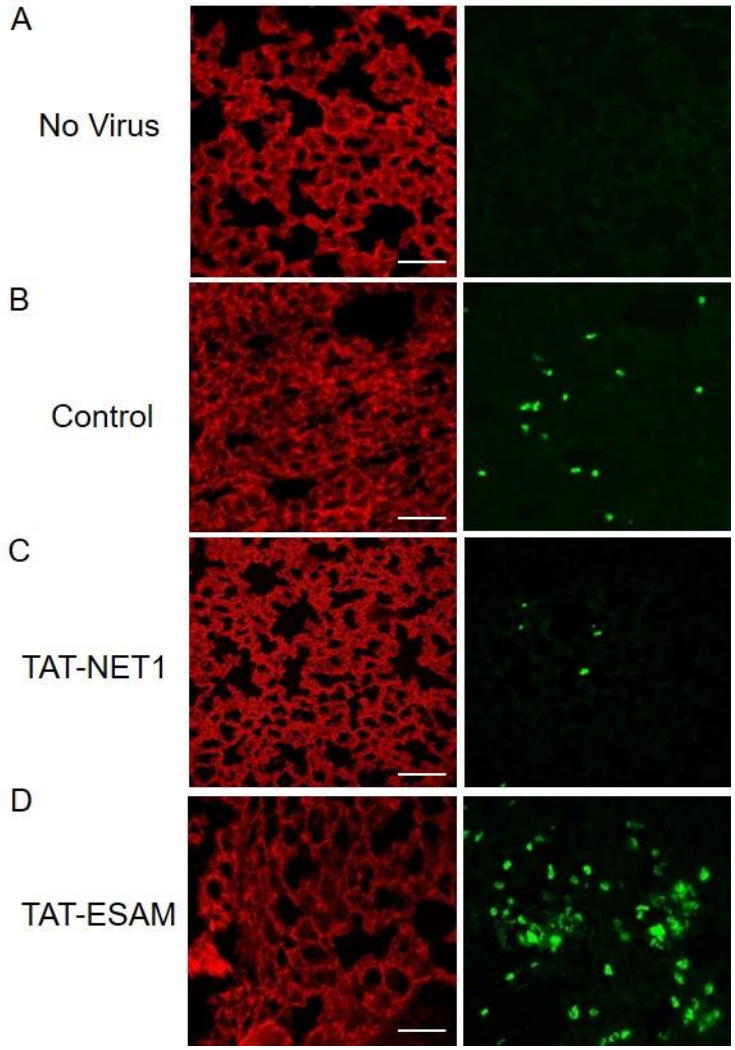

Figure 69. MAGI-1 PDZ1 binding peptides decrease AdV5-Cre infection whereas PDZ3 binding peptides increase AdV5-Cre infection *in vivo*.

Analysis of lung cryosections from tdT mice pretreated with A) No virus, B) Control (PBS or TAT-CAR^{Ex8}-9cAA), C) PDZ1 TAT-NET1 binding peptide, or D) PDZ3 TAT-ESAM binding peptide 4 h prior to AdV5-Cre intranasal infection. 20x confocal microscopy, Scale bar= 50µm

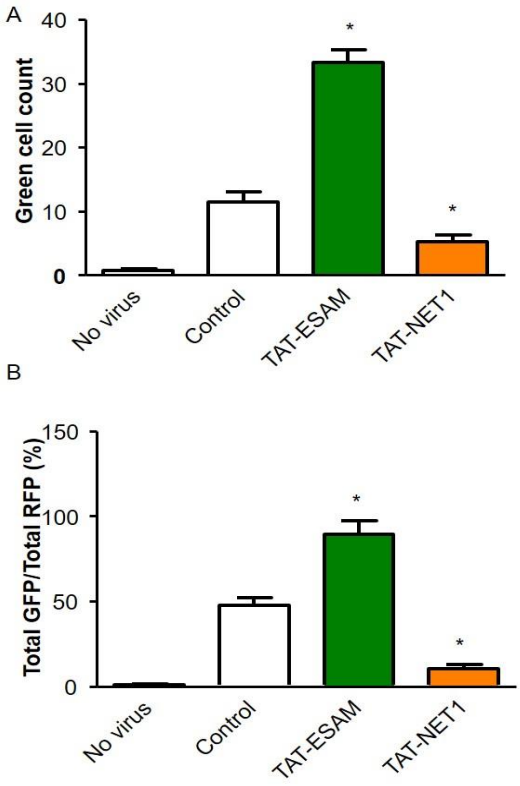

Figure 70. MAGI-1 PDZ1 binding peptides decrease AdV5-Cre infection whereas MAGI-1 PDZ3 binding peptides increase AdV5-Cre infection *in vivo*.

Quantitative analysis of GFP expression in lung cryosections from tdT mice with no virus, pre-treated with control, PDZ3 TAT-ESAM peptides, or PDZ1 TAT-NET1 peptides. (A) Total GFP expressing cells counted in lung sections from different treatment conditions. (B) Quantification of total GFP/Total RFP fluorescence in lung section of different treated conditions by image J. There is significantly higher or lower GFP expression in TAT-ESAM or TAT-NET1 treated mice, respectively. Data are average of quantification from 10 sections. * $P<0.05$ compare to control

TAT-PDZ1 peptides decrease viral genomes whereas TAT-PDZ3 increased viral genomes in lung tissue of td-Tomato mice

I further confirmed the change in AdV-Cre transduction in the lungs of td-Tomato mice by quantitation of the GFP expression. GFP mRNA was first extracted from lung sections of treated mice, then cDNA was synthesized as described in the material and methods. Data were normalized to control. QPCR of the synthesized DNA showed a significant increase in GFP expression in TAT-ESAM treated mice as compared to control. Moreover, TAT-NET1 treated mice showed significantly less GFP expression compared to control (Figure 71). To further confirm that the formed GFP was due to change in AdV-Cre transduction in the lung epithelia, AdV genomic copies were assessed by qPCR of the viral genome. As expected, TAT-ESAM treated mice had increased viral genome copies in their lung tissue compared to control while TAT-NET1 treated mice had significantly decreased AdV genome copies in their lungs (Figure 71). These results showed the efficacy of TAT-PDZ peptide in altering AdV transduction *in vivo* and validate the use TAT-PDZ1 peptides as prophylactic treatment against AdV infection and PDZ3 peptides as agents to promote AdV mediated gene therapy.

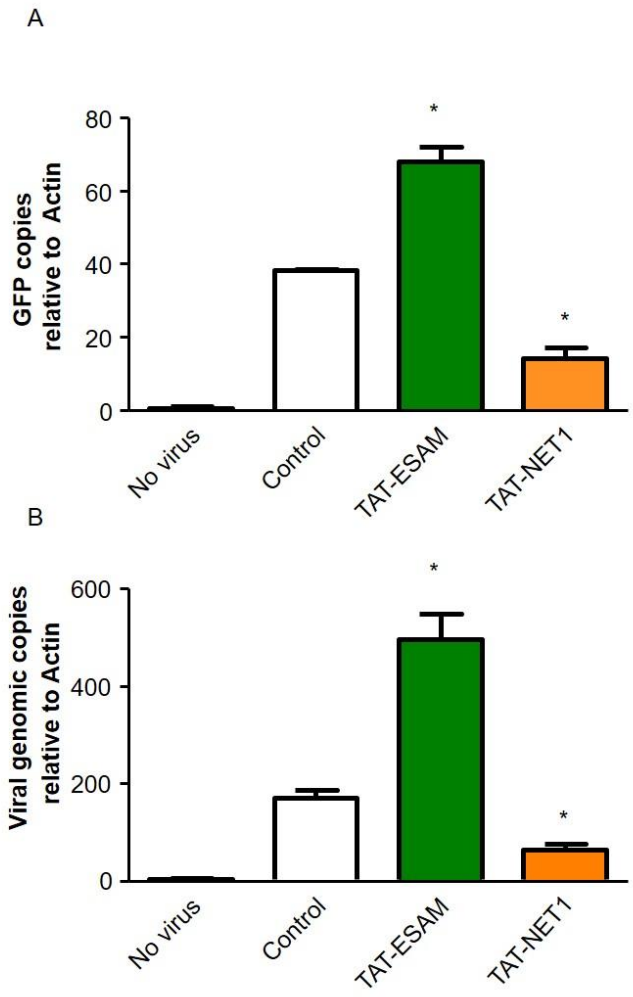

Figure 71. MAGI-1 PDZ1 binding peptides decrease AdV5-Cre infection whereas MAGI-1 PDZ3 binding peptides increase AdV5-Cre infection *in vivo*.

(A) RT-PCR for GFP mRNA expression after isolation of total RNA from lung tissue of control or peptide treated mice. (B) QPCR of viral genome copies in lung tissue from control or peptide treated mice. There is a significant increase or decrease of GFP expression as well as viral genome copies in lung tissue from TAT-PDZ3 or TAT-PDZ1 treated mice, respectively. * $P<0.05$ compare to control

Conclusions

In this chapter, I have performed pre-clinical evaluation of new potential therapeutics that alters AdV infection *in vivo.* By using a novel transgenic td-Tomato mouse model, TAT-PDZ binding peptides showed promising outcomes that can be used to either promote AdV mediate gene therapy or as prophylactic treatment against AdV infection *in vivo*. The advantage of using the td-Tomato mouse model is the non-invasive and easy assessment of the efficacy of TAT-PDZ peptides *in vivo*. TAT-PDZ1 peptides treatment lowered the number of AdV-Cre infected cells as well as AdV genome whereas TAT-PDZ3 peptides increased the AdV-Cre transduction. One shortage of the *in vivo* work was the relatively small N (N= 2-3). Nevertheless, more studies need to be done with a larger "n/group" to further elucidate the safety and effectiveness of the TAT-PDZ peptides *in vivo.* Future work will also focus on pathogenesis studies and gene therapy studies to demonstrate peptide efficacy.

CHAPTER 6: Discussion

We have shown for the first time that AdV transduction can be modulated by targeting the apically localized CAR isoform using cell permeable peptides that interrupt MAGI-1-CAR^{Ex8} interactions. We were able to dissect the mechanism by which MAGI-1 triggers CAR^{Ex8} degradation. TAT-PDZ1 binding peptides showed decreased CAR^{Ex8} and AdV infection in cancer epithelial cell lined, primary human airway epithelia, and epithelia from animal models of AdV pathogenicity (cotton rats), and *in vivo*. Together this reveals a novel mechanism for prophylactic therapeutics that can reduce AdV entry and infection of populations susceptible to AdV infection. Moreover, we used a similar approach to develop therapeutics that would enhance AdV entry. By using TAT-PDZ3 binding peptides that block MAGI-1 PDZ3 domain, we were able to increase the apical CAR^{Ex8} levels and enhance AdV entry *in vitro* and *in vivo*. This suggests the application of these peptides as potential therapeutics to enhance AdV mediated gene therapy.

I showed that MAGI-1 mediates a ternary interaction between ADAM17 and CAR^{Ex8} through its PDZ domains and that TAT-PDZ1 peptides mediate their effect by blocking interactions with the MAGI-1 PDZ1 domain. I validated the selectivity of the peptides to the corresponding PDZ domain by a direct binding assay. Furthermore, I showed that MAGI-1 is a main mediator in this pathway and that silencing MAGI-1 can reverse the effect of the TAT peptides on CAR^{Ex8}. However, taking in consideration the structural similarity between PDZ domains, as well as the fact that CAR^{Ex8} interacts with

many PDZ domain containing proteins (47, 102-105), it is possible that these peptides can bind and block other cellular PDZ domains. It is unknown how such off-target effects might affect the level of CAR^{Ex8}, however, I have shown the TAT-PDZ peptides do not change epithelial cell integrity, which rules out any possible overt toxicity from such potential off-target effects (if present) and suggests these peptides may be safe.

My data also showed that TAT-PDZ peptides indirectly targeting the nascent translated protein of CAR^{Ex8}. This was supported by the fact that the effect of the TAT-PDZ peptides was reversed upon inhibition the protein translation. Moreover, the peptides effect was worn off after 24 hrs of treatment suggesting a reversible effect. Furthermore, there was no change in the level of MAGI-1 protein upon treatment with TAT-PDZ peptides which proved that TAT-PDZ peptides are transiently disrupting the interaction between CAR^{Ex8} and MAGI-1 PDZ domains. Together, these data suggest a safe and reliable therapeutic approach for regulating the susceptibility of epithelia to AdV infection.

We and others were able to detect CAR expression at the apical membrane of epithelial cells (45, 61, 171). It is believed that the newly discovered TAT-PDZ1 binding peptides can abolish AdV entry by two phases. The first phase, acute phase, involves a decrease in the apical membrane-associated CAR^{Ex8} protein level which diminished the AdV entry due to a reduction in available receptor. This phase take place during the early time of TAT-PDZ1 peptide treatment that causes a shift of CAR^{Ex8} binding with the savior domain of MAGI-1, PDZ1, to the degradation domain, PDZ3. This shift causes a transient but significant decrease in the membrane level of CAR^{Ex8} and AdV entry. The second phase, chronic phase, is initiated by the shed CAR^{Ex8} ECD, providing long-term

protection against AdV infection. This happened when CAR^{Ex8} bound to MAGI-1 PDZ3 domain becomes increasingly a substrate available for ADAM17. The resulting cleaved ECD is secreted outside the cells and acts as decoy that binds AdV outside of the cell and protects the epithelia from further AdV entry. I speculate that it may also act as a scavenger for the nascent replicating AdV inside epithelial cells.

My data suggests that ADAM17 is responsible for CAR^{Ex8} but not CAR^{Ex7} shedding which is triggered by PDZ1 binding peptides. It is possible for ADAM10, which has the closest homology with ADAM17, to be a candidate for CAR^{Ex8} shedding (158). However, ADAM17 involvement in CAR^{Ex8} degradation is more likely for several reasons. First, ADAM10 is involved in constitutive shedding (172) whereas ADAM17 is involved in stimulated shedding (173). Second, in epithelial cells, ADAM10 has been shown to be localized at the basolateral surface (174), in contrast, ADAM17 sequestered mainly in the lipid rafts (175, 176), which is consistent with being localized at the apical membrane in polarized epithelia (177). Third, the C-term domain of ADAM17 (-ETEC) contains a class I PDZ binding motif, which enables ADAM17 to interact with PDZ domain containing proteins (178, 179), while ADAM10 C-term domain lacks such a sequence (-HMRR).

It is also worth noting that CAR^{Ex7} (which has identical transmembrane and extracellular domains as CAR^{Ex8}) interacts with the third PDZ domain of MAGI-1 (150). However, the level of CAR^{Ex7} was not affected by treatment with TAT-PDZ1 peptides. There are many possible explanations for why that happens. One of the most plausible reasons is different sorting between the two isoforms in the polarized epithelia. In polarized airway epithelia, CAR^{Ex8} is localized at the apical membrane whereas CAR^{Ex7} is localized at the

basolateral membrane (45, 163). Therefore, it is predicted that ADAM17 is localized with CAR^{Ex8} at the apical surface (175, 176), whereas ADAM10 is localized at the basolateral membrane and if there was an interaction, ADAM10 would be responsible for CAR^{Ex7} shedding (174). This hypothesis can be tested by testing the effect of ADAM17 on CAR^{Ex7} in non-polarized cell lines. Another possibility is that CAR^{Ex7} has 13 amino acids more than CAR^{Ex8} at the C-term domain. This could cause a shift of the ADAM17 cleavage site within CAR^{Ex8} ECD. Such shift in the cleavage site may render CAR^{Ex7} inaccessible to cleavage by ADAM17. One possibility to test this hypothesis is by replacing the CAR^{Ex7} cytoplasmic domain (including the PDZ binding motif) with that on CAR^{Ex8} or alternatively by deletion some from CAR^{Ex7} to make the full length same size as CAR^{Ex8}. Finally, it is possible that each isoform is associated with a different family of proteins due to the difference in the extreme C-term domains, which render CAR^{Ex8} but not CAR^{Ex7} accessible for cleavage by ADAM17.

ADAM17, but not ADAM10, has a PDZ binding motif and interacts with the third PDZ domain of another cellular PDZ-domain containing protein Dlg/SAP97 (178, 179). Interestingly, this interaction plays important role in the regulation ADAM17 activity. Disruption the ADAM17 interaction with the SAP97 PDZ domain significantly increased epidermal growth factor receptor (EGFR) shedding by ADAM17 into the cell media (178). If this is true, it would mean that ADAM17 activity can be regulated by interfering with its interactions with the PDZ domain. This strategy can be used to increase ADAM17 activity in conditions where ADAM17 is a potential therapeutic target. My data showed that blocking the ADAM17 interaction with MAGI-1 PDZ2

domain via TAT-PDZ2 targeted peptides reversed the degradation of CAR^{Ex8}, although I do not have evidence on how would that change ADAM17 activity.

MAGI-1 is a widely expressed scaffold protein in the body. Data from our lab has suggested that MAGI-1 is part of the endoplasmic reticulum associated degradation (ERAD). ERAD is a quality control mechanism that can target transmembrane proteins to the degradation pathway. The discovery that ADAM17 interacts with MAGI-1 is a novel finding and may link MAGI-1 mediated degradation to other associated proteins. This new finding can potentially explain the mechanism behind degradation of other MAGI-1 interacting proteins. For example, Delta-like ligand (Dll), which plays important role in cell communication and cell division, interacts with the fourth PDZ domain of MAGI-1 (180), and is known to undergo cleavage by ADAMs and secretases (181).

My data showed that silencing ADAM17 reversed the effect of TAT-PDZ1 peptides on CAR^{Ex8} degradation, nevertheless, many bands of CAR^{Ex8} were detected only in the ADAM17 silencing condition. The exact reason for these bands is still unknown but it is possible that silencing ADAM17 makes CAR^{Ex8} susceptible to post-translational modifications such as ubiquitination. Another strong hypothesis is that ADAM17 could be important for the proper glycosylation and folding of the full length CAR^{Ex8} (182). The actual molecular wt of CAR^{Ex8} is 38 KD but it runs at 46 KD on a SDS-PAGE gel. The is due to glycosylation of the extracellular domain of CAR^{Ex8}. It has been shown that glycosylation is necessary for the proper folding and for the functional effect of CAR (182). Therefore, the non-glycosylated CAR^{Ex8} is considered misfolded and it is trapped in the ER until it is fully glycosylated. The multiple bands of CAR^{Ex8} that appeared upon ADAM17 silencing could be the non- or partially-glycosylated forms of CAR. If this is

true, that would mean that ADAM17 acts as scavenger that degrades the non-functional forms of CAR^{Ex8}, which can be novel new role for the ADAM17 enzyme.

Several studies have shown that administration of "soluble CAR" ectodomain (sCAR) is a potential antiviral strategy for both wildtype AdV and CVB infection (162, 183, 184), however, systemic administration of the sCAR is immunogenic and can aggravate heart failure (184). Our approach is unique because it is expected to only augment the natural pathways that release the endogenous CAR extracellular domain in the local environment. Given the limited amount of receptor, it is predicted to be non-toxic and, since it is an endogenous pathway, is not expected be immunogenic.

There are reports that ADAM17 is responsible for cleavage of many other viral receptors. For example, both CD163, a receptor for Porcine reproductive and respiratory syndrome virus (PRRSV) infection, and Angiotensin Converting Enzyme 2 (ACE2) a well-known receptor for severe acute respiratory syndrome (SARS) virus, have been shown to undergo shedding by ADAM17, an effect that leads to decreased entry of the corresponding virus (185, 186). Moreover, there is an argument that the efficiency of AdV entry depends on additional stepwise interactions with co-receptors, such as integrins (72, 73). As its names implies, (A Dis-integrins And Metalloprotease), ADAM17 may cause shedding of the integrins from the cell surface (95, 128) and, therefore, it is possible that this could be an additional mechanism to decreases the AdV transduction in airway epithelia.

Although we have no preliminary data to indicate that AdV binding to CAR^{Ex8} will initiate RIP, it will be very exciting if it does. First, it is well known that AdV infection can activate numerous cellular signaling and transcription pathways, many of

which remain unknown but could affect viral virulence (187, 188). Second, published evidence indicates that AdV and CVB bind CAR at the cell surface initially but that CAR does not enter cells with the virus (75, 189, 190). Finally, shedding of the CAR ectodomain could interfere with viral entry mechanism by endocytosis (75, 191). This would explain a longstanding gap in the field. Insights into any of these processes could enhance drug discovery for reduction of viral infection, and potentially even CAR-related diseases such as dilated cardiomyopathy (183).

PDZ3 binding peptides are basically the opposite of PDZ1 binding peptides. Blocking the interaction between MAGI-1 PDZ3 and CAR^{Ex8} led to increased CAR^{Ex8} interaction with the savior PDZ1 domain and rescued CAR^{Ex8} from degradation. My data suggests that this increase is associated with more CAR^{Ex8} initially co-localized with the nucleus but then with the various endosomes within the cells. It is possible that CAR^{Ex8} is simply escaping the MAGI-1 ERAD-like surveillance. Interestingly, MAGI-1 does not end up at the apical surface so there must be a step of release, potentially within the Golgi sorting steps or upon packing into endosomes. Although the pathway through the cell was not fully characterized, blocking only the PDZ3 domain with TAT-ESAM or blocking both PDZ1 and PDZ3 domains with TAT-CAR^{Ex8}-9C appeared to be similar. Moreover, both of these peptides behaved similarly *in vivo* and increased AdV-Cre transduction of tdT mice equally. Further studies are needed to fully elucidate the mechanism of such effects.

Future directions

In the future, we would like to test the protective effect of TAT-PDZ1 peptides *in vivo* against AdV infection using animal model of pathogenicity. We would also test the efficacy of TAT-PDZ1 peptides in protecting against the Coxsackievirus infection which also uses CAR for binding and entry. We will also test the effectiveness of TAT-PDZ3 peptides in increase the AdV transduction and correction the cystic fibrosis *in vitro* and *in vivo*. Even though we did not detect any toxicity in our epithelia or *in vivo*, developing new peptides or other small molecule therapeutics with more specificity toward MAGI-1 PDZ1 or PDZ3 domains are more likely to have less off target effects and yield a more specific response.

References

1. Rowe WP, Huebner RJ, Gilmore LK, Parrott RH, Ward TG. 1953. Isolation of a cytopathogenic agent from human adenoids undergoing spontaneous degeneration in tissue culture. *Proc Soc Exp Biol Med* 84: 570-3
2. Hilleman MR, Werner JH. 1954. Recovery of New Agent from Patients with Acute Respiratory Illness. *Proceedings of the Society for Experimental Biology and Medicine* 85: 183-8
3. Ginsberg HS, Badger GF, Dingle JH, Jordan WS, Katz S. 1955. Etiologic Relationship of the Ri-67 Agent to Acute Respiratory Disease (Ard). *Journal of Clinical Investigation* 34: 820-31
4. Lynch JP, 3rd, Fishbein M, Echavarria M. 2011. Adenovirus. *Semin Respir Crit Care Med* 32: 494-511
5. Lai CY, Lee CJ, Lu CY, Lee PI, Shao PL, Wu ET, Wang CC, Tan BF, Chang HY, Hsia SH, Lin JJ, Chang LY, Huang YC, Huang LM, Taiwan Pediatric Infectious Disease A. 2013. Adenovirus serotype 3 and 7 infection with acute respiratory failure in children in Taiwan, 2010-2011. *PLoS One* 8: e53614
6. Sandrock C, Stollenwerk N. 2008. Acute febrile respiratory illness in the ICU: reducing disease transmission. *Chest* 133: 1221-31
7. Berk A. 2007. Adenoviridae: The Viruses and Their Replication. In *Fields Virology*, ed. DKaP Howley. Philadelphia: Lippincott Williams and Wilkins
8. Mahl MC, Sadler C. 1975. Virus survival on inanimate surfaces. *Can J Microbiol* 21: 819-23
9. Kramer A, Schwebke I, Kampf G. 2006. How long do nosocomial pathogens persist on inanimate surfaces? A systematic review. *BMC Infect Dis* 6: 130
10. Kolavic-Gray SA, Binn LN, Sanchez JL, Cersovsky SB, Polyak CS, Mitchell-Raymundo F, Asher LV, Vaughn DW, Feighner BH, Innis BL. 2002. Large epidemic of adenovirus type 4 infection among military trainees: epidemiological, clinical, and laboratory studies. *Clin Infect Dis* 35: 808-18
11. Jernigan JA, Lowry BS, Hayden FG, Kyger SA, Conway BP, Groschel DH, Farr BM. 1993. Adenovirus type 8 epidemic keratoconjunctivitis in an eye clinic: risk factors and control. *J Infect Dis* 167: 1307-13
12. Van R, Wun CC, O'Ryan ML, Matson DO, Jackson L, Pickering LK. 1992. Outbreaks of human enteric adenovirus types 40 and 41 in Houston day care centers. *J Pediatr* 120: 516-21
13. Tsou TP, Tan BF, Chang HY, Chen WC, Huang YP, Lai CY, Chao YN, Wei SH, Hung MN, Hsu LC, Lu CY, Shao PL, Mu JJ, Chang LY, Liu MT, Unknown Pathogen Discovery/Investigation G, Huang LM. 2012. Community outbreak of adenovirus, Taiwan, 2011. *Emerg Infect Dis* 18: 1825-32
14. William S. M. Wold MSH. 2007. Adenoviruses. In *Fields Virology*, ed. PMH David M. Knipe, pp. 2395-436. Philadelphia: Lippincott Williams and Wilkins

15. Russell KL, Hawksworth AW, Ryan MA, Strickler J, Irvine M, Hansen CJ, Gray GC, Gaydos JC. 2006. Vaccine-preventable adenoviral respiratory illness in US military recruits, 1999-2004. *Vaccine* 24: 2835-42
16. Kajon AE, Moseley JM, Metzgar D, Huong HS, Wadleigh A, Ryan MA, Russell KL. 2007. Molecular epidemiology of adenovirus type 4 infections in US military recruits in the postvaccination era (1997-2003). *J Infect Dis* 196: 67-75
17. Radin JM, Hawksworth AW, Blair PJ, Faix DJ, Raman R, Russell KL, Gray GC. 2014. Dramatic Decline of Respiratory Illness among US Military Recruits after the Renewed Use of Adenovirus Vaccines. *Clin Infect Dis* pii: ciu507.
18. Safrin S, Cherrington J, Jaffe HS. 1997. Clinical uses of cidofovir. *Rev Med Virol* 7: 145-56
19. Gavin PJ, Katz BZ. 2002. Intravenous ribavirin treatment for severe adenovirus disease in immunocompromised children. *Pediatrics* 110: e9
20. Matthes-Martin S, Feuchtinger T, Shaw PJ, Engelhard D, Hirsch HH, Cordonnier C, Ljungman P, Fourth European Conference on Infections in L. 2012. European guidelines for diagnosis and treatment of adenovirus infection in leukemia and stem cell transplantation: summary of ECIL-4 (2011). *Transpl Infect Dis* 14: 555-63
21. Holcakova J, Tomasec P, Bugert JJ, Wang EC, Wilkinson GW, Hrstka R, Krystof V, Strnad M, Vojtesek B. 2010. The inhibitor of cyclin-dependent kinases, olomoucine II, exhibits potent antiviral properties. *Antivir Chem Chemother* 20: 133-42
22. Grosche P, Sirockin F, Mac Sweeney A, Ramage P, Erbel P, Melkko S, Bernardi A, Hughes N, Ellis D, Combrink KD, Jarousse N, Altmann E. 2015. Structure-based design and optimization of potent inhibitors of the adenoviral protease. *Bioorg Med Chem Lett* 25: 438-43
23. Mac Sweeney A, Grosche P, Ellis D, Combrink K, Erbel P, Hughes N, Sirockin F, Melkko S, Bernardi A, Ramage P, Jarousse N, Altmann E. 2014. Discovery and structure-based optimization of adenain inhibitors. *ACS Med Chem Lett* 5: 937-41
24. Caruso Brown AE, Cohen MN, Tong S, Braverman RS, Rooney JF, Giller R, Levin MJ. 2015. Pharmacokinetics and safety of intravenous cidofovir for life-threatening viral infections in pediatric hematopoietic stem cell transplant recipients. *Antimicrob Agents Chemother* 59: 3718-25
25. Symeonidis N, Jakubowski A, Pierre-Louis S, Jaffe D, Pamer E, Sepkowitz K, O'Reilly RJ, Papanicolaou GA. 2007. Invasive adenoviral infections in T-cell-depleted allogeneic hematopoietic stem cell transplantation: high mortality in the era of cidofovir. *Transpl Infect Dis* 9: 108-13
26. Kinchington PR, Romanowski EG, Jerold Gordon Y. 2005. Prospects for adenovirus antivirals. *J Antimicrob Chemother* 55: 424-9
27. Spjut S, Qian W, Bauer J, Storm R, Frangsmyr L, Stehle T, Arnberg N, Elofsson M. 2011. A potent trivalent sialic acid inhibitor of adenovirus type 37 infection of human corneal cells. *Angew Chem Int Ed Engl* 50: 6519-21
28. Wirth T, Parker N, Yla-Herttuala S. 2013. History of gene therapy. *Gene* 525: 162-9

29. Edelstein ML, Abedi MR, Wixon J. 2007. Gene therapy clinical trials worldwide to 2007--an update. *J Gene Med* 9: 833-42
30. Bergelson JM, Cunningham JA, Droguett G, Kurt-Jones EA, Krithivas A, Hong JS, Horwitz MS, Crowell RL, Finberg RW. 1997. Isolation of a common receptor for Coxsackie B viruses and adenoviruses 2 and 5. *Science* 275: 1320-3
31. Tomko RP, Xu R, Philipson L. 1997. HCAR and MCAR: the human and mouse cellular receptors for subgroup C adenoviruses and group B coxsackieviruses. *Proc Natl Acad Sci U S A* 94: 3352-6
32. Carson SD, Chapman NN, Tracy SM. 1997. Purification of the putative coxsackievirus B receptor from HeLa cells. *Biochemical and Biophysical Research Communications* 233: 325-8
33. Wang X, Bergelson JM. 1999. Coxsackievirus and adenovirus receptor cytoplasmic and transmembrane domains are not essential for coxsackievirus and adenovirus infection. *J Virol* 73: 2559-62
34. Walters RW, van't Hof W, Yi SM, Schroth MK, Zabner J, Crystal RG, Welsh MJ. 2001. Apical localization of the coxsackie-adenovirus receptor by glycosyl-phosphatidylinositol modification is sufficient for adenovirus-mediated gene transfer through the apical surface of human airway epithelia. *J Virol* 75: 7703-11
35. Stonebraker JR, Wagner D, Lefensty RW, Burns K, Gendler SJ, Bergelson JM, Boucher RC, O'Neal WK, Pickles RJ. 2004. Glycocalyx restricts adenoviral vector access to apical receptors expressed on respiratory epithelium in vitro and in vivo: role for tethered mucins as barriers to lumenal infection. *J Virol* 78: 13755-68
36. Wood M, Perrotte P, Onishi E, Harper ME, Dinney C, Pagliaro L, Wilson DR. 1999. Biodistribution of an adenoviral vector carrying the luciferase reporter gene following intravesical or intravenous administration to a mouse. *Cancer Gene Ther* 6: 367-72
37. Huch M, Abate-Daga D, Roig JM, Gonzalez JR, Fabregat J, Sosnowski B, Mazo A, Fillat C. 2006. Targeting the CYP2B 1/cyclophosphamide suicide system to fibroblast growth factor receptors results in a potent antitumoral response in pancreatic cancer models. *Hum Gene Ther* 17: 1187-200
38. Printz MA, Gonzalez AM, Cunningham M, Gu DL, Ong M, Pierce GF, Aukerman SL. 2000. Fibroblast growth factor 2-retargeted adenoviral vectors exhibit a modified biolocalization pattern and display reduced toxicity relative to native adenoviral vectors. *Hum Gene Ther* 11: 191-204
39. Reynolds PN, Zinn KR, Gavrilyuk VD, Balyasnikova IV, Rogers BE, Buchsbaum DJ, Wang MH, Miletich DJ, Grizzle WE, Douglas JT, Danilov SM, Curiel DT. 2000. A targetable, injectable adenoviral vector for selective gene delivery to pulmonary endothelium in vivo. *Mol Ther* 2: 562-78
40. Eto Y, Gao JQ, Sekiguchi F, Kurachi S, Katayama K, Maeda M, Kawasaki K, Mizuguchi H, Hayakawa T, Tsutsumi Y, Mayumi T, Nakagawa S. 2005. PEGylated adenovirus vectors containing RGD peptides on the tip of PEG show high transduction efficiency and antibody evasion ability. *J Gene Med* 7: 604-12
41. Wu H, Seki T, Dmitriev I, Uil T, Kashentseva E, Han T, Curiel DT. 2002. Double modification of adenovirus fiber with RGD and polylysine motifs improves

coxsackievirus-adenovirus receptor-independent gene transfer efficiency. *Hum Gene Ther* 13: 1647-53
42. Sengupta S, Ulasov IV, Thaci B, Ahmed AU, Lesniak MS. 2011. Enhanced transduction and replication of RGD-fiber modified adenovirus in primary T cells. *PLoS One* 6: e18091
43. Kimball KJ, Preuss MA, Barnes MN, Wang M, Siegal GP, Wan W, Kuo H, Saddekni S, Stockard CR, Grizzle WE, Harris RD, Aurigemma R, Curiel DT, Alvarez RD. 2010. A phase I study of a tropism-modified conditionally replicative adenovirus for recurrent malignant gynecologic diseases. *Clin Cancer Res* 16: 5277-87
44. Thomas CE, Ehrhardt A, Kay MA. 2003. Progress and problems with the use of viral vectors for gene therapy. *Nat Rev Genet* 4: 346-58
45. Excoffon KJ, Gansemer ND, Mobily ME, Karp PH, Parekh KR, Zabner J. 2010. Isoform-specific regulation and localization of the coxsackie and adenovirus receptor in human airway epithelia. *PLoS One* 5: e9909
46. van Raaij MJ, Chouin E, van der Zandt H, Bergelson JM, Cusack S. 2000. Dimeric structure of the coxsackievirus and adenovirus receptor D1 domain at 1.7 A resolution. *Structure* 8: 1147-55
47. Cohen CJ, Shieh JT, Pickles RJ, Okegawa T, Hsieh JT, Bergelson JM. 2001. The coxsackievirus and adenovirus receptor is a transmembrane component of the tight junction. *Proc Natl Acad Sci U S A* 98: 15191-6
48. Excoffon KJ, Avenarius MR, Hansen MR, Kimberling WJ, Najmabadi H, Smith RJ, Zabner J. 2006. The Coxsackievirus and Adenovirus Receptor: a new adhesion protein in cochlear development. *Hear Res* 215: 1-9
49. Excoffon KJDA, Traver GL, Zabner J. 2005. The role of the extracellular domain in the biology of the Coxsackievirus and Adenovirus Receptor. *American Journal of Respiratory Cell and Molecular Biology* 32: 498-503
50. Morton PE, Hicks A, Nastos T, Santis G, Parsons M. 2013. CAR regulates epithelial cell junction stability through control of E-cadherin trafficking. *Sci Rep* 3: 2889
51. van't Hof W, Crystal RG. 2002. Fatty acid modification of the coxsackievirus and adenovirus receptor. *J Virol* 76: 6382-6
52. Gao Y, Lui WY. 2014. Synergistic effect of interferon-gamma and tumor necrosis factor-alpha on coxsackievirus and adenovirus receptor expression: an explanation of cell sloughing during testicular inflammation in mice. *Biol Reprod* 90: 59
53. Raschperger E, Thyberg J, Pettersson S, Philipson L, Fuxe J, Pettersson RF. 2006. The coxsackie- and adenovirus receptor (CAR) is an in vivo marker for epithelial tight junctions, with a potential role in regulating permeability and tissue homeostasis. *Exp Cell Res* 312: 1566-80
54. Dorner AA, Wegmann F, Butz S, Wolburg-Buchholz K, Wolburg H, Mack A, Nasdala I, August B, Westermann J, Rathjen FG, Vestweber D. 2005. Coxsackievirus-adenovirus receptor (CAR) is essential for early embryonic cardiac development. *J Cell Sci* 118: 3509-21
55. Asher DR, Cerny AM, Weiler SR, Horner JW, Keeler ML, Neptune MA, Jones SN, Bronson RT, Depinho RA, Finberg RW. 2005. Coxsackievirus and

adenovirus receptor is essential for cardiomyocyte development. *Genesis* 42: 77-85
56. Chen JW, Zhou B, Yu QC, Shin SJ, Jiao K, Schneider MD, Baldwin HS, Bergelson JM. 2006. Cardiomyocyte-specific deletion of the coxsackievirus and adenovirus receptor results in hyperplasia of the embryonic left ventricle and abnormalities of sinuatrial valves. *Circ Res* 98: 923-30
57. Noutsias M, Fechner H, de Jonge H, Wang X, Dekkers D, Houtsmuller AB, Pauschinger M, Bergelson J, Warraich R, Yacoub M, Hetzer R, Lamers J, Schultheiss HP, Poller W. 2001. Human coxsackie-adenovirus receptor is colocalized with integrins alpha(v)beta(3) and alpha(v)beta(5) on the cardiomyocyte sarcolemma and upregulated in dilated cardiomyopathy: implications for cardiotropic viral infections. *Circulation* 104: 275-80
58. Tomko RP, Johansson CB, Totrov M, Abagyan R, Frisen J, Philipson L. 2000. Expression of the adenovirus receptor and its interaction with the fiber knob. *Exp Cell Res* 255: 47-55
59. Raschperger E, Thyberg J, Pettersson S, Philipson L, Fuxe J, Pettersson RF. 2006. The coxsackie- and adenovirus receptor (CAR) is an in vivo marker for epithelial tight junctions, with a potential role in regulating permeability and tissue homeostasis. *Experimental Cell Research* 312: 1566-80
60. Kotha PL, Sharma P, Kolawole AO, Yan R, Alghamri MS, Brockman TL, Gomez-Cambronero J, Excoffon KJ. 2015. Adenovirus entry from the apical surface of polarized epithelia is facilitated by the host innate immune response. *PLoS Pathog* 11: e1004696
61. Diaz F, Gravotta D, Deora A, Schreiner R, Schoggins J, Falck-Pedersen E, Rodriguez-Boulan E. 2009. Clathrin adaptor AP1B controls adenovirus infectivity of epithelial cells. *Proc Natl Acad Sci U S A* 106: 11143-8
62. Carson SD, Chapman NN, Tracy SM. 1997. Purification of the putative coxsackievirus B receptor from HeLa cells. *Biochem Biophys Res Commun* 233: 325-8
63. Kolawole AO, Sharma P, Yan R, Lewis KJ, Xu Z, Hostetler HA, Ashbourne Excoffon KJ. 2012. The PDZ1 and PDZ3 domains of MAGI-1 regulate the eight-exon isoform of the coxsackievirus and adenovirus receptor. *J Virol* 86: 9244-54
64. Sharma P, Kolawole AO, Core SB, Kajon AE, Excoffon KJ. 2012. Sidestream smoke exposure increases the susceptibility of airway epithelia to adenoviral infection. *PLoS One* 7: e49930
65. Ohka S, Ohno H, Tohyama K, Nomoto A. 2001. Basolateral sorting of human poliovirus receptor alpha involves an interaction with the mu1B subunit of the clathrin adaptor complex in polarized epithelial cells. *Biochem Biophys Res Commun* 287: 941-8
66. Gaggar A, Shayakhmetov DM, Lieber A. 2003. CD46 is a cellular receptor for group B adenoviruses. *Nat Med* 9: 1408-12
67. Sirena D, Lilienfeld B, Eisenhut M, Kalin S, Boucke K, Beerli RR, Vogt L, Ruedl C, Bachmann MF, Greber UF, Hemmi S. 2004. The human membrane cofactor CD46 is a receptor for species B adenovirus serotype 3. *J Virol* 78: 4454-62

68. Marttila M, Persson D, Gustafsson D, Liszewski MK, Atkinson JP, Wadell G, Arnberg N. 2005. CD46 is a cellular receptor for all species B adenoviruses except types 3 and 7. *J Virol* 79: 14429-36
69. Segerman A, Atkinson JP, Marttila M, Dennerquist V, Wadell G, Arnberg N. 2003. Adenovirus type 11 uses CD46 as a cellular receptor. *J Virol* 77: 9183-91
70. Roelvink PW, Lizonova A, Lee JG, Li Y, Bergelson JM, Finberg RW, Brough DE, Kovesdi I, Wickham TJ. 1998. The coxsackievirus-adenovirus receptor protein can function as a cellular attachment protein for adenovirus serotypes from subgroups A, C, D, E, and F. *J Virol* 72: 7909-15
71. Roelvink PW, Mi Lee G, Einfeld DA, Kovesdi I, Wickham TJ. 1999. Identification of a conserved receptor-binding site on the fiber proteins of CAR-recognizing adenoviridae. *Science* 286: 1568-71
72. Wickham TJ, Mathias P, Cheresh DA, Nemerow GR. 1993. Integrins alpha v beta 3 and alpha v beta 5 promote adenovirus internalization but not virus attachment. *Cell* 73: 309-19
73. Li E, Brown SL, Stupack DG, Puente XS, Cheresh DA, Nemerow GR. 2001. Integrin alpha(v)beta1 is an adenovirus coreceptor. *J Virol* 75: 5405-9
74. Wang K, Huang S, Kapoor-Munshi A, Nemerow G. 1998. Adenovirus internalization and infection require dynamin. *J Virol* 72: 3455-8
75. Greber UF, Willetts M, Webster P, Helenius A. 1993. Stepwise dismantling of adenovirus 2 during entry into cells. *Cell* 75: 477-86
76. Wiethoff CM, Wodrich H, Gerace L, Nemerow GR. 2005. Adenovirus protein VI mediates membrane disruption following capsid disassembly. *J Virol* 79: 1992-2000
77. Meier O, Greber UF. 2004. Adenovirus endocytosis. *J Gene Med* 6 Suppl 1: S152-63
78. Excoffon KJDA, Moninger T, Zabner J. 2003. The coxsackie B virus and adenovirus receptor resides in a distinct membrane microdomain. *Journal of Virology* 77: 2559-67
79. Leopold PL, Kreitzer G, Miyazawa N, Rempel S, Pfister KK, Rodriguez-Boulan E, Crystal RG. 2000. Dynein- and microtubule-mediated translocation of adenovirus serotype 5 occurs after endosomal lysis. *Hum Gene Ther* 11: 151-65
80. Suomalainen M, Nakano MY, Keller S, Boucke K, Stidwill RP, Greber UF. 1999. Microtubule-dependent plus- and minus end-directed motilities are competing processes for nuclear targeting of adenovirus. *J Cell Biol* 144: 657-72
81. Coughlan L, Alba R, Parker AL, Bradshaw AC, McNeish IA, Nicklin SA, Baker AH. 2010. Tropism-modification strategies for targeted gene delivery using adenoviral vectors. *Viruses* 2: 2290-355
82. Cho KO, Hunt CA, Kennedy MB. 1992. The rat brain postsynaptic density fraction contains a homolog of the Drosophila discs-large tumor suppressor protein. *Neuron* 9: 929-42
83. Woods DF, Bryant PJ. 1991. The discs-large tumor suppressor gene of Drosophila encodes a guanylate kinase homolog localized at septate junctions. *Cell* 66: 451-64
84. Itoh M, Nagafuchi A, Yonemura S, Kitani-Yasuda T, Tsukita S, Tsukita S. 1993. The 220-kD protein colocalizing with cadherins in non-epithelial cells is identical

to ZO-1, a tight junction-associated protein in epithelial cells: cDNA cloning and immunoelectron microscopy. *J Cell Biol* 121: 491-502
85. Cushing PR, Fellows A, Villone D, Boisguerin P, Madden DR. 2008. The relative binding affinities of PDZ partners for CFTR: a biochemical basis for efficient endocytic recycling. *Biochemistry* 47: 10084-98
86. Funke L, Dakoji S, Bredt DS. 2005. Membrane-associated guanylate kinases regulate adhesion and plasticity at cell junctions. *Annu Rev Biochem* 74: 219-45
87. Montgomery JM, Zamorano PL, Garner CC. 2004. MAGUKs in synapse assembly and function: an emerging view. *Cell Mol Life Sci* 61: 911-29
88. Laura RP, Ross S, Koeppen H, Lasky LA. 2002. MAGI-1: a widely expressed, alternatively spliced tight junction protein. *Exp Cell Res* 275: 155-70
89. Garner CC, Nash J, Huganir RL. 2000. PDZ domains in synapse assembly and signalling. *Trends Cell Biol* 10: 274-80
90. Dev KK. 2004. Making protein interactions druggable: targeting PDZ domains. *Nat Rev Drug Discov* 3: 1047-56
91. Morais Cabral JH, Petosa C, Sutcliffe MJ, Raza S, Byron O, Poy F, Marfatia SM, Chishti AH, Liddington RC. 1996. Crystal structure of a PDZ domain. *Nature* 382: 649-52
92. Ebnet K, Aurrand-Lions M, Kuhn A, Kiefer F, Butz S, Zander K, Meyer zu Brickwedde MK, Suzuki A, Imhof BA, Vestweber D. 2003. The junctional adhesion molecule (JAM) family members JAM-2 and JAM-3 associate with the cell polarity protein PAR-3: a possible role for JAMs in endothelial cell polarity. *J Cell Sci* 116: 3879-91
93. Lee HJ, Zheng JJ. 2010. PDZ domains and their binding partners: structure, specificity, and modification. *Cell Commun Signal* 8: 8
94. Nie J, McGill MA, Dermer M, Dho SE, Wolting CD, McGlade CJ. 2002. LNX functions as a RING type E3 ubiquitin ligase that targets the cell fate determinant Numb for ubiquitin-dependent degradation. *EMBO J* 21: 93-102
95. Cheng J, Guggino W. 2013. Ubiquitination and degradation of CFTR by the E3 ubiquitin ligase MARCH2 through its association with adaptor proteins CAL and STX6. *PLoS One* 8: e68001
96. Yan P, Fu J, Qu Z, Li S, Tanaka T, Grusby MJ, Xiao G. 2009. PDLIM2 suppresses human T-cell leukemia virus type I Tax-mediated tumorigenesis by targeting Tax into the nuclear matrix for proteasomal degradation. *Blood* 113: 4370-80
97. Pieczynski J, Margolis B. 2011. Protein complexes that control renal epithelial polarity. *Am J Physiol Renal Physiol* 300: F589-601
98. Nooh MM, Naren AP, Kim SJ, Xiang YK, Bahouth SW. 2013. SAP97 controls the trafficking and resensitization of the beta-1-adrenergic receptor through its PDZ2 and I3 domains. *PLoS One* 8: e63379
99. Kim E, Niethammer M, Rothschild A, Jan YN, Sheng M. 1995. Clustering of Shaker-type K+ channels by interaction with a family of membrane-associated guanylate kinases. *Nature* 378: 85-8
100. Petitprez S, Zmoos AF, Ogrodnik J, Balse E, Raad N, El-Haou S, Albesa M, Bittihn P, Luther S, Lehnart SE, Hatem SN, Coulombe A, Abriel H. 2011. SAP97

and dystrophin macromolecular complexes determine two pools of cardiac sodium channels Nav1.5 in cardiomyocytes. *Circ Res* 108: 294-304
101. Craven SE, Bredt DS. 1998. PDZ proteins organize synaptic signaling pathways. *Cell* 93: 495-8
102. Coyne CB, Voelker T, Pichla SL, Bergelson JM. 2004. The coxsackievirus and adenovirus receptor interacts with the multi-PDZ domain protein-1 (MUPP-1) within the tight junction. *J Biol Chem* 279: 48079-84
103. Excoffon KJ, Hruska-Hageman A, Klotz M, Traver GL, Zabner J. 2004. A role for the PDZ-binding domain of the coxsackie B virus and adenovirus receptor (CAR) in cell adhesion and growth. *J Cell Sci* 117: 4401-9
104. Mirza M, Raschperger E, Philipson L, Pettersson RF, Sollerbrant K. 2005. The cell surface protein coxsackie- and adenovirus receptor (CAR) directly associates with the Ligand-of-Numb Protein-X2 (LNX2). *Exp Cell Res* 309: 110-20
105. Sollerbrant K, Raschperger E, Mirza M, Engstrom U, Philipson L, Ljungdahl PO, Pettersson RF. 2003. The Coxsackievirus and adenovirus receptor (CAR) forms a complex with the PDZ domain-containing protein ligand-of-numb protein-X (LNX). *J Biol Chem* 278: 7439-44
106. Excoffon KJ, Kolawole AO, Kusama N, Gansemer ND, Sharma P, Hruska-Hageman AM, Petroff E, Benson CJ. 2012. Coxsackievirus and adenovirus receptor (CAR) mediates trafficking of acid sensing ion channel 3 (ASIC3) via PSD-95. *Biochem Biophys Res Commun* 425: 13-8
107. Javier RT, Rice AP. 2011. Emerging theme: cellular PDZ proteins as common targets of pathogenic viruses. *J Virol* 85: 11544-56
108. Glaunsinger BA, Lee SS, Thomas M, Banks L, Javier R. 2000. Interactions of the PDZ-protein MAGI-1 with adenovirus E4-ORF1 and high-risk papillomavirus E6 oncoproteins. *Oncogene* 19: 5270-80
109. Massimi P, Gammoh N, Thomas M, Banks L. 2004. HPV E6 specifically targets different cellular pools of its PDZ domain-containing tumour suppressor substrates for proteasome-mediated degradation. *Oncogene* 23: 8033-9
110. Dobrosotskaya I, Guy RK, James GL. 1997. MAGI-1, a membrane-associated guanylate kinase with a unique arrangement of protein-protein interaction domains. *J Biol Chem* 272: 31589-97
111. Thomas M, Narayan N, Pim D, Tomaic V, Massimi P, Nagasaka K, Kranjec C, Gammoh N, Banks L. 2008. Human papillomaviruses, cervical cancer and cell polarity. *Oncogene* 27: 7018-30
112. Zhang Y, Dasgupta J, Ma RZ, Banks L, Thomas M, Chen XS. 2007. Structures of a human papillomavirus (HPV) E6 polypeptide bound to MAGUK proteins: mechanisms of targeting tumor suppressors by a high-risk HPV oncoprotein. *J Virol* 81: 3618-26
113. Muller M, Jacob Y, Jones L, Weiss A, Brino L, Chantier T, Lotteau V, Favre M, Demeret C. 2012. Large scale genotype comparison of human papillomavirus E2-host interaction networks provides new insights for e2 molecular functions. *PLoS Pathog* 8: e1002761
114. Kranjec C, Banks L. 2011. A systematic analysis of human papillomavirus (HPV) E6 PDZ substrates identifies MAGI-1 as a major target of HPV type 16 (HPV-16)

and HPV-18 whose loss accompanies disruption of tight junctions. *J Virol* 85: 1757-64
115. van den Berg A, Dowdy SF. 2011. Protein transduction domain delivery of therapeutic macromolecules. *Curr Opin Biotechnol* 22: 888-93
116. Schwarze SR, Dowdy SF. 2000. In vivo protein transduction: intracellular delivery of biologically active proteins, compounds and DNA. *Trends Pharmacol Sci* 21: 45-8
117. Jones AT, Sayers EJ. 2012. Cell entry of cell penetrating peptides: tales of tails wagging dogs. *J Control Release* 161: 582-91
118. Schwarze SR, Ho A, Vocero-Akbani A, Dowdy SF. 1999. In vivo protein transduction: delivery of a biologically active protein into the mouse. *Science* 285: 1569-72
119. Cai SR, Xu G, Becker-Hapak M, Ma M, Dowdy SF, McLeod HL. 2006. The kinetics and tissue distribution of protein transduction in mice. *Eur J Pharm Sci* 27: 311-9
120. Takayama K, Hirose H, Tanaka G, Pujals S, Katayama S, Nakase I, Futaki S. 2012. Effect of the attachment of a penetration accelerating sequence and the influence of hydrophobicity on octaarginine-mediated intracellular delivery. *Mol Pharm* 9: 1222-30
121. Villegas-Mendez A, Fender P, Garin MI, Rothe R, Liguori L, Marques B, Lenormand JL. 2012. Functional characterisation of the WW minimal domain for delivering therapeutic proteins by adenovirus dodecahedron. *PLoS One* 7: e45416
122. Hill MD, Martin RH, Mikulis D, Wong JH, Silver FL, Terbrugge KG, Milot G, Clark WM, Macdonald RL, Kelly ME, Boulton M, Fleetwood I, McDougall C, Gunnarsson T, Chow M, Lum C, Dodd R, Poublanc J, Krings T, Demchuk AM, Goyal M, Anderson R, Bishop J, Garman D, Tymianski M, investigators Et. 2012. Safety and efficacy of NA-1 in patients with iatrogenic stroke after endovascular aneurysm repair (ENACT): a phase 2, randomised, double-blind, placebo-controlled trial. *Lancet Neurol* 11: 942-50
123. Long W, Corbet A, Cotton R, Courtney S, McGuiness G, Walter D, Watts J, Smyth J, Bard H, Chernick V. 1991. A controlled trial of synthetic surfactant in infants weighing 1250 g or more with respiratory distress syndrome. The American Exosurf Neonatal Study Group I, and the Canadian Exosurf Neonatal Study Group. *N Engl J Med* 325: 1696-703
124. Bakker EM, Volpi S, Salonini E, Mullinger B, Kroneberg P, Bakker M, Hop WC, Assael BM, Tiddens HA. 2014. Small airway deposition of dornase alfa during exacerbations in cystic fibrosis; a randomized controlled clinical trial. *Pediatr Pulmonol* 49: 154-61
125. Kotelevets L, van Hengel J, Bruyneel E, Mareel M, van Roy F, Chastre E. 2005. Implication of the MAGI-1b/PTEN signalosome in stabilization of adherens junctions and suppression of invasiveness. *FASEB J* 19: 115-7
126. D'Mello R, Marchand F, Pezet S, McMahon SB, Dickenson AH. 2011. Perturbing PSD-95 interactions with NR2B-subtype receptors attenuates spinal nociceptive plasticity and neuropathic pain. *Mol Ther* 19: 1780-92
127. Bach A, Clausen BH, Moller M, Vestergaard B, Chi CN, Round A, Sorensen PL, Nissen KB, Kastrup JS, Gajhede M, Jemth P, Kristensen AS, Lundstrom P,

Lambertsen KL, Stromgaard K. 2012. A high-affinity, dimeric inhibitor of PSD-95 bivalently interacts with PDZ1-2 and protects against ischemic brain damage. *Proc Natl Acad Sci U S A* 109: 3317-22

128. Qian Z, Xu X, Amacher JF, Madden DR, Cormet-Boyaka E, Pei D. 2015. Intracellular Delivery of Peptidyl Ligands by Reversible Cyclization: Discovery of a PDZ Domain Inhibitor that Rescues CFTR Activity. *Angew Chem Int Ed Engl* 54: 5874-8
129. Thorsen TS, Madsen KL, Rebola N, Rathje M, Anggono V, Bach A, Moreira IS, Stuhr-Hansen N, Dyhring T, Peters D, Beuming T, Huganir R, Weinstein H, Mulle C, Stromgaard K, Ronn LC, Gether U. 2010. Identification of a small-molecule inhibitor of the PICK1 PDZ domain that inhibits hippocampal LTP and LTD. *Proc Natl Acad Sci U S A* 107: 413-8
130. Nagai Y, Fujikake N, Ohno K, Higashiyama H, Popiel HA, Rahadian J, Yamaguchi M, Strittmatter WJ, Burke JR, Toda T. 2003. Prevention of polyglutamine oligomerization and neurodegeneration by the peptide inhibitor QBP1 in Drosophila. *Hum Mol Genet* 12: 1253-9
131. Popiel HA, Nagai Y, Fujikake N, Toda T. 2007. Protein transduction domain-mediated delivery of QBP1 suppresses polyglutamine-induced neurodegeneration in vivo. *Mol Ther* 15: 303-9
132. Zhang W, Penmatsa H, Ren A, Punchihewa C, Lemoff A, Yan B, Fujii N, Naren AP. 2011. Functional regulation of cystic fibrosis transmembrane conductance regulator-containing macromolecular complexes: a small-molecule inhibitor approach. *Biochem J* 435: 451-62
133. Zhang Y, Appleton BA, Wiesmann C, Lau T, Costa M, Hannoush RN, Sidhu SS. 2009. Inhibition of Wnt signaling by Dishevelled PDZ peptides. *Nat Chem Biol* 5: 217-9
134. Patrie KM, Drescher AJ, Welihinda A, Mundel P, Margolis B. 2002. Interaction of two actin-binding proteins, synaptopodin and alpha-actinin-4, with the tight junction protein MAGI-1. *J Biol Chem* 277: 30183-90
135. Shiratsuchi T, Oda K, Nishimori H, Suzuki M, Takahashi E, Tokino T, Nakamura Y. 1998. Cloning and characterization of BAP3 (BAI-associated protein 3), a C2 domain-containing protein that interacts with BAI1. *Biochem Biophys Res Commun* 251: 158-65
136. Dobrosotskaya IY, James GL. 2000. MAGI-1 interacts with beta-catenin and is associated with cell-cell adhesion structures. *Biochem Biophys Res Commun* 270: 903-9
137. Xu Z, Peng AW, Oshima K, Heller S. 2008. MAGI-1, a candidate stereociliary scaffolding protein, associates with the tip-link component cadherin 23. *J Neurosci* 28: 11269-76
138. Ohno H, Hirabayashi S, Kansaku A, Yao I, Tajima M, Nishimura W, Ohnishi H, Mashima H, Fujita T, Omata M, Hata Y. 2003. Carom: a novel membrane-associated guanylate kinase-interacting protein with two SH3 domains. *Oncogene* 22: 8422-31
139. Wegmann F, Ebnet K, Du Pasquier L, Vestweber D, Butz S. 2004. Endothelial adhesion molecule ESAM binds directly to the multidomain adaptor MAGI-1 and recruits it to cell contacts. *Exp Cell Res* 300: 121-33

140. Hirabayashi S, Tajima M, Yao I, Nishimura W, Mori H, Hata Y. 2003. JAM4, a junctional cell adhesion molecule interacting with a tight junction protein, MAGI-1. *Mol Cell Biol* 23: 4267-82
141. Tanemoto M, Toyohara T, Abe T, Ito S. 2008. MAGI-1a functions as a scaffolding protein for the distal renal tubular basolateral K+ channels. *J Biol Chem* 283: 12241-7
142. Patrie KM, Drescher AJ, Goyal M, Wiggins RC, Margolis B. 2001. The membrane-associated guanylate kinase protein MAGI-1 binds megalin and is present in glomerular podocytes. *J Am Soc Nephrol* 12: 667-77
143. Hirabayashi S, Mori H, Kansaku A, Kurihara H, Sakai T, Shimizu F, Kawachi H, Hata Y. 2005. MAGI-1 is a component of the glomerular slit diaphragm that is tightly associated with nephrin. *Lab Invest* 85: 1528-43
144. Dobrosotskaya IY. 2001. Identification of mNET1 as a candidate ligand for the first PDZ domain of MAGI-1. *Biochem Biophys Res Commun* 283: 969-75
145. Chastre E, Abdessamad M, Kruglov A, Bruyneel E, Bracke M, Di Gioia Y, Beckerle MC, van Roy F, Kotelevets L. 2009. TRIP6, a novel molecular partner of the MAGI-1 scaffolding molecule, promotes invasiveness. *FASEB J* 23: 916-28
146. He J, Bellini M, Inuzuka H, Xu J, Xiong Y, Yang X, Castleberry AM, Hall RA. 2006. Proteomic analysis of beta1-adrenergic receptor interactions with PDZ scaffold proteins. *J Biol Chem* 281: 2820-7
147. Mino A, Ohtsuka T, Inoue E, Takai Y. 2000. Membrane-associated guanylate kinase with inverted orientation (MAGI)-1/brain angiogenesis inhibitor 1-associated protein (BAP1) as a scaffolding molecule for Rap small G protein GDP/GTP exchange protein at tight junctions. *Genes Cells* 5: 1009-16
148. Ridgway LD, Kim EY, Dryer SE. 2009. MAGI-1 interacts with Slo1 channel proteins and suppresses Slo1 expression on the cell surface. *Am J Physiol Cell Physiol* 297: C55-65
149. Thomas M, Kranjec C, Nagasaka K, Matlashewski G, Banks L. 2011. Analysis of the PDZ binding specificities of Influenza A virus NS1 proteins. *Virol J* 8: 25
150. Yan R, Sharma P, Kolawole AO, Martin SC, Readler JM, Kotha PL, Hostetler HA, Excoffon KJ. 2015. The PDZ3 domain of the cellular scaffolding protein MAGI-1 interacts with the Coxsackievirus and adenovirus receptor (CAR). *Int J Biochem Cell Biol* 61: 29-34
151. Tennant JR. 1964. Evaluation of the Trypan Blue Technique for Determination of Cell Viability. *Transplantation* 2: 685-94
152. Alghamri MS, Morris M, Meszaros JG, Elased KM, Grobe N. 2014. Novel role of aminopeptidase-A in angiotensin-(1-7) metabolism post myocardial infarction. *Am J Physiol Heart Circ Physiol* 306: H1032-40
153. Merluzzi S, Moretti M, Altamura S, Zwollo P, Sigvardsson M, Vitale G, Pucillo C. 2004. CD40 stimulation induces Pax5/BSAP and EBF activation through a APE/Ref-1-dependent redox mechanism. *J Biol Chem* 279: 1777-86
154. Grobe N, Di Fulvio M, Kashkari N, Chodavarapu H, Somineni HK, Singh R, Elased KM. 2015. Functional and molecular evidence for expression of the renin angiotensin system and ADAM17-mediated ACE2 shedding in COS7 cells. *Am J Physiol Cell Physiol* 308: C767-77

155. Strengert M, Knaus UG. 2011. Analysis of epithelial barrier integrity in polarized lung epithelial cells. *Methods Mol Biol* 763: 195-206
156. Cramm-Behrens CI, Dienst M, Jacob R. 2008. Apical cargo traverses endosomal compartments on the passage to the cell surface. *Traffic* 9: 2206-20
157. Prince GA, Porter DD, Jenson AB, Horswood RL, Chanock RM, Ginsberg HS. 1993. Pathogenesis of adenovirus type 5 pneumonia in cotton rats (Sigmodon hispidus). *J Virol* 67: 101-11
158. Houri N, Huang KC, Nalbantoglu J. 2013. The Coxsackievirus and Adenovirus Receptor (CAR) undergoes ectodomain shedding and regulated intramembrane proteolysis (RIP). *PLoS One* 8: e73296
159. Le Gall SM, Bobe P, Reiss K, Horiuchi K, Niu XD, Lundell D, Gibb DR, Conrad D, Saftig P, Blobel CP. 2009. ADAMs 10 and 17 represent differentially regulated components of a general shedding machinery for membrane proteins such as transforming growth factor alpha, L-selectin, and tumor necrosis factor alpha. *Mol Biol Cell* 20: 1785-94
160. Sahin U, Weskamp G, Kelly K, Zhou HM, Higashiyama S, Peschon J, Hartmann D, Saftig P, Blobel CP. 2004. Distinct roles for ADAM10 and ADAM17 in ectodomain shedding of six EGFR ligands. *J Cell Biol* 164: 769-79
161. Goodfellow IG, Evans DJ, Blom AM, Kerrigan D, Miners JS, Morgan BP, Spiller OB. 2005. Inhibition of coxsackie B virus infection by soluble forms of its receptors: binding affinities, altered particle formation, and competition with cellular receptors. *J Virol* 79: 12016-24
162. Roger C, Pozzuto T, Klopfleisch R, Kurreck J, Pinkert S, Fechner H. 2015. Expression of an engineered soluble coxsackievirus and adenovirus receptor by a dimeric AAV9 vector inhibits adenovirus infection in mice. *Gene Ther* 22: 458-66
163. Carvajal-Gonzalez JM, Gravotta D, Mattera R, Diaz F, Perez Bay A, Roman AC, Schreiner RP, Thuenauer R, Bonifacino JS, Rodriguez-Boulan E. 2012. Basolateral sorting of the coxsackie and adenovirus receptor through interaction of a canonical YXXPhi motif with the clathrin adaptors AP-1A and AP-1B. *Proc Natl Acad Sci U S A* 109: 3820-5
164. Nishimura N, Sasaki T. 2009. Rab family small G proteins in regulation of epithelial apical junctions. *Front Biosci (Landmark Ed)* 14: 2115-29
165. Silvis MR, Bertrand CA, Ameen N, Golin-Bisello F, Butterworth MB, Frizzell RA, Bradbury NA. 2009. Rab11b regulates the apical recycling of the cystic fibrosis transmembrane conductance regulator in polarized intestinal epithelial cells. *Mol Biol Cell* 20: 2337-50
166. Brunetti-Pierri N, Ng P. 2009. Progress towards liver and lung-directed gene therapy with helper-dependent adenoviral vectors. *Curr Gene Ther* 9: 329-40
167. Kim EH, Park HJ, Han GY, Song MK, Pereboev A, Hong JS, Chang J, Byun YH, Seong BL, Nguyen HH. 2014. Intranasal adenovirus-vectored vaccine for induction of long-lasting humoral immunity-mediated broad protection against influenza in mice. *J Virol* 88: 9693-703
168. Podolska K, Stachurska A, Hajdukiewicz K, Malecki M. 2012. Gene therapy prospects--intranasal delivery of therapeutic genes. *Adv Clin Exp Med* 21: 525-34
169. Davis B, Nguyen J, Stoltz D, Depping D, Excoffon KJ, Zabner J. 2004. Adenovirus-mediated erythropoietin production by airway epithelia is enhanced

by apical localization of the coxsackie-adenovirus receptor in vivo. *Mol Ther* 10: 500-6
170. Muzumdar MD, Tasic B, Miyamichi K, Li L, Luo L. 2007. A global double-fluorescent Cre reporter mouse. *Genesis* 45: 593-605
171. Lutschg V, Boucke K, Hemmi S, Greber UF. 2011. Chemotactic antiviral cytokines promote infectious apical entry of human adenovirus into polarized epithelial cells. *Nat Commun* 2: 391
172. Hundhausen C, Misztela D, Berkhout TA, Broadway N, Saftig P, Reiss K, Hartmann D, Fahrenholz F, Postina R, Matthews V, Kallen KJ, Rose-John S, Ludwig A. 2003. The disintegrin-like metalloproteinase ADAM10 is involved in constitutive cleavage of CX3CL1 (fractalkine) and regulates CX3CL1-mediated cell-cell adhesion. *Blood* 102: 1186-95
173. Vincent B, Paitel E, Saftig P, Frobert Y, Hartmann D, De Strooper B, Grassi J, Lopez-Perez E, Checler F. 2001. The disintegrins ADAM10 and TACE contribute to the constitutive and phorbol ester-regulated normal cleavage of the cellular prion protein. *J Biol Chem* 276: 37743-6
174. Wild-Bode C, Fellerer K, Kugler J, Haass C, Capell A. 2006. A basolateral sorting signal directs ADAM10 to adherens junctions and is required for its function in cell migration. *J Biol Chem* 281: 23824-9
175. Tellier E, Canault M, Rebsomen L, Bonardo B, Juhan-Vague I, Nalbone G, Peiretti F. 2006. The shedding activity of ADAM17 is sequestered in lipid rafts. *Exp Cell Res* 312: 3969-80
176. Thiel KW, Carpenter G. 2006. ErbB-4 and TNF-alpha converting enzyme localization to membrane microdomains. *Biochem Biophys Res Commun* 350: 629-33
177. Mellman I, Nelson WJ. 2008. Coordinated protein sorting, targeting and distribution in polarized cells. *Nat Rev Mol Cell Biol* 9: 833-45
178. Surena AL, de Faria GP, Studler JM, Peiretti F, Pidoux M, Camonis J, Chneiweiss H, Formstecher E, Junier MP. 2009. DLG1/SAP97 modulates transforming growth factor alpha bioavailability. *Biochim Biophys Acta* 1793: 264-72
179. Peiretti F, Deprez-Beauclair P, Bonardo B, Aubert H, Juhan-Vague I, Nalbone G. 2003. Identification of SAP97 as an intracellular binding partner of TACE. *J Cell Sci* 116: 1949-57
180. Mizuhara E, Nakatani T, Minaki Y, Sakamoto Y, Ono Y, Takai Y. 2005. MAGI1 recruits Dll1 to cadherin-based adherens junctions and stabilizes it on the cell surface. *J Biol Chem* 280: 26499-507
181. Six E, Ndiaye D, Laabi Y, Brou C, Gupta-Rossi N, Israel A, Logeat F. 2003. The Notch ligand Delta1 is sequentially cleaved by an ADAM protease and gamma-secretase. *Proc Natl Acad Sci U S A* 100: 7638-43
182. Excoffon KJ, Gansemer N, Traver G, Zabner J. 2007. Functional effects of coxsackievirus and adenovirus receptor glycosylation on homophilic adhesion and adenoviral infection. *J Virol* 81: 5573-8
183. Pinkert S, Westermann D, Wang X, Klingel K, Dorner A, Savvatis K, Grossl T, Krohn S, Tschope C, Zeichhardt H, Kotsch K, Weitmann K, Hoffmann W, Schultheiss HP, Spiller OB, Poller W, Fechner H. 2009. Prevention of cardiac

dysfunction in acute coxsackievirus B3 cardiomyopathy by inducible expression of a soluble coxsackievirus-adenovirus receptor. *Circulation* 120: 2358-66
184. Dorner A, Grunert HP, Lindig V, Chandrasekharan K, Fechner H, Knowlton KU, Isik A, Pauschinger M, Zeichhardt H, Schultheiss HP. 2006. Treatment of coxsackievirus-B3-infected BALB/c mice with the soluble coxsackie adenovirus receptor CAR4/7 aggravates cardiac injury. *J Mol Med* 84: 842-51
185. Smith RA, von Eschenbach AC, Wender R, Levin B, Byers T, Rothenberger D, Brooks D, Creasman W, Cohen C, Runowicz C, Saslow D, Cokkinides V, Eyre H, Comm APCA, Comm ACCA, Comm AECA. 2001. American Cancer Society guidelines for the early detection of cancer: Update of early detection guidelines for prostate, colorectal, and endometrial cancers - ALSO: Update 2001 - Testing for early lung cancer detection. *Ca-a Cancer Journal for Clinicians* 51: 38-75
186. Tao M, Kruhlak M, Xia S, Androphy E, Zheng ZM. 2003. Signals that dictate nuclear localization of human papillomavirus type 16 oncoprotein E6 in living cells. *J Virol* 77: 13232-47
187. Wolfrum N, Greber UF. 2013. Adenovirus signalling in entry. *Cell Microbiol* 15: 53-62
188. Coyne CB, Bergelson JM. 2005. CAR: a virus receptor within the tight junction. *Adv Drug Deliv Rev* 57: 869-82
189. Coyne CB, Bergelson JM. 2006. Virus-induced Abl and Fyn kinase signals permit coxsackievirus entry through epithelial tight junctions. *Cell* 124: 119-31
190. Coyne CB, Shen L, Turner JR, Bergelson JM. 2007. Coxsackievirus entry across epithelial tight junctions requires occludin and the small GTPases Rab34 and Rab5. *Cell Host Microbe* 2: 181-92
191. Nakano MY, Boucke K, Suomalainen M, Stidwill RP, Greber UF. 2000. The first step of adenovirus type 2 disassembly occurs at the cell surface, independently of endocytosis and escape to the cytosol. *J Virol* 74: 7085-95